



TECHNISCHE
UNIVERSITÄT
DARMSTADT

Factors regulating late stages of homologous recombination and sub-pathway choice in G2

Vom Fachbereich Biologie der Technischen Universität Darmstadt

zur Erlangung des Grades

Doctor rerum naturalium

(Dr. rer. nat.)


Dissertation von

M.Sc. Amira Elbakry

Erstgutachter: Prof. Dr. Markus Löbrich

Zweitgutachter: Prof. Dr. Alexander Löwer

Darmstadt 2020



Elbakry, Amira: Factors regulating late stages of homologous recombination and sub-pathway choice in G2

Darmstadt, Technische Universität Darmstadt,

Jahr der Veröffentlichung der Dissertation auf TUPrints: 2021

URN: urn:nbn:de:tuda-tuprints-175757

Tag der mündlichen Prüfung: 05.06.2020

Veröffentlicht unter CC BY-SA 4.0 International



For those who stayed.

Preface

Due to the progression of the work presented here, this thesis is written in as a monography but is structured to provide an optimal presentation of the findings. The data are grouped into two independent chapters, each composed in a manuscript-like layout, with separate introduction, methods, results and discussion sections. General introduction and discussion sections border the chapters and unite the themes discussed in them, and a common materials section applying to both is included at the end. For simplicity and to avoid unnecessary redundancy, any new methods are described only once and abbreviations (listed below) are spelled out only when they first appear in the main document and then used in the short version henceforth. The first chapter encompasses work that has been carried out as a part of a bigger project and features in the final manuscript by Juhász *et al.* “ATR_X promotes extended DNA synthesis and sister chromatid exchange during homologous recombination” published in *Molecular Cell* in 2018. A follow-up commentary on this study by Elbakry *et al.* “DNA repair synthesis and histone deposition partner during homologous recombination” was also published in *Molecular and Cellular Oncology* in 2018. The second chapter involves follow up work that builds on the initial findings and expands on the model proposed and is in preparation as a separate manuscript. Therefore, the general discussion takes into account the data presented here as well as data from others that has been published and amalgamates them into a comprehensive bird’s eye view.

Table of contents

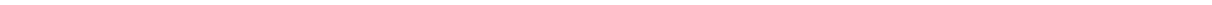
1. SUMMARY	1
2. INTRODUCTION	5
2.1 HOMOLOGOUS RECOMBINATION PROCESSES	5
2.1.1 INITIATION AND PROGRESSION OF HR	6
2.1.2 HR SUB-PATHWAYS: SYNTHESIS-DEPENDENT STRAND ANNEALING	11
2.1.3 HR SUB-PATHWAYS: DOUBLE HOLLIDAY JUNCTION	12
2.1.4 HR SUB-PATHWAYS: BREAK-INDUCED REPLICATION	15
2.1.5 HR FACTORS AND REPLICATION	16
2.2 CHROMATIN STRUCTURE AND DYNAMICS	18
2.2.1 HISTONE VARIANTS	19
2.2.2 CHROMATIN DYNAMICS AND THE DDR	20
2.2.3 VARIANTS ON THE MOVE FOLLOWING DNA DAMAGE	22
2.2.4 REPAIR PATHWAY CHOICE AND REGULATION OF HR	22
2.3 AIM OF THE STUDY	25
3. THE HISTONE VARIANT H3.3 IS REQUIRED DURING HOMOLOGOUS RECOMBINATION	27
3.1 INTRODUCTION	27
3.2 METHODS	28
3.2.1 CELL CULTURE	28
3.2.2 SIRNA AND PLASMID TRANSFECTION	29
3.2.3 DNA DAMAGE INDUCTION	30
3.2.4 CELL CYCLE-SPECIFIC DSB REPAIR ANALYSIS	31
3.2.5 IMMUNOFLUORESCENCE	31
3.2.6 SNAP-H3.3 DETECTION	32
3.2.7 REPORTER ASSAY	32
3.2.8 BRDU INCORPORATION ASSAY	32
3.2.9 CLONOGENIC SURVIVAL ASSAY	33
3.2.10 SISTER CHROMATID EXCHANGES ANALYSIS	33
3.2.11 CHROMATIN IMMUNOPRECIPITATION (CHIP)	34
3.2.12 SDS-PAGE AND IMMUNOBLOTTING	35
3.2.13 BACTERIAL TRANSFORMATION	36
3.2.14 QUANTIFICATION AND STATISTICAL ANALYSIS	36
3.3 RESULTS	37
3.3.1 THE HISTONE VARIANT H3.3 HAS A ROLE IN THE REPAIR OF X-RAY-INDUCED DSBs IN S/G2	37
3.3.2 H3.3 IS REQUIRED FOR HR IN A MANNER EPISTATIC TO THE CHROMATIN REMODELER ATRX	38
3.3.3 H3.3 IS REQUIRED DURING THE LATE STEPS OF HR	40
3.3.4 NEWLY SYNTHESIZED H3.3 IS DEPOSITED EARLY AT SITES OF DAMAGE INDEPENDENTLY OF ATRX	43
3.3.5 LATE DEPOSITION OF NEWLY SYNTHESIZED H3.3 AT SITES OF DAMAGE IS DEPENDENT ON RAD51, ATRX AND DAXX	45
3.3.6 HISTONE H3.3 DEPOSITION AND DNA REPAIR SYNTHESIS ARE INTERLINKED	47
3.3.7 HISTONE H3.3 DEPOSITION BY OTHER CHROMATIN REMODELERS AND CHAPERONS	49

3.4	DISCUSSION	51
3.5	CONCLUSION	54
4.	<u>ATRX AND RECQ5 DEFINE DISTINCT SUB-PATHWAYS OF HOMOLOGOUS RECOMBINATION</u>	55
4.1	INTRODUCTION	55
4.2	METHODS	57
4.2.1	CELL CULTURE	57
4.2.2	SIRNA, PLASMID TRANSFECTION AND INHIBITORS	58
4.2.3	X-RAY IRRADIATION	58
4.2.4	IMMUNOFLUORESCENCE	58
4.2.5	SISTER CHROMATID EXCHANGES ANALYSIS	58
4.2.6	ULTRA-FINE BRIDGES ANALYSIS	59
4.2.7	SDS-PAGE AND IMMUNOBLOTTING	59
4.2.8	BACTERIAL TRANSFORMATION	59
4.2.9	QUANTIFICATION AND STATISTICAL ANALYSIS	59
4.3	RESULTS	60
4.3.1	ATRX AND RECQ5 DEFINE TWO DISTINCT SUB-PATHWAYS OF HR	60
4.3.2	ATRX DOMINATES OVER RECQ5 TO PROMOTE HIGH SCE FREQUENCY	63
4.3.3	ATRX-DEPENDENT HR LEADS TO THE FORMATION OF IR-INDUCED MUS81-DEPENDENT HR INTERMEDIATES	66
4.3.4	PROCESSING OF ATRX-DEPENDENT HR INTERMEDIATES IS BLM-INDEPENDENT	69
4.4	DISCUSSION	71
4.4.1	HR BY SDSA AND THE DHJ PATHWAY	71
4.4.2	SCEs FREQUENTLY ARISE IN G2-IRRADIATED MAMMALIAN CELLS	71
4.4.3	ATRX-DEPENDENT HR INTERMEDIATES ARE EXCLUSIVELY CHanneLED INTO THE RESOLUTION PATHWAY	72
4.4.4	A ROLE FOR CHROMATIN IN HR SUB-PATHWAY CHOICE	73
4.4.5	CONCLUSION	73
5.	<u>DISCUSSION</u>	75
5.1	HR SUB-PATHWAYS AND THE FREQUENCY OF COS	75
5.2	CHROMATIN REMODELING AND REGULATION OF REPAIR OUTCOME	76
5.3	PATHWAY CHOICE AND THE FIDELITY OF HR	78
5.4	HR SUB-PATHWAY CHOICE: CLINICAL RELEVANCE	80
5.5	CONCLUSION AND OUTLOOK	82
6.	<u>MATERIALS</u>	83
6.1	CONSUMABLES	83
6.2	LAB EQUIPMENT AND SOFTWARE	83
6.3	CHEMICALS	84
6.4	OLIGONUCLEOTIDES (SIRNA AND PRIMERS)	86
6.5	DNA CONSTRUCTS	87
6.6	ANTIBODIES	87
6.7	KITS, ENZYMES AND LADDERS	88
6.8	BUFFERS, SOLUTIONS AND MEDIA	89

6.9	CELL LINES AND BACTERIA	91
7.	REFERENCES	92
8.	APPENDIX	105
8.1	ABBREVIATIONS	105
8.2	EHRENWÖRTLICHE ERKLÄRUNG	108
8.3	CURRICULUM VITAE	109
8.4	ACKNOWLEDGMENTS	111

List of Figures

FIGURE 2.1: Cell cycle pathway regulation and HR initiation	7
FIGURE 2.2: Rad51 loading and nucleofilament formation	8
FIGURE 2.3: Homology search, D-loop formation and DNA synthesis	10
FIGURE 2.4: HR sub-pathways	14
FIGURE 2.5: HR at replication-associated lesions	17
FIGURE 2.6: Structure and dynamics of chromatin.	20
FIGURE 2.7: General chromatin responses to DNA damage	21
FIGURE 2.8: Histone exchange and DSB pathway choice	23
FIGURE 3.1: The histone variant H3.3 has a role in the repair of X-ray-induced DSBs in G2 cells	38
FIGURE 3.2: H3.3 is required for HR in a manner epistatic to the chromatin remodeler ATRX	41
FIGURE 3.3: H3.3 is required during the late steps of HR	42
FIGURE 3.4: Newly synthesized H3.3 is deposited early at sites of damage independently of ATRX	44
FIGURE 3.5: Late deposition of newly synthesized H3.3 at sites of damage is dependent on Rad51, ATRX and DAXX	46
FIGURE 3.6: Histone H3.3 deposition and DNA repair synthesis are interlinked	48
FIGURE 3.7: Histone H3.3 deposition by other chromatin remodelers and chaperons	50
FIGURE 3.8: Model for histone deposition during homologous recombination	53
FIGURE 4.1: ATRX and RECQ5 define two distinct sub-pathways of HR	62
FIGURE 4.2: ATRX dominates over RECQ5 to promote high SCE frequency.	65
FIGURE 4.3: ATRX-dependent HR leads to the formation of IR-induced Mus81-dependent HR intermediates	68
FIGURE 4.4: Processing of ATRX-dependent HR intermediates is BLM-independent	70
FIGURE 4.5: Model depicting the interplay between ATRX and RECQ5 to regulate distinct sub-pathways of HR	74
FIGURE 5.1: Repair of one-ended breaks and formation of chromosomal rearrangements	79



1. SUMMARY

Cells have evolved multiple mechanisms to preserve genome integrity and restore structural and functional properties of the genome following deoxyribonucleic acid (DNA) damage. DNA double-strand breaks (DSBs) are critical lesions whose timely and faithful repair is important for cellular viability and genomic stability. Among the multiple pathways dedicated for handling DSBs, homologous recombination (HR) provides a high-fidelity mechanism for error-free repair in cycling cells. HR is also important for the faithful duplication of the genome by providing means of tolerating replication stress and overcoming a variety of lesions occurring as a result of replication errors such as single-strand breaks, gaps and one-ended DSBs that impede progressing replication forks. HR at two-ended DSBs can proceed through two known sub-pathways with distinct genetic outcomes: the double Holliday junction (dHJ) pathway and synthesis-dependent strand annealing (SDSA), which result in crossover (CO) and non-CO recombination products, respectively. Although the initial steps of HR, such as resection, have been extensively studied, less is known about late stages of HR, especially in mammalian cell, as well as the factors governing sub-pathway choice. Here, experiments were set up to specifically analyse HR-mediated repair of X-ray-induced DSBs in G2 cells, a setup that avoids the complications of S-phase induced damage and focuses on two-ended breaks. The first part of this study shows that the histone variant H3.3 is required during late stages of HR, in a step following Rad51 loading and removal, and in a manner epistatic to the chromatin remodeler ATRX. Indeed, H3.3 is needed for DNA repair synthesis in G2 cells, and subsequent formation of sister chromatid exchanges (SCEs). To monitor *in vivo* histone deposition, a stable cell line system expressing SNAP-H3.3 was used to visualize newly synthesized histone incorporation following laser-induced DNA damage. Consistent with previous reports, H3.3 is deposited early (up to 1 h) post IR, but through an HR-independent mechanism. However, late H3.3 incorporation (8 h) was dependent on Rad51, ATRX and the chaperon DAXX, corroborating an active deposition of H3.3 at sites of DNA damage during HR. Furthermore, H3.3 deposition was also dependent on the processivity factor PCNA and its loader RFC-1, suggesting a tight association with DNA synthesis. The results collectively inspire a model where ATRX-DAXX-mediated H3.3 deposition is tightly coupled to DNA repair synthesis and serves to facilitate progression of the displacement loop (D-loop) and repair completion in a sub-pathway of HR that leads to the formation of CO products.

To further understand the regulation of HR sub-pathway choice, cells lacking ATRX and the SDSA factor RECQ5 were analysed for their HR repair capacity. ATRX-deficient U2OS cells with inducible ATRX expression and HeLa cells were used to establish comparisons of pathways usage. While both cell lines are dependent on Rad51 for repair of G2-induced DSBs, ATRX-deficient cells rely entirely on RECQ5-mediated SDSA for the repair of these breaks, while HeLa cells can employ both pathways. Further analysis revealed that ATRX-dependent HR dominates in cells that have both factors, resulting in elevated IR-induced SCEs in cells with induced ATRX expression. Additional factors were analysed to show that SDSA surprisingly does not require the essential HR factor Rad54 for repair, indicating the deeper inherent differences between these two sub-pathways and suggesting a more complex regulation of pathway choice.

Quantitative analysis of HR events showed that approximately 50% of ATRX-dependent HR events result in a CO product, a much higher frequency than previously thought. This led to further analysis of HR intermediates formed in this pathway manifesting as IR-induced ultra-fine bridges (UFBs) visualized in anaphase cells lacking the resolvases Mus81 and Gen1. IR-induced UFBs formed in an ATRX-dependent manner, suggesting that these HR intermediates are largely processed by the resolution pathway. Furthermore, Mus81 foci analysis showed that Mus81 was recruited to DSBs in mitotic HeLa cells but not in U2OS cells, suggesting the presence of distinct HR intermediates in these cells. Recruitment of Mus81 was not affected by BLM depletion, suggesting that Mus81 is occupying all suitable substrates even in the presence of BLM and that these structures are not subject to dissolution. Similarly, BLM depletion did not affect Rad51 foci formation, γ H2AX foci dynamics, or the level of IR-induced SCEs, further corroborating the notion that BLM is not active in this sub-pathway of HR. Taken together, the data suggest that ATRX-dependent HR dominates over RECQ5-dependent SDSA for the repair of two-ended breaks in G2 cells. This pathway involves the formation of HR intermediates that are exclusively resolved by the structure-specific nucleases Mus81 and Gen1 while being refractory to dissolution, explaining the observed high frequency of SCEs observed. This dominance could be explained by a model whereby ATRX-dependent histone deposition inside an expanding D-loop structurally hinders both strands displacement during SDSA and the dissolution of a dHJ by BLM.

Zusammenfassung

Zur Erhaltung der Integrität des Genoms haben Zellen vielfältige Mechanismen entwickelt, um die strukturellen und funktionellen Eigenschaften des Genoms nach einem DNA-Schaden wiederherzustellen. Eine schnelle und fehlerfreie Reparatur von DNA-Doppelstrangbrüchen (DSBs) ist essenziell für die genomische Stabilität und das Überleben der Zellen. Die homologe Rekombination (HR) ist ein fehlerfreier DSB-Reparaturmechanismus, der proliferierenden Zellen zur Verfügung steht. HR ist außerdem an der fehlerfreien Duplikation des Genoms beteiligt, indem es dazu beiträgt Replikationsstress zu tolerieren und Schäden, die die Replikationsgabel blockieren zu prozessieren (Einzelstrangbrüche, *gaps* oder einendige DSBs). An zweiendigen DSBs können zwei Unterwege der HR ablaufen, die unterschiedliche genetische Endprodukte haben: der double Holliday junction (dHJ) pathway, wodurch crossover (CO) Produkte entstehen und synthesis dependent strand annealing (SDSA) wodurch non-CO Produkte entstehen. Wobei über die ersten Schritte der HR, wie z.B. die Resektion, sehr viel bekannt ist, ist über die späteren HR-Schritte und die Faktoren, die an der Wahl des Unterwegs beteiligt sind, vor allem in Säugerzellen nur wenig bekannt. In dieser Studie wurde die HR-Reparatur von Röntgenstrahl (IR)-induzierten DSBs in der G2 Phase untersucht. Durch die spezifische Analyse von G2-Phase Brüchen konnten S-Phase Brüche ausgeschlossen werden und somit die Analyse auf 2-endige DSBs fokussiert werden. Im ersten Teil dieser Arbeit konnte gezeigt werden, dass die Histon-Variante H3.3 nach der Entfernung von Rad51 und somit in einem späten Stadium der HR erforderlich ist. Außerdem konnte gezeigt werden, dass H3.3 epistatisch mit dem Chromatin-remodeler ATRX wirkt. H3.3 wird für die Reparatursynthese und die darauffolgende Ausbildung von Schwesterchromatidaustauschen (SCEs) in G2 Zellen benötigt. Um den Chromatineinbau von H3.3 *in vivo* zu messen wurde eine stabile Zelllinie hergestellt, die SNAP-H3.3 exprimiert. Mithilfe dieser Zelllinie konnte der Einbau von neu synthetisierten H3.3 Histonen an Laser-induzierten DNA-Schäden visualisiert werden. H3.3 wird zu frühen Zeitpunkten (bis 1 h) post IR mithilfe eines HR-unabhängigen Mechanismus in das Chromatin eingebaut. Zu späteren Zeitpunkten (8 h) post IR wird H3.3 aktiv am DNA-Schaden durch HR in das Chromatin eingebaut und ist daher abhängig von Rad51, ATRX und DAXX. Des Weiteren ist der aktive Einbau von H3.3 abhängig von PCNA und RCF-1, was eine direkte Verbindung mit der DNA-Synthese nahelegt. Diese Ergebnisse legen ein Modell nahe, bei dem der Einbau von H3.3 in das Chromatin durch ATRX und DAXX vermittelt wird und eng an die DNA-Reparatursynthese gekoppelt ist. Dabei wird die Progression des D-Loops unterstützt und CO Produkte entstehen.

Um die Regulierung der Wahl des HR Unterwegs besser zu verstehen wurde die HR-Reparaturkapazität von ATRX- und RECQ5-defizienten Zellen untersucht. Für den direkten Vergleich der beiden Unterwege wurden U2OS Zellen mit induzierbarer ATRX-Expression und HeLa Zellen verwendet. Während beide Zelllinien für die Reparatur von G2-induzierten DSBs Rad51 benötigen, können ATRX-defiziente Zellen ihre DSBs ausschließlich mit Hilfe des RECQ5-abhängigen SDSA reparieren, während HeLa Zellen von beiden Unterwegen Gebrauch machen können. Weiterhin konnte gezeigt werden, dass Zellen denen beide Unterwege zur Verfügung stehen, ATRX-abhängiges HR bevorzugt verwenden. Dies führt zu erhöhten IR-induzierten SCEs in Zellen mit induzierter ATRX Expression. Überraschenderweise konnte gezeigt werden, dass der essenzielle HR-Faktor Rad54 für die Reparatur mittels SDSA nicht benötigt wird, was auf die tieferen inhärenten Unterschiede zwischen diesen beiden Unterwegen hinweist und eine komplexere Regulierung der Wegwahl nahelegt.

Die quantitative Analyse von HR-Ereignissen zeigte, dass etwa 50% der ATRX-abhängigen HR-Ereignisse zu einem CO-Produkt führen, eine viel höhere Frequenz als bisher angenommen. Die weiterführende Analyse der ausgebildeten HR-Strukturen zeigte, dass IR-induzierte ultrafeine Brücken (UFBs) in Anaphasezellen sichtbar werden. Die Anzahl der UFBs, die nach IR gebildet werden, ist signifikant höher in Zellen ohne die Resolvasen Mus81 und Gen1. Dies zeigt, dass HR-Strukturen weitgehend durch *resolution* aufgelöst werden. Darüber hinaus zeigte die Analyse der Mus81-Foci, dass Mus81 zu DSBs in mitotischen HeLa-Zellen rekrutiert wird, jedoch nicht in U2OS-Zellen. Dieses Ergebnis deutet darauf hin, dass unterschiedliche HR-Intermediatstrukturen in diesen Zellen vorliegen. Die Rekrutierung von Mus81 wurde durch eine BLM-Depletion nicht beeinträchtigt, was darauf hindeutet, dass Mus81 alle geeigneten Substrate in Anwesenheit von BLM besetzt und dass diese Strukturen nicht durch *dissolution* aufgelöst werden. Des Weiteren hatte eine BLM-Depletion keinen Effekt auf Rad51-Foci, γ H2AX-Foci oder die Anzahl der IR-induzierten SCEs, was die Vermutung, dass die BLM in diesem HR-Unterweg nicht aktiv ist, weiter bestätigt. Insgesamt deuten die Daten darauf hin, dass ATRX-abhängiges HR gegenüber dem RECQ5-abhängigen SDSA bei der Reparatur von zweiendigen DSBs in G2-Zellen überwiegt. Bei diesem Reparaturweg werden HR-Intermediate ausgebildet, die ausschließlich von den strukturspezifischen Nukleasen Mus81 und Gen1 aufgelöst werden, und somit nicht durch *dissolution* aufgelöst werden können, was die erhöhte Anzahl von SCEs erklärt. Dies legt ein Modell nahe, bei dem die ATRX-abhängige Histonablagerung innerhalb des D-loops die Verdrängung des DNA Strangs während SDSA und die *dissolution* einer dHJ durch BLM strukturell behindert.

2. INTRODUCTION

Protecting the genome is of critical importance to cell and organismal survival as excessive deoxyribonucleic acid (DNA) damage can cause cell death or the accumulation of pathological mutations. With thousands of lesions bombarding the DNA daily, the cell faces the challenging endeavor of faithful and timely DNA repair, for which an arsenal of specialized mechanisms is in place. Among the most lethal events compromising genomic stability and cellular viability is the double-strand break (DSB), as it physically disconnects regions of the genome and can initiate chromosomal rearrangements and disruption of gene structure and function. DSBs can arise from endogenous processes such as replication errors, radical-producing metabolic activities, and enzymatic cleavage that initiates recombination events during meiosis and antigen receptor diversification. They can also be caused by external sources, including ionizing radiation and genotoxic drugs. Multiple pathways work non-redundantly to repair DSBs, operating with different fidelities, efficiencies and temporal dynamics within a regulation complex network to ensure the restoration of genomic integrity. Two main pathways are described for DSB repair, in addition to a variety of sub- and back-up pathways, which are homologous recombination (HR) and canonical non-homologous end joining (c-NHEJ). This work will focus on mechanisms of HR and its sub-pathways in somatic cells and particularly at DSBs.

2.1 HOMOLOGOUS RECOMBINATION PROCESSES

HR is an essential process for preserving genomic integrity that relies on the presence of identical or near-identical sequences in sister chromatids and homologous sequences (on homologous chromosomes or distinct genomic loci), respectively. The importance of HR in unperturbed cells and in response to DNA damage is underscored by the excessive genomic instabilities and chromosomal aberrations observed in cells harboring HR mutants. These HR deficiencies and their associated mutagenic signatures are often linked to higher predisposition to various types of cancer¹. HR provides a high-fidelity mechanism to respond to a variety of toxic DNA damages in the form of stalled or broken replication forks, single-strand (ss) gaps, and one-ended and two-ended DSBs arising during perturbed DNA replication and as a result of exogenous genomic assaults. HR-mediated DSB repair in somatic yeast and mammalian cells is largely restricted to the sister chromatid of the damaged region, where identical sequences are used and thereby no genetic information is lost^{2,3}. On the other hand, HR during meiosis serves to create genetic diversity by targeting the homologous chromosome for use as

a template, promoting exchange between maternal and paternal sequences⁴. During meiosis, and in contrast to mitotic HR, a large number of DSBs are introduced in a highly regulated manner, the repair of which is coordinated to favor the homolog instead of the sister chromatid and intricately balances the recombination products to a narrow range of crossing over events⁴. While functionally distinct, mitotic- and meiotic-HR are mechanistically similar and share common steps and factors that have been extensively studied in yeast and mammalian models to provide a more comprehensive picture about the HR process. Although far from complete, current knowledge has provided invaluable insights fueling pioneering work in cancer diagnostics and therapeutics. A prime example is applying the concept of synthetic lethality, where tumors deficient for HR factors are specifically targeted with agents that inhibit another DNA repair pathway, and a double-deficiency leads to tumor cell death, while normal cells remain unaffected⁵. Understanding HR is also revolutionizing genetic engineering approaches, making CRISPR technologies for example, more effective, versatile and far-reaching⁶. Therefore, HR is a multifaceted process that supports various essential biological functions, warranting extensive investigation of the mechanisms of recombination.

2.1.1 *Initiation and progression of HR*

In mitotically dividing cells, HR is regulated spatially and temporally, through a variety of mechanisms, to ensure timely and faithful repair of DNA lesions, most notably DSBs. The use of a sister chromatid for HR ensures an error-free repair, consistent with its restriction to the S/G2 phase of the cell cycle (Figure 2.1 A) during which the genome is duplicated. This regulation orchestrated by a tightly controlled network of cyclin-dependent kinases (CDKs)⁷. Interestingly, new evidence also indicates a role of newly replicated chromatin to favor HR, adding another layer of regulation to ensure cell-cycle specificity⁸. In contrast, c-NHEJ occurs throughout the cell cycle and is generally regarded as a fast, but an error-prone DSB repair pathway⁹. Additionally, recent genome-wide data show that the location of a DSB in the genome also influences repair pathway choice, where DSBs in transcriptionally active regions are preferentially repaired by HR¹⁰. A key mechanistic determinant in the choice of HR versus c-NHEJ is processing of the breaks ends^{11,12}. While c-NHEJ mostly requires little end processing (depending on the nature and complexity of the break), HR requires extensive 5'-to-3' resection of the break ends to produce 3'-OH single-stranded overhangs (Figure 2.1 B). This is a two-step, bidirectional process that is initiated in mammalian cells by MRE11-Rad50-NBS1 (MRN) complex together with CtBP-interacting protein (CtIP) that catalyze an endonucleolytic cleavage behind the break. MRE11 then initiates short-range resection in the

3'-to-5' direction, resulting in small (up to 300 bp) overhangs¹³. This has the advantage of removing highly modified bases and/or bound proteins blocking the break end that could impede repair. Resection is then extended in the 5'-to-3' direction by two redundant pathways involving EXO1 and BLM/DNA2, generating long stretches of single-stranded (ssDNA) (>1000 bp) and committing the cell to HR, although other pathways are also able to repair these intermediates, such as single strand annealing (SSA) and alternative NHEJ (alt-NHEJ)^{12,14,15}. This process is regulated by various mechanisms, including CDK-dependent phosphorylation of CtIP that promotes its activation in S/G2 and interaction with breast cancer type 1 susceptibility protein (BRCA1), thereby ensuring timely usage of resection factors^{16,17}. Moreover, BRCA1 functions to overcome resection inhibition by the DNA damage response factor 53BP1, constituting a key node for pathway choice^{18,19}. Additionally, EXO1 and NBS1 are also phosphorylated by CDKs to provide another layer of temporal regulation of extended resection^{20,21}.

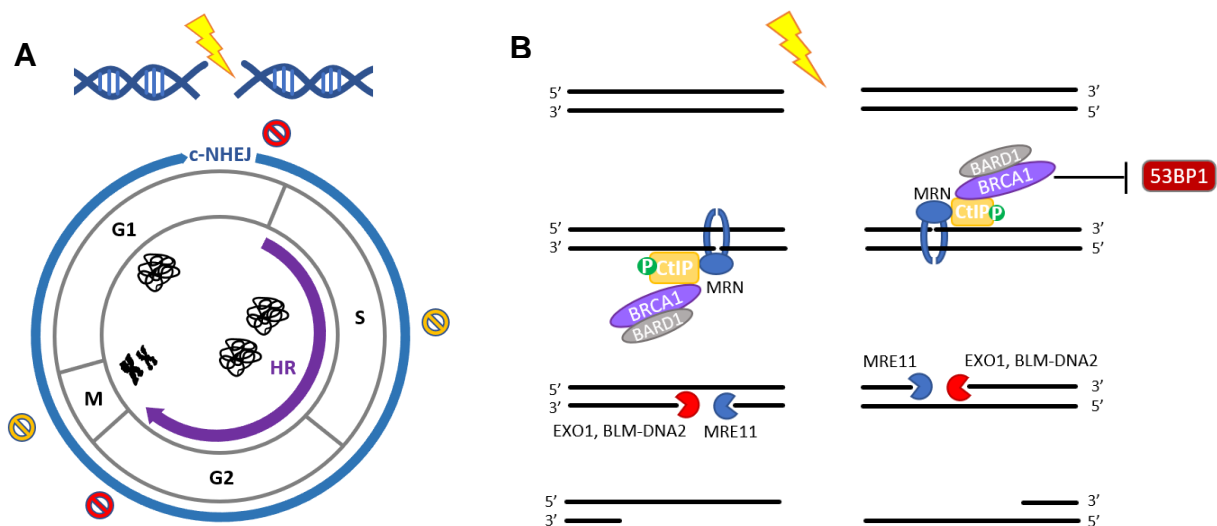


Figure 2.1. Cell cycle pathway regulation and HR initiation.

(A) DSBs are repaired by c-NHEJ throughout the cell cycle, while HR occurs only during S/G2. DNA damage-induced check points arrest (red) or slow down (yellow) cell cycle progression to allow for DNA repair. (B) End resection commits DSB repair to HR. Resection is initiated in S/G2 by CDK--mediated phosphorylation of CtIP, which interacts with MRN to catalyze an endonucleolytic cleavage behind the break. BRCA1-BARD1 also overcome resection inhibition by 53BP1. Short-range 3'-to-5' resection by MRE11 and long-range 5'-to-3' resection by EXO1 or BLM-DNA2 results in large ssDNA 3' overhangs.

The large sections of resected DNA are coated initially by replication protein A (RPA) complex which protects DNA ends from nuclease-mediated degradation and relaxes secondary structures to prime the ssDNA for subsequent repair steps^{22,23} (Figure 2.2). It is also suggested that RPA prevents microhomology-mediated annealing, thereby suppressing error-prone

pathways from dominating ²⁴. However, RPA strongly competes with Rad51 for ssDNA and inhibits the nucleation step needed for the formation of the presynaptic filament, a central step in HR ²⁵. This inhibition is overcome by the mediator function of BRCA2, which interacts with Rad51 and promotes its loading on ssDNA, replacing RPA to initiate nucleation and allow 3'-

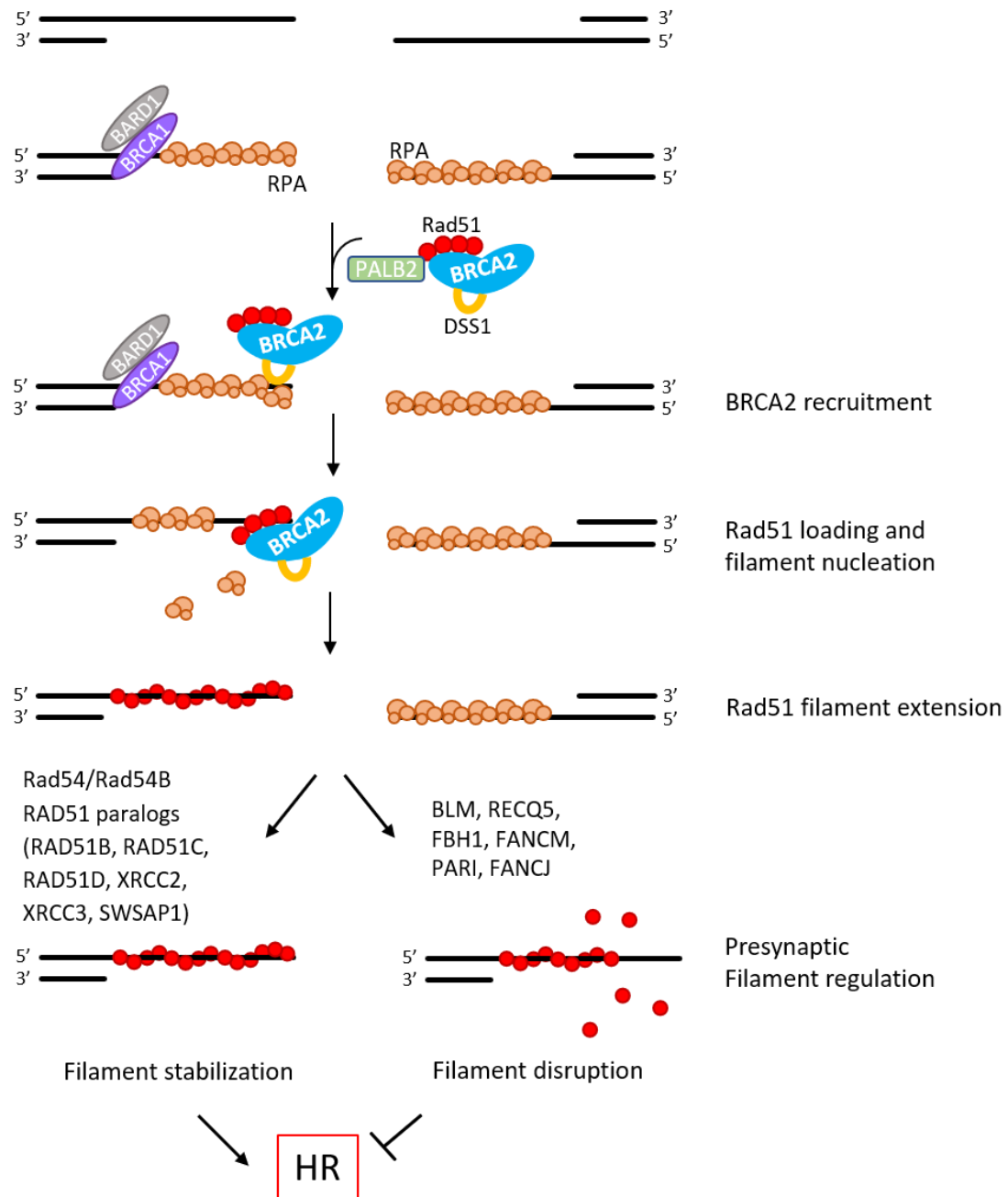


Figure 2.2. Rad51 loading and nucleofilament formation.

Resected DNA ends are coated by RPA, which is replaced by Rad51 in a BRCA2-DSS1-mediated reaction, promoted by interaction with BRCA1-BARD1 through PALB2. The initial nucleation event is followed by filament extension in the 3'-to-5' direction. The pre-synaptic filament is stabilized by Rad54/Rad54B and the Rad51 paralogs to promote recombination, where helicases displace Rad51 from ssDNA in anti-recombination processes.

to-5' filament extension²⁶⁻²⁹. The function of BRCA2 in Rad51 loading requires other interactors to support nucleofilament formation, such as DSS1 and all four known mammalian Rad51 paralogs^{27,30}. Additionally, BRCA2 recruitment requires an interaction with BRCA1-BARD1 mediated through partner and localizer of BRCA2 (PALB2), thereby bridging the resection and Rad51 loading steps³¹. Each Rad51 monomer interacts with three nucleotides of the ssDNA and assembles in a right-handed helical filament, termed the presynaptic filament, that drives homology search and subsequent strand exchange between the double-stranded DNA (dsDNA) donor and ssDNA at regions of homology (Figure 2.3)³². During homology search, the donor helix is destabilized and the bases are sampled for complementarity in a process known as base-flipping³³. Homology recognition proceeds precise three-nucleotide steps in which tracts of at least eight-nucleotide microhomology are required for subsequent strand exchange^{34,35}. Interestingly, any sequence on the ssDNA of the filament can be used for homology search, thereby not restricting the process to the invading end³⁶. Once homology is found, a three-molecule structure, known as the synaptic complex, or the paranemic joint, is formed and is made up of the invading ssDNA interacting with the donor dsDNA without strand intertwining and relying on protein interactions for stabilization^{37,38}.

The synaptic complex then progresses to form the displacement loop (D-loop), an important HR intermediate in which the invading strand pairs with the complementary sequence in the donor and the original strand is displaced to allow the intertwining of the new paired strands, a region referred to as heteroduplex DNA (hDNA) (Figure 2.3)³⁹. A key factor for multiple steps leading to D-loop formation is Rad54, an ATP-dependent motor protein with translocase activity that associates with Rad51 and stabilizes the initial ssDNA filaments and formation of the synaptic complex⁴⁰⁻⁴². In this process Rad54 exerts a quality control function, ensuring correct associations of homologous sequences by sensing and dissociating heterologous pairings⁴². Additionally, Rad54 is also required for D-loop formation *in vitro*, where interaction with Rad51 and ssDNA junction DNA stimulates Rad54 ATPase activity and serves to drive hDNA formation and extension, using Rad54 motor activity to convert synaptic complexes into D-loops, a reaction coupled to Rad51 removal from hDNA^{36,43}. This reaction is regulated *in vivo* by Nek1 kinase, which phosphorylates Rad54 specifically in G2 to promote Rad51 removal and promote HR progression⁴⁴. The premature activation of Rad54 in S phase causes unregulated removal of Rad51 at stalled replication forks, leading to fork degradation and persistent DNA damage, thereby highlighting the importance of temporally regulating this process⁴⁴.

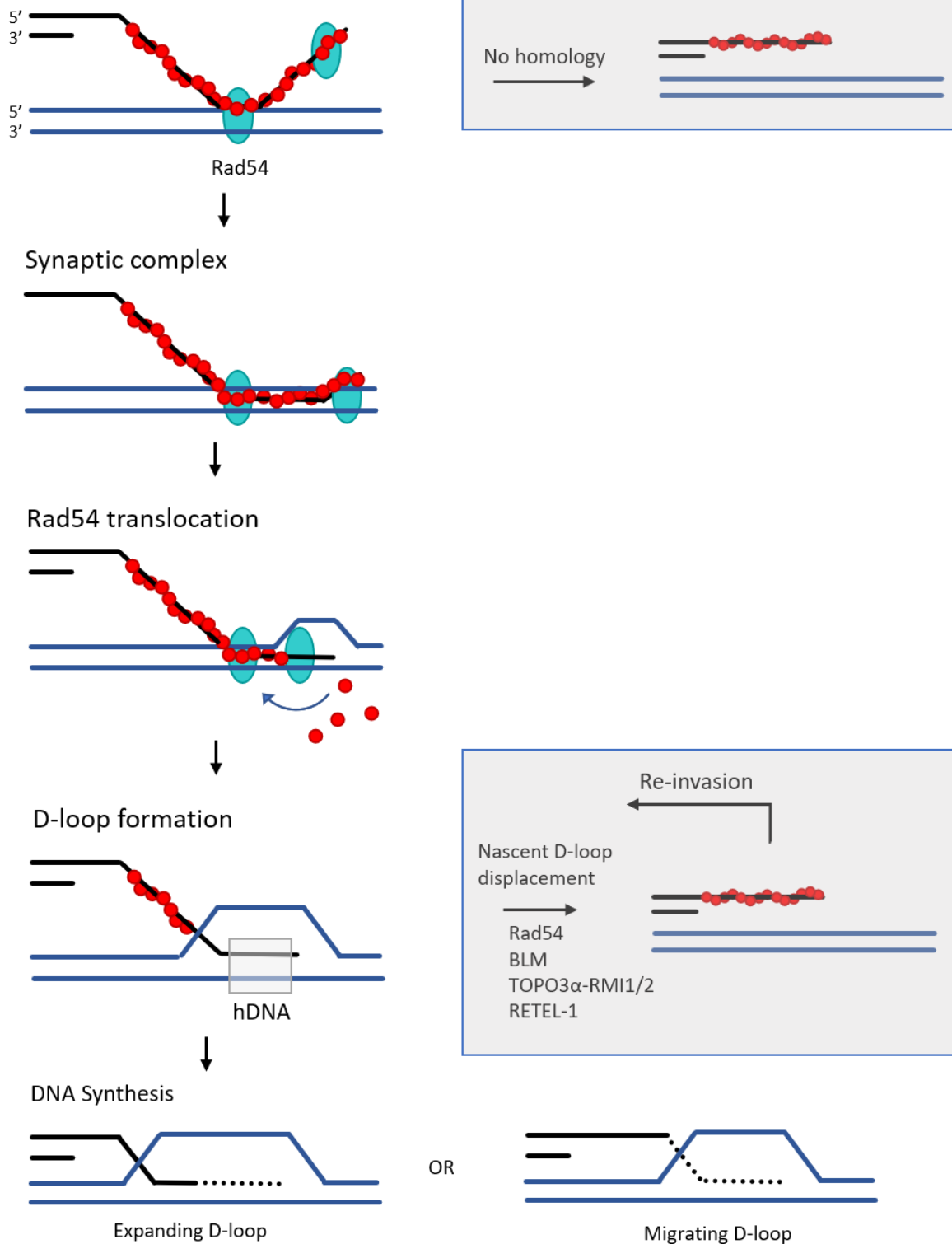


Figure 2.3. Homology search, D-loop formation and DNA synthesis.

Rad54-mediated homology search is followed by synaptic complex formation upon homology recognition. Rad54 translocates along dsDNA, removing Rad51 and allowing D-loop formation and hDNA generation. The 3' end of the invading strand primes DNA synthesis in either an expanding or migrating D-loop model. Quality control of proper homologies is mediated by Rad54, while nascent, non-extended D-loops can be dismantled by helicases to prime re-invasion or HR termination.

The formation of the D-loop is critical to provide the primer-template junction required for DNA synthesis to complete the faithful restoration of sequence information. *In vitro* studies using short oligonucleotide ssDNA and plasmid donors identified essential factors for DNA synthesis following D-loop formation to be the proliferating cell nuclear antigen (PCNA), replication factor C (RFC) complex, and the DNA polymerase δ (Pol δ)⁴⁵. How these complexes function *in vivo* or if additional factors are required is not yet clear, but it is likely that the complex nature of chromatin and nuclear environment would dictate the need for a more elaborate mechanism. One concern is the topological changes that arise during both D-loop formation and the subsequent DNA synthesis. The invading strand's intertwining is favored in regions of negative supercoils, which relax during D-loop formation, where the longer the hDNA, the more the DNA is relaxed³⁹. DNA synthesis can proceed until the negative supercoils pre-existing in the donor are consumed, and positive supercoils start to form, eventually leading to a topological block³⁶. At this stage, different modes of progression could apply: one is a 'migrating bubble' where the D-loop remains at a relatively constant size, but the invading strand is constantly being displaced on the 5' side, a process that could be performed by a helicase (Figure 2.3). Evidence for this comes from studies in the budding yeast *Saccharomyces cerevisiae* describing a process called break-induced replication (BIR, discussed below), where the helicase Pif1 is required for long-range synthesis⁴⁶. Additionally, a newly identified HR factor, HROB, was shown to recruit the helicase proteins MCM8 and MCM9 to sites of DNA damage to promote the repair of inter-strand crosslinks (ICL)-induced DSBs in a step following Rad51 loading⁴⁷. However, their exact function during D-loop formation and extension is still unclear. An alternative model is an expanding D-loop where the positive supercoils must be dissipated ahead of the DNA synthesis complex, a function normally carried out by topoisomerases during replication and transcription. Neither of these models has been fully explored; with questions still remaining regarding the regulation of D-loop size and range, termination of DNA synthesis and the factors involved.

2.1.2 ***HR sub-pathways: Synthesis-Dependent Strand Annealing***

Following DNA synthesis, HR at two-ended DSBs can proceed in one of two main sub-pathways: synthesis-dependent strand annealing (SDSA) or a double Holliday junction (dHJ) forming pathway. SDSA proceeds by the disruption of the extended D-loop as the invading end is ejected and anneals back to the other complementary end of the DSB. This pathway therefore inherently precludes the formation of cleavable HR intermediates and results in strictly non-crossover (CO) products (Figure 2.4 A)⁴⁸. Since the displacement step is central

to this pathway, it has been the focus of many studies, resulting in the implication of various helicases in this process, including the budding yeast proteins Srs2, Sgs1 and Mph1. Sgs1 is the yeast homolog of the human Bloom syndrome protein (BLM), and was shown to dismantle protein-free D-loops, but not those constituted with RPA, Rad51 and Rad54⁴⁹. However, the topoisomerase complex Topo3-Rmi1, which associates with Sgs1, can dismantle Rad51-Rad54-dependent D-loops⁴⁹. Dissociating nascent (non-extended) D-loops prior to DNA synthesis is an anti-recombination reaction, which could serve to control for the proper formation of these HR intermediates (Figure 2.3). On the other hand, D-loops that have been extended through DNA synthesis represent a different substrate, and their dissociation is important for the completion of HR and thereby is a pro-recombinogenic event. Although Srs2 has been shown to dissociate Rad51 from single-stranded presynaptic filaments *in vitro*, suggesting an anti-recombinase function, it can also disrupt Rad51-containing extended D-loops, thereby promoting SDSA^{50,51}. Similarly, biochemical assays revealed that Mph1, yeast ortholog of human FANCM, can dissociate both nascent and extended D-loops in a manner independent from Srs2 and Sgs1⁵². How these helicases distinguish between extended and nascent D-loops, and therefore exert pro- and anti-recombination functions respectively, is unclear. One means of regulation is proposed through interaction with PCNA, where SUMO-modified PCNA leads to Srs2 preferentially targeting extended D-loops, providing a mechanism for recruitment, as well as ensuring DNA synthesis has taken place prior to D-loop disruption⁵¹. While multiple studies have address the displacement step in yeast, the analogous human cells is less elucidated, in which multiple helicases have been implicated, such as RECQ5, RECQ1, RTEL1, FANCI and FBH1⁵³⁻⁵⁷. After D-loop displacement, the now-free end anneals to the other complementary end of the DSB, using the homology generated from the DNA synthesis step. This is followed by further DNA synthesis to fill in the gaps and restore the remaining missing sequences and then ligation to seal the DNA backbone and complete repair. However, the factors promoting the annealing, synthesis and ligation steps are still unidentified.

2.1.3 *HR sub-pathways: double Holliday junction*

Another possible pathway following D-loop extension involves a step known as second end capture, where the second end of the DSB anneals to, or ‘captures’ the displaced strand of the D-loop which is then used as a template for DNA synthesis (Figure 2.4 B). Alternatively, it has been proposed that this step could in fact be another invasion process mirroring the one at the opposite end, also allowing DNA synthesis and sequence restoration, albeit circumventing the

need for a strand annealing factor³⁹. In both cases, ligation of these structures will result in the formation of a four-way joint molecule (JM) on either side of the break that covalently links the two chromatids, resulting in a dHJ (Figure 2. 4 B)⁵⁸. These JMs are substrates to multiple enzymes that process them to generate distinct genetic outcomes. The human BTR complex consisting of BLM, topoisomerase III α (TopoIII α) and RecQ-mediated genome instability protein 1/2 (RMI1/2) mediates a ‘dissolution’ step; the helicase activity of BLM drives 3’-to-5’ DNA unwinding and, together with TopoIII α -RMI1/2, promotes the bidirectional branch migration of the dHJ to converge into a hemicatenane that is then dissociated by topoisomerase action⁵⁹⁻⁶¹. The dissolution of a dHJ leads to strictly non-CO products where no exchange of strands between the recombining molecules takes place and is considered a non-mutagenic pathway⁶¹. This is substantiated by the genomic instability of cells from Bloom syndrome (BS) patients, which harbor inactivating mutations in BLM and are characterized by substantially elevated levels of sister chromatid exchanges (SCEs)^{62,63}. The observed high levels of COs in BS cells are generated by the action of structure-selective endonucleases that function in distinct complexes to spearhead the ‘resolution’ pathway of dHJs: Mus81-EME1, SLX1-SLX4 and Gen1⁶⁴. Resolution of HJs by these endonucleases leads to both CO and non-CO products, depending on the site of incisions, at equal probability given random cleavage reactions. Mus81 is the active nuclease in the Mus81-EME1 complex, but requires EME1 for stability and activity⁶⁵. Interestingly, intact HJs are not the preferred substrate for the Mus81-EME1, where cutting efficiency was found to be very low, compared to other substrates, such as nicked HJs, 3’-flaps and replication forks^{64,65}. The requirement of Mus81-EME1 for HJ resolution despite lack of biochemical compatibility was clarified upon the discovery and characterization of the SLX1-SLX4 complex. SLX1 is the catalytic nuclease in the complex, with SLX4 acting as a scaffold for structural stability and activity⁶⁶. SLX1-SLX4 can act on a variety of substrates, including 3’ and 5’ flaps, branched DNA structures, replication forks, and stem loops. SLX4 also acts as a scaffold for other proteins, including Mus81-EME1, XPF-ERCC1 and MSH2-MSH3^{64,66,67}. Importantly, SLX1-SLX4 was shown to cooperate with Mus81-EME1 to resolve HJs in a nick-counter-nick mechanism, where SLX1-SLX4 introduces the initial, rate-limiting incision creating a nicked HJ that is a suitable substrate for Mus81-EME1, which introduces the second cut on the opposite strand^{64,67}. The SLX-MUS combined cleavage frequently yields asymmetrical products, resulting in gaps and flaps that require further processing. On the other hand, Gen1 cleaves HJs by introducing symmetrical incisions, and unlike the other nucleases,

does not have any known interaction partners^{64,68}. The action of these resolvases is temporally regulated as to limit promiscuous resolution of branched structures during replication, where

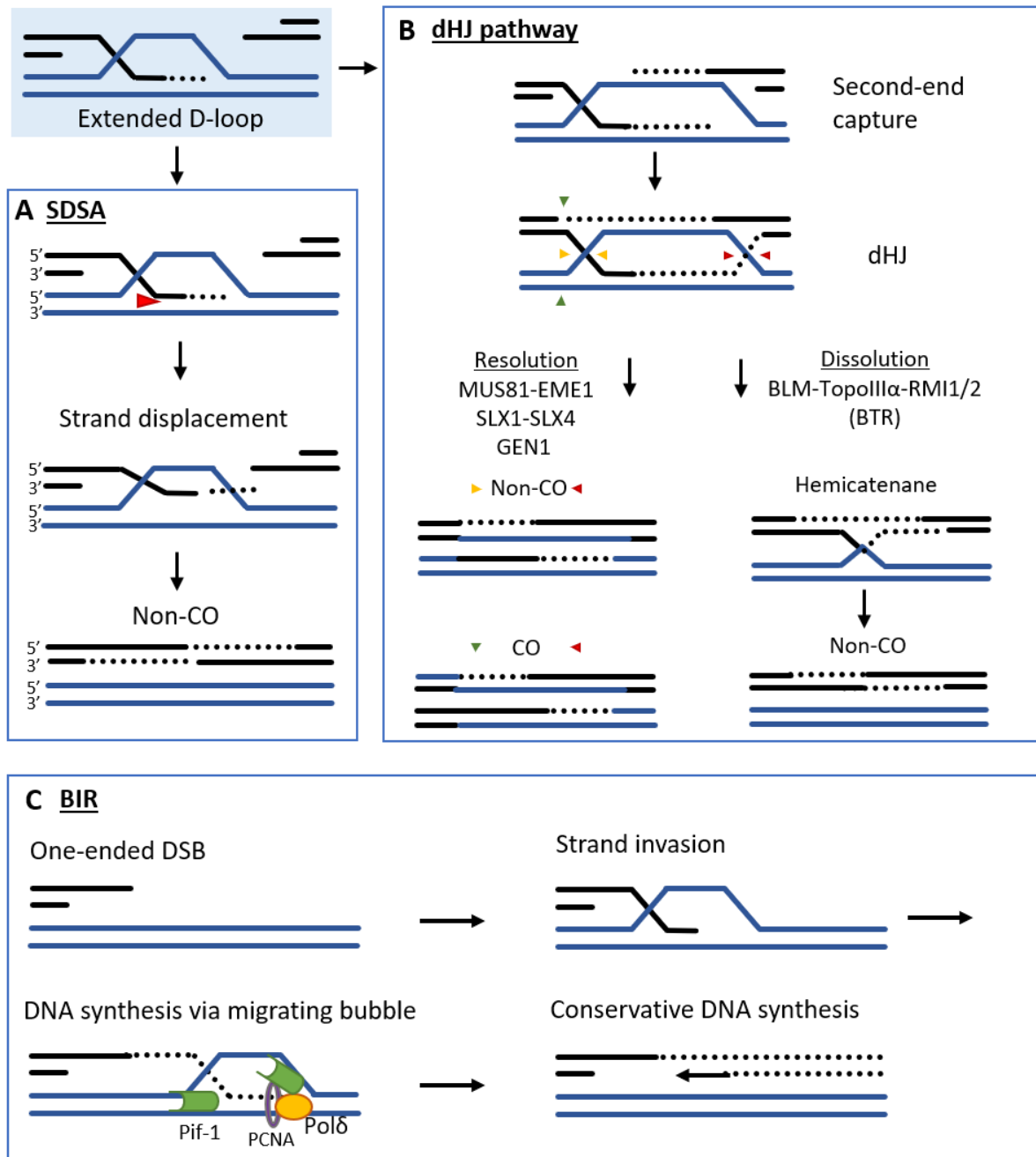


Figure 2.4. HR sub-pathways.

HR of two-ended DSBs can proceed by two main sub-pathways following D-loop extension. (A) SDSA: the invading strand is displaced and re-anneals to the other break end, resulting in non-CO recombination products. (B) dHJ pathway: the second DSB end “captures” the displaced strand of the D-loop, leading to the formation of two, four-way junctions that can be dissolved by the BTR complex to form non-CO products or resolved by structure-selective nucleases that have the potential for both CO and non-CO formation (colored arrows indicate location of incision corresponding to each outcome). (C) One-ended breaks can be repaired by BIR, where a migrating D-loop is promoted by Pif1 helicase and Pol δ leading and the newly synthesized strand is the template for the lagging strand, in a conservative DNA synthesis process.

their activation takes place at the G2/M transition⁶⁹. CDK-mediated phosphorylation of Mus81 triggers interaction with SLX1-SLX4, while PLK kinases phosphorylate EME1 and SLX4^{69,70}. Gen1 is active later in the cell cycle, as its subcellular localization is limited to the cytoplasm by S-phase specific CDK-mediated phosphorylation until nuclear envelope breakdown during anaphase allows access to the DNA. Consolidating the notion that SLX-MUS and Gen1 act in independent resolution pathways, depletion of SLX1/4 is epistatic to Mus81 depletion in rescuing the elevated SCE phenotype observed in BS cells, while Gen1 depletion has an additive rescue effect^{64,71}. Therefore, cells have evolved two distinct HJ resolution mechanisms, highlighting the importance of processing HR intermediates before the completion of mitosis. Although it has been generally accepted that these resolution pathways act largely as a back-up to BTR-mediated dissolution, accumulating evidence points to an independent role of the endonucleases; the absence of SLX-MUS or Gen1 leads to chromosome segregation defects and sensitivity to ICL-inducing agents, even in the presence of a functional BTR complex⁷².

2.1.4 *HR sub-pathways: Break-induced replication*

The above described pathways necessitate the presence of the two DSB ends, which ensure proper repair completion. However, cells often encounter situations where the break is asymmetrical, i.e. has only one end or one of the break ends fails to find and/or engage with a homologous sequence. Such one-ended breaks arise when the replication fork stalls due to a persisting lesion and then collapses, resulting in a DSB whose other end has not yet been generated (unless a converging fork reaches the break site). Under conditions of excessive DNA damage cells employ the specialized HR pathway BIR (Figure 2.4 C)⁷³. BIR was first described in yeast and has been observed also in human cells in two modes: a dominant Rad51-dependent process, and a less frequent Rad51-independent pathway that depends on Rad52, reflecting different means of pairing to the homologous sequences^{74,75}. BIR is initiated by 5'-to-3' resection of the broken DNA end, followed by long-range DNA synthesis that extends to hundreds of kilobase pairs, up to the end of the chromosome in yeast⁷⁶. A distinctive feature of BIR is a conservative mode of DNA replication, where the lagging strand synthesis is initiated after the completion of the leading strand, using it as a template (Figure 2.4 C)⁷⁶. This is facilitated by the Pif1 helicase, an essential BIR factor that promotes a migrating bubble mode of synthesis and is important for the recruitment of Pol δ to Rad51-mediated D-loops where the subunit Pol32 (and its human homolog POLD3) is required for efficient leading strand synthesis^{46,77}. BIR is normally suppressed in S-phase, likely due to its low fidelity and

propensity for mutations ⁷⁸. The asynchronous DNA synthesis of the leading and lagging strands involves the formation of very long patches of ssDNA that are sensitive to damage ⁷⁹. Additionally, the frequent dissociation of Pol32/POLD3 entails multiple rounds of reinvasion and synthesis restart, increasing the chance of misaligning to the template and template switching, especially in repetitive regions, thereby leading to genomic alterations such as duplications and copy number variations (CNVs) ⁸⁰. Much of the knowledge about BIR comes from studies in yeast, but similar observations in human cells demonstrated that BIR is required for replication fork restart under conditions of cyclin E overexpression-induced replication stress ⁸¹. Similarly, replication fork collapse at common fragile sites (CFSs) induces BIR-like long-range mitotic DNA synthesis, termed MiDAS that ensures replication completion before mitotic progression ⁸². Additionally, BIR was recently described to drive telomere elongation in tumor cells employing alternative lengthening of telomeres (ALT), and also exhibit a bimodal dependency on Rad51 similar to that observed in yeast ⁸³. Despite increasing interest, BIR is still poorly understood, especially in mammalian cells. However, it is clear that it is an important process affecting genomic integrity that shares common mechanisms with other DNA repair processes and better characterization of the factors involved will provide key insights into multiple fields of research.

2.1.5 *HR factors and replication*

HR is also critical for the faithful duplication of the genome, emerging as a safeguard for the replication process as evidenced by the gross genomic instability of HR mutants even in undamaged cells. The replication fork can face multiple obstacles, including modified or bulky bases, protein-DNA linkages, DNA secondary structures and DNA:RNA hybrids ⁸⁴. These lesions block the replication fork, causing fork uncoupling, stalling and/or collapse, thereby severely compromising the integrity of the genome. To ensure timely genome duplication, cells employ multiple processes to bypass the damage, collectively termed DNA damage tolerance (DDT), or to repair subsequent toxic intermediates ⁸⁵. In eukaryotes, when a fork stalls, it is often rescued by a converging fork progressing from a nearby origin of replication or, alternatively, the fork is restarted by the recombination machinery. In either case, fork protection is necessary to prevent degradation of the single-stranded regions by nucleases (such as MRE11, CtIP, EXO1), which requires BRCA2-mediated Rad51 filament formation in addition to factors from the Fanconi Anemia (FA) pathway, depending on the lesion involved ⁸⁶⁻⁸⁸. The uncoupling between the helicase and polymerase causes the accumulation of large regions of ssDNA gaps that need to be filled (Figure 2.5) ⁸⁹. While this can be carried out by error-

prone translesion synthesis (TLS), HR pathways are employed for a more faithful restoration of sequences⁸⁵. This involves a process of fork reversal, whereby the fork regresses backwards and the newly synthesized strands anneal to each other while the parental strands forming a

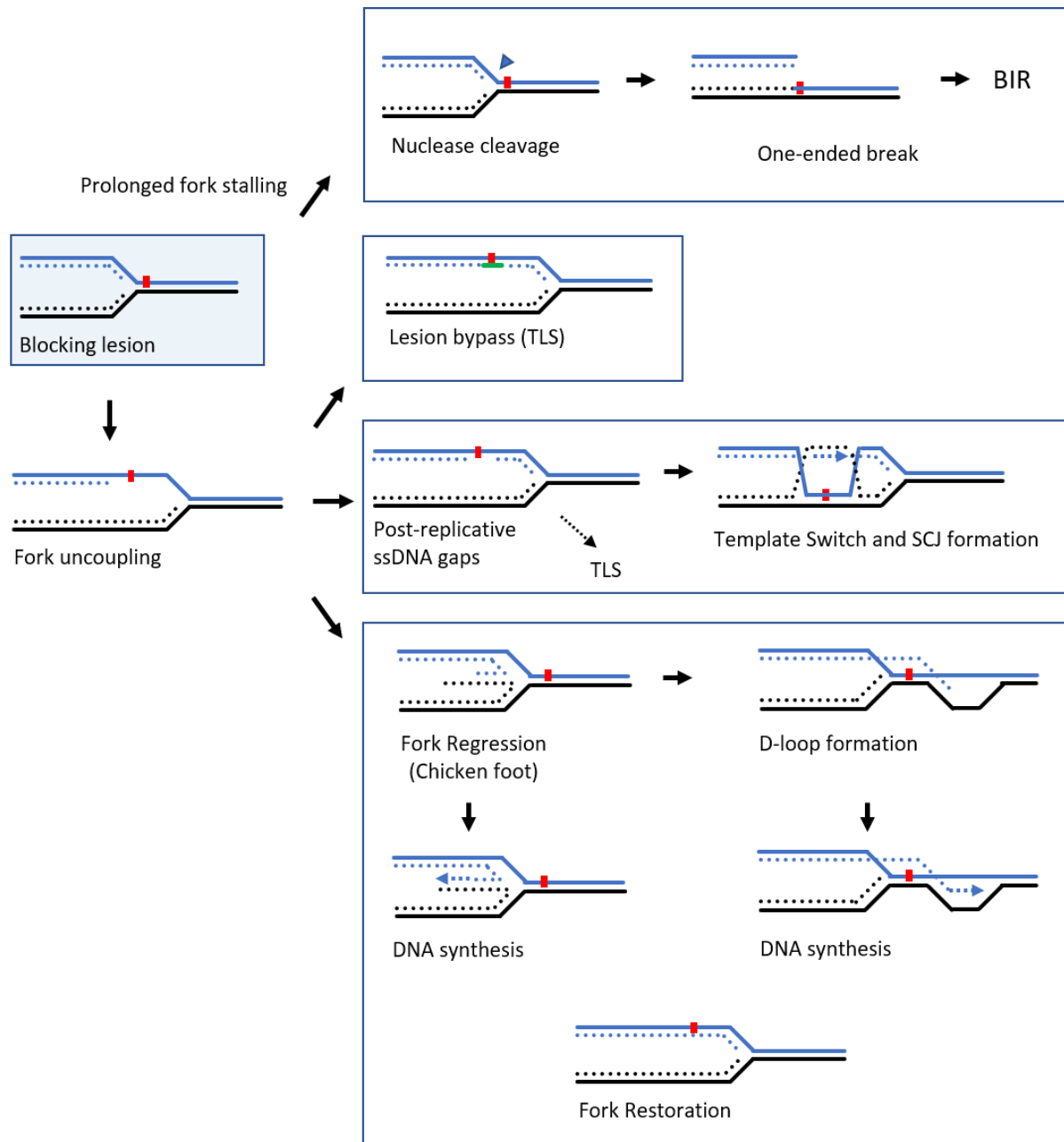


Figure 2.5. HR at replication-associated lesions.

Lesions blocking a replication fork can lead to fork uncoupling, generating large regions of ssDNA that can be filled by error-prone TLS polymerases. Alternatively, Rad51 mediates fork regression and template switch, leading to the formation of a four-way “chicken-foot” structure, or the invasion of intact regions ahead of the the lesion to form a D-loop. This is followed by DNA synthesis and fork recovery. Replication can also be restarted through DNA re-priming past the lesion, leading to post-replicative ssDNA gaps that can initiate a Rad51-mediated template switch, resulting in SCJ which can be dissociated by helicases, including BLM, part of the BTR complex. TLS polymerases can also fill these ssDNA gaps. Persisting fork stalling leads to nuclease-mediated cleavage generating a one-ended DSB that can then be repaired by HR repair mechanisms.

four-way junction called the chicken foot structure that is bound and stabilized by Rad51 following regulated resection (Figure 2.5)^{90,91}. This template switch can be followed by DNA synthesis to allow lesion bypass, or Rad51-mediated strand invasion of the parental strands ahead of the fork and fork restoration. Additionally, post-replicative ssDNA gaps can be generated by DNA re-priming and re-initiation of DNA synthesis behind the lesion (Figure 2.5). Rad51 loading to ssDNA at the gaps allows template switch to the newly synthesized strand, which, if not displaced by helicases, can lead to a sister chromatid junction (SCJ) that is then dissolved by the BTR complex⁹². Furthermore, extensive fork stalling could lead to fork collapse or cleavage by structure-specific nucleases, such as Mus81, to generate one-ended DSBs that can initiate BIR (Figure 2.5). Therefore, there are multiple mechanisms in place for handling replication stress, which require canonical HR factors, but also other cofactors that are not needed for DSB repair, highlighting fundamental differences between the two processes. How these factors are spatially and temporally regulated to sustain appropriate responses to DNA damage and replication stress is still under investigation to further the understanding of cell-cycle regulation of DNA damage responses and mechanisms.

2.2 CHROMATIN STRUCTURE AND DYNAMICS

While the elucidation of DNA repair protein networks and mechanisms is critical for understanding the DNA damage response (DDR), it is important to consider this knowledge in the context of genomic architecture. In eukaryotes, genomic DNA is tightly packed into a highly organized multidimensional complex structure known as chromatin. The simplest building block of chromatin is the nucleosome, the ‘bead’ in the known ‘bead-on-a-string’ representation first describing these structures as repeating units. The canonical nucleosome consists of 145-147 bp of DNA wrapped around an octameric core of two copies of each of four histone proteins: H2A, H2B, H3 and H4, organized as a heterotetramer of H3-H4 and two H2A-H2B dimers. Linker DNA and the linker histone H1 (existing as one copy), complete the nucleosome unit (Figure 2.6)^{93,94}. The nucleosome core is stabilized by hydrophobic interactions between conserved regions in the core histones, while histone-DNA interactions occur through exposed positive residues⁹³. Lysine-rich histone tails protrude from the histone core and mediate inter-nucleosomal interactions, as well as binding with an array of non-histone proteins, allowing the formation of high-order structures, such as the 10-nm and 30-nm nucleosomal fibers, and regulating their sub-nuclear organization.

Despite the stability of the nucleosomal core, it is far from a static structure, as access to the bound DNA sequences is required for various cellular processes and is an intricately regulated

process. Therefore, the nucleosome is highly dynamic, undergoing constant modifications in various modes. One of the most studied types of histone alterations is post-translational modifications (PTMs) to the free histone tails, which regulate histone-histone and nucleosomal interactions as well as protein binding. These modifications include, but are not limited to, phosphorylation, methylation, acetylation, ubiquitination and SUMOylation and regulate essential cellular processes, such as transcription, replication, DNA repair, in response to intrinsic and extrinsic effectors⁹⁵. Furthermore, a large array of chromatin remodelers is in place to modulate chromatin architecture through an ATP-dependent activity resulting in sliding or spacing of nucleosomes, histones eviction and histone exchange. Chromatin remodelers often function in large complexes with histone chaperons, helicases, histone-readers and other accessory proteins and carry out specialized functions in various cellular processes⁹⁶.

2.2.1 *Histone variants*

The nucleosome core can be additionally modified through the incorporation of so-called histone variants, which have diverged from the canonical histones and carry out specific functions in cellular physiology. In higher eukaryotes, there are multiple histone variants of the core histones H3 H2A, H2B and H1 which have been curated and classified by multiple efforts (Figure 2.6)^{94,97}. As a general paradigm, canonical histones are required during DNA replication as the genome doubles in size, and therefore are transcribed mainly in S-phase and are incorporated in a DNA synthesis-dependent manner. On the other hand, histone variants are available throughout the cell cycle and are incorporated independently of DNA synthesis, but rather are linked to specific processes (such as transcription) and/or genomic loci (such as telomeres and centromeres) (Figure 2.6)^{98,99}. The incorporation of histone variants introduces physical and biochemical changes to the nucleosome, affecting PTMs and protein-DNA interactions and thereby can cause profound alterations to the overall chromatin architecture. For example, the centromeric H3 histone variant, known as CENPA in vertebrates, is enriched at deposited at centromeric regions by the Holliday junction recognition protein (HJURP) in G1 phase and is important for kinetochore formation¹⁰⁰. Lack of CENPA leads to chromosome misalignment, missegregation, aneuploidy and micronuclei, demonstrating the importance of this histone variant in maintaining proper centromeric structure and function^{100,101}.

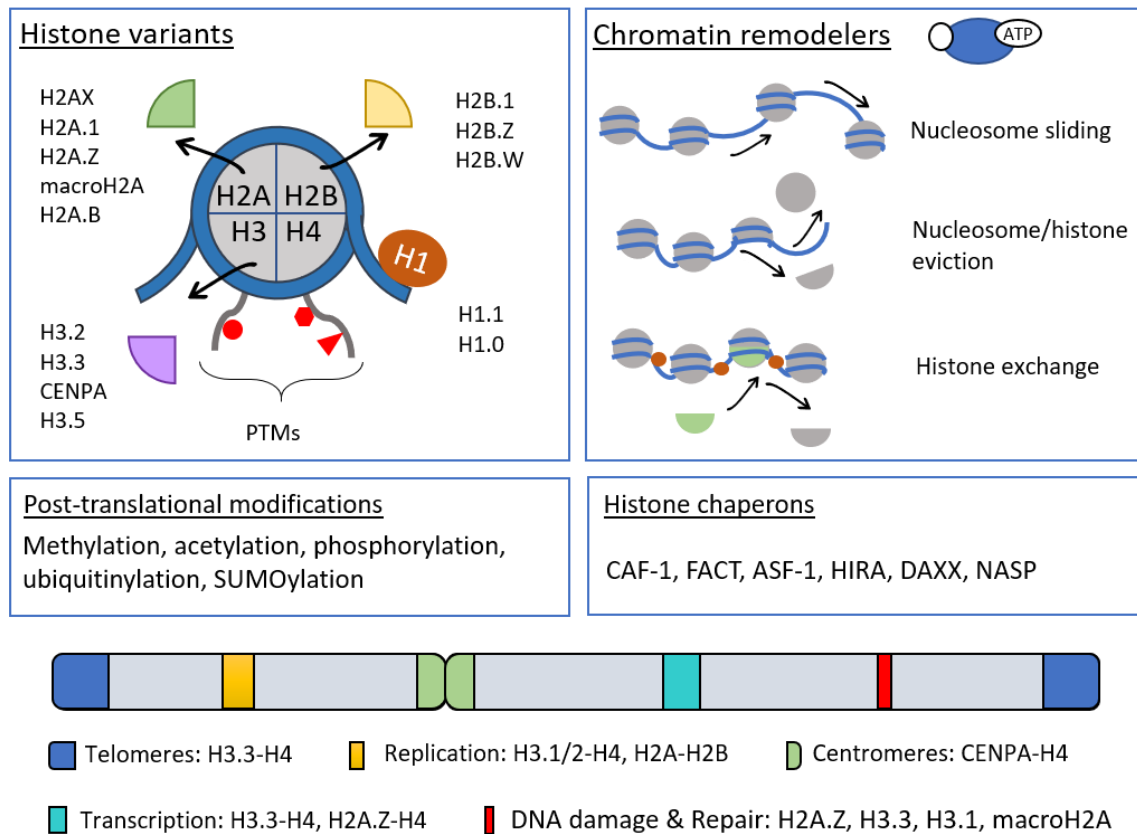


Figure 2.6. Structure and dynamics of chromatin.

The basic unit of chromatin is the nucleosome, made up of 147 bp of DNA wrapped twice around two copies of each of four histone core proteins, H2A, H2B, H3 and H4, with one copy of linker H1. Variants of most histones have been identified (examples shown), and often localize to specific genomic loci and serve various functions. Histones can undergo a variety of post translational modifications on their protruding N-terminal “tails”. The nucleosome can be modified by ATP-dependent chromatin remodelers that can slide nucleosomes and/or evict or exchange histones, often aided by histone-specific chaperons.

2.2.2 Chromatin dynamics and the DDR

In response to DNA damage, the chromatin undergoes various changes. Challenging a rigid ‘access-repair-restore’ model in which chromatin is little more than a physical hindrance that needs deconstruction, more studies are evidencing a more active role of chromatin reorganization in the repair process¹⁰². Indeed, genome-wide mapping of histone modifications linked chromatin signatures to specific repair pathways at DSBs¹⁰³. General chromatin responses to DNA damage include transient states of condensation and relaxation where condensation possibly serves to stabilize breaks and prevent further damage to break ends and to scaffold repair proteins (Figure 2.7)¹⁰⁴. Chromatin relaxation is necessary to allow access for repair machinery, especially when extensive end processing is required. This is not strictly chronological, where evidence points to the concomitant existence of repressive and relaxing

factors at varying spatial resolutions, where the immediate vicinity of the break is accessible while the surrounding chromatin is more compact ¹⁰⁵. Additionally, the large-scale chromatin state contributes to DSB-induced DNA mobility, which influences DSB clustering and sub-nuclear localization, repair foci formation and homology search ¹⁰⁶. Therefore, nucleosome remodeling and histone exchange are progressively shown to be central to the regulation of these processes, with more cross-talk between the different remodelers and histone variants likely taking place.

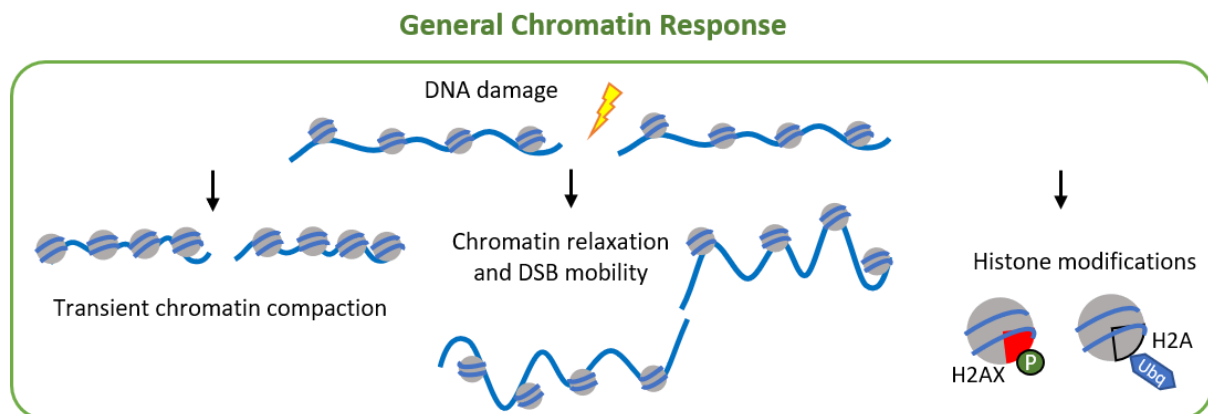


Figure 2.7. General chromatin responses to DNA damage.

Following DSB induction, chromatin undergoes transient structural changes, including compaction, relaxation to allow DSB mobility and sub-nuclear re-localization, and histone PTMs, including but not limited to H2AX phosphorylation and H2A ubiquitination

One of the most pronounced DNA damage signals is the phosphorylation of the histone variant H2AX on the C-terminal serine 139 (in mammals) to form γ H2AX, a signature mark of DSBs. Upon the induction of a DSB, H2AX is phosphorylated by ataxia telangiectasia mutated (ATM), allowing binding of the DNA damage checkpoint protein 1 (MDC1) protein ^{107,108}. This provides docking sites for multiple proteins and allows for further ATM-mediated phosphorylation and spreading of the γ H2AX signal for up to two Mb flanking the DSB, forming microscopically visible foci ¹⁰⁹. Additionally MDC1 recruits effector ubiquitin ligases RNF8 and RNF168 to ubiquitinate H2A and H2AX, as well as other chromatin components, further recruiting DNA repair proteins, such as 53BP1 and BRCA1 that modulate pathway choice ^{110,111}. While H2AX represents about 10-25% of H2A variants in the genome, its distribution is neither random nor static. H2AX was found to be non-randomly distributed in the genome, but rather enriched in regions prone to replication-associated stress including active transcription sites, sub-telomeric regions, and early-replicating common fragile sites, a distribution specific to dividing cells versus resting cells ^{112,113}. These studies point to a damage-induced enrichment of H2AX that could act as a marker for damaged regions.

Consistent with this notion, *de novo* H2AX deposition via the chromatin remodeler FACT was observed after UVC damage and is coupled to DNA synthesis and the removal of H2A.Z¹¹⁴. This new deposition of H2AX further modulates the DNA damage response and also changes the chromatin landscape post-repair, reflecting the far-reaching effects of chromatin responses during the DDR.

2.2.3 *Variants on the move following DNA damage*

In addition to histone PTMs, an increasing number of studies are showing a strong link between histone variant deposition and DSB repair protein recruitment, pathway choice, and post repair remodeling (Figure 2.8). The remodeler SMARCA5 has been shown to cooperate with the remodeling and spacing factor 1 (RSF-1) to deposit the centromeric histone variants CENP-S and CENP-X in at sites of DSBs. These variants, in turn, direct the mono-ubiquitination of FANCD2 and FANCI to recruit DSBs proteins for both HR and c-NHEJ repair pathways¹¹⁵. Interestingly, RSF-1-mediated deposition of CENP-S and CENP-X at DSBs, independently of SMARCA5, was also shown to promote c-NHEJ by facilitating the recruitment of XRCC4¹¹⁶. The mechanism through which these variants affect the repair pathway choice or factor recruitment is not fully determined, but mounting evidence suggest their importance for regulating such processes. Similarly, the histone variant H3.3 has also been proposed to be involved in DSB repair, where poly (ADP-ribose) polymerase 1 (PARP1) promotes the rapid recruitment of the chromatin remodeler CHD2 to allow chromatin expansion and H3.3 deposition at sites of DSBs¹¹⁷. This was shown to be important for the recruitment of the c-NHEJ factors Ku80 and XRCC4 and subsequent efficient repair. Additionally, c-NHEJ-mediated repair of enzyme-induced DSBs is followed by chromatin assembly factor 1 (CAF-1) and histone regulator A (HIRA)-mediated deposition of the histones H3.1 and H3.3, respectively¹¹⁸. However, this remodeling step is independent of repair and constitutes a post-repair nucleosome reassembly step, likely to reestablish epigenetic marks and maintain chromatin integrity. Interestingly, H3.3 has been also linked to HR, where HAT-1 mediated acetylation of H4K5/K12 in concert with HIRA-mediated H3.3 deposition promotes Rad51 loading and subsequent HR-mediated repair¹¹⁹.

2.2.4 *Repair pathway choice and regulation of HR*

In addition to recruitment of repair factors, histone variants affect chromatin states and function at the interface of multiple pathways, often influencing pathway usage. A prominent example is the histone variant H2A.Z, which has been implicated in initial steps of DSB detection and pathway choice (Figure 2.8). H2A.Z is rapidly deposited at the sites of DSBs minutes after

damage induction by the p400 ATPase subunit of NuA4 where H2A.Z deposition restricts CtIP-mediated resection and therefore acts as an antagonist to HR in favor of c-NHEJ¹²⁰. However, H2A.Z is then rapidly removed redundantly by INO80 and Anpe32 and exchanged with canonical H2A, an exchange that has multiple effects on DSB repair^{121,122}. This regulated exchange of H2A.Z was shown to also promote HR by promoting both end resection and also

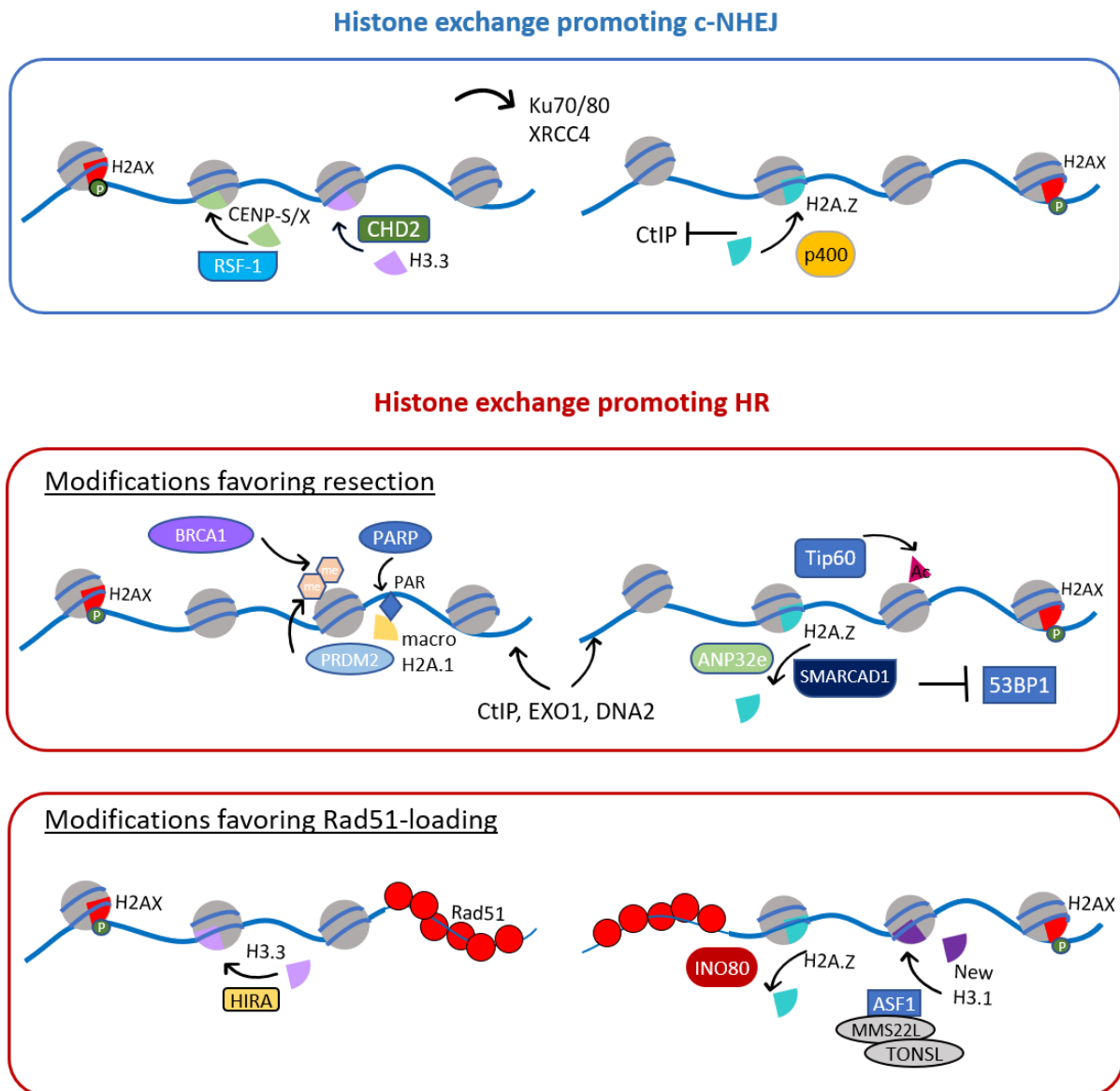



Figure 2.8. Histone exchange and DSB pathway choice.

Histone variant deposition at DSBs promotes either c-NHEJ or HR by influencing resection and/or recruiting repair factors. Deposition of H3.3 and CENP-S/X recruits XRCC4 and Ku70-80, while H2A.Z prevents CtIP-mediated resection, collectively promoting c-NHEJ. H2A.Z removal and macroH2A.1 recruitment promote resection through recruitment of BRCA1, CtIP, EXO1 and DNA2, while inhibiting 53BP1. New H3.1 and H3.3 deposition, H2A.Z removal by INO80 promote Ra51 loading. Variants can have multiple roles, depending on the remodeler associated with their deposition. removal induces Tip60-mediated H4 acetylation thereby forming open and flexible chromatin.



the downstream replacement of RPA by Rad51 for the formation of the presynaptic filament required for homology search and HR progression in yeast and human cells ^{122,123}. Other chromatin remodelers, such as the yeast Fun30 and its human homolog SMARCAD1, are also required for long-range resection through EXO1 and DNA2, likely involving H2A.Z histone exchange as well ^{124,125}.

Another H2A variant, macroH2A1, has also been linked to DSB repair and the regulation of resection. MacroH2A.1 is recruited to sites of DSBs through a PARP-dependent mechanism, where, interestingly, the variant is not incorporated into nucleosome, but rather interacts directly with PARylated DNA ¹²⁶. MacroH2A1 enrichment promotes the recruitment of the methyltransferase PRDM2 which drives the dimethylation of H3K9 and the formation of condensed chromatin. Together these events recruit BRCA1 to breaks, thereby promoting resection and subsequent HR ¹²⁷. Interestingly, macroH2A.1 deposition at telomeric breaks has been suggested to promote HR-mediated repair to promote alternative lengthening of telomeres in cells lacking alpha-thalassemia mental retardation X-linked protein (ATRX), highlighting the versatility of histone variants at different genomic loci ¹²⁸.

2.3 AIM OF THE STUDY

Collectively, the studies discussed above provide ample evidence for the regulation of DSB pathway choice, as well as early HR events through the timely exchange of histone variants to provide distinct chromatin landscapes and scaffolds for repair proteins. However, less is known about the regulation of later stages of HR repair by chromatin remodelers or histone variants. While it is expected that chromatin remodeling is required for processes such as homology search and DNA repair synthesis where large regions of DNA need to be exposed, little information is available about potential factors involved in these stages. Some studies have implicated Rad54 as a chromatin remodeler required for synaptic complex formation, but further investigation showed that neither does Rad54 require its ATPase activity for this role nor is it required for strand invasion using nucleosome-bound substrates^{42,129,130}. The work presented here aims to investigate late stages of HR and to understand the regulation of HR sub-pathway choice and repair outcome. The first part of this work examines the role of the histone variant H3.3 during HR-mediated repair of DSBs, motivated by data implicating the chromatin remodeler ATRX, associated with H3.3 deposition, in this process. This is addressed by measuring the effect of H3.3 knockdown on DSB repair and cell survival in cellular assays as well as tracking the *in vivo* deposition of H3.3 following DNA damage and investigating the factors involved in this process. Furthermore, the contribution of this ATRX-promoted pathway to overall HR events is assessed in the second part of this thesis with a quantitative comparison with RECQ5-mediated SDSA and an analysis of the mechanism leading to the generation of CO recombination products and governing their frequency. The study aims to provide a better understanding of the mechanisms regulating late stages of HR in G2 cells, the factors involved in distinct HR-sub-pathways, and the possible contribution of chromatin remodeling in influencing repair sub-pathway choice and outcome.



3. THE HISTONE VARIANT H3.3 IS REQUIRED DURING HOMOLOGOUS RECOMBINATION

3.1 INTRODUCTION

The repair of DSBs requires extensive chromatin reorganization and modification, not only to allow access to the damaged DNA, but also as an active regulator of subsequent repair^{104,131,132}. An emerging key facet of chromatin remodeling during the DNA damage response is the exchange of canonical histones for variants that are specific for various physiological functions. The H3 histone variant H3.3 is one of the main variants whose role in DNA repair is becoming increasingly prominent. H3.3 differs from H3.1 by 5 amino acids, where the 87, 89 and 90 amino acid positions seem to dictate the genome-wide distribution of the histone variants potentially by interacting with distinct assembly machinery¹³³. These three residues may vary between species, but always distinguish H3.3 from H3, suggesting a critical role for these residues⁹³. The canonical histone H3.1 is expressed mainly in S-phase and is deposited in a replication-associated manner by CAF-1^{134,135}. Conversely, H3.3 is constitutively expressed throughout the cell cycle and has a DNA synthesis- independent incorporation dynamics through multiple interaction partners^{135,136}. H3.3 has a bimodal incorporation pattern that is mediated by two distinct chaperon complexes. The chaperon HIRA directs H3.3 deposition in promoters of actively transcribed genes and gene bodies and is associated with active chromatin marks, such as H3K4me3^{133,137,138}. In contrast, H3.3 is also associated with silent chromatin, where the chromatin remodeler ATRX together with the H3.3-specific chaperon death domain associated protein (DAXX) mediate its deposition in telomeric and pericentric regions^{133,139}. ATRX-DAXX also direct H3.3 deposition to other repeat-rich regions in the genome, which serves to maintain a repressive heterochromatin state and structural stability¹⁴⁰. In the context of DNA damage, H3.3 was shown to be rapidly deposited at sites of UVC-induced damage to facilitate recovery of transcription post repair, but is not involved in the repair process¹⁴¹. Similarly, H3.3 was observed to have a role in replication fork recovery following UV damage in chicken DT40 cells¹⁴². Furthermore, H3.3 is exchanged into chromatin shortly after DSB induction to promote c-NHEJ and is also involved in post-repair chromatin assembly^{118,143}. Interestingly, H3.3 is mutated in a variety of cancers, including pediatric high grade glioblastoma, diffuse intrinsic pontine glioma, chondroblastoma and giant cell tumors of the bone¹⁴⁴. While the majority of the mutations reported occur in the N-terminal tail of the

histone, there is considerable overlap between their occurrence and mutations in ATRX or DAXX¹⁴⁵. Loss of the ATRX-DAXX-H3.3 pathway has also been strongly associated with a subset of tumors that employ a process known as the alternative lengthening of telomeres (ALT) instead of telomerase reactivation to maintain telomere length¹⁴⁶. ALT cells and cell lines are characterized by loss-of-function mutations in ATRX, and to lesser extents, DAXX and H3.3 and have been linked to DSB repair defects and chromosomal rearrangements, suggesting a role for this complex to suppress the ALT pathway, possibly through DNA repair functions^{147,148}. Additionally, ATRX and DAXX have also been shown to have a role during replication, where they function to protect forks from MRE11-mediated degradation and to maintain fork processivity¹⁴⁹. Therefore, ATRX-DAXX-dependent H3.3 deposition seems to be important for genomic integrity, possibly through multiple mechanisms that have not been fully elucidated yet.

The study presented here uncovers a role for the histone H3.3 during HR-mediated repair of exogenously induced DSBs in G2 cells. H3.3 deposition occurs following Rad51-dependent homology search and promotes extended DNA repair synthesis and the formation of sister chromatid exchanges. Additionally, H3.3 incorporation is dependent on DNA synthesis factors, supporting a model in which DNA synthesis is coupled to H3.3 incorporation in an inter-dependent process that is required for repair completion. The tight coupling of histone deposition to repair synthesis is novel for this histone variant and could reflect a requirement for high histone turnover, possibly to alleviate topological stress, but could also suggest a special need for this specific histone variant, with potential implications for post translational modification or additional interaction partners to be involved in this highly regulated process.

3.2 METHODS

3.2.1 Cell culture

Cell lines

HeLa-S3 and HeLa ATRX KO¹⁵⁰ cells were cultured in DMEM supplemented with 10% FBS and 1% NEAA. HeLa-pGC reporter cells were a gift from Jochen Dahm-Daphi¹⁵¹ and were cultured in DMEM with 0.6 µg/ml puromycin. HeLa-SNAP-H3.3 cells were a gift from Geneviève Almouzni¹⁵² and cultured in DMEM with 1 µg/ml blasticidin S. Only sterile media, buffers, reagents and consumables were used and cells were routinely tested for mycoplasma contamination by PCR. All cell lines were maintained at 37°C in a 5% CO₂ incubator.

Cell line maintenance and passaging

Fresh cells were routinely thawed from liquid nitrogen stocks to obtain cells with low passage number. For thawing, cryovials were incubated in a 37°C water bath for approximately 1 min and then the cell suspension was diluted in 10 ml of fresh medium. Cells were centrifuged for 5 min at 4°C at 200 x g. The supernatant was removed and the cell pellet was resuspended in 5 ml of fresh medium and seeded in a small culture vessel (25 cm² flask or 60 mm dish) then transferred 24 h later to a 100 mm dish. For cell passaging, cells at 80-90% confluency were washed with 5 ml sterile PBS then incubated with 1 ml pre-warmed trypsin/EDTA for 2-5 min at 37°C. Cell detachment was confirmed by the observation of round cells under an inverted microscope. Trypsin was quenched with 5-8 ml medium and cells were seeded at a ratio of 1:5-1:10 (see section 6.9).

Cell seeding

Depending on the experimental need, cells were seeded on sterile cover slips in 35 mm and 60 mm dishes, or directly on plastic in 100 mm dishes, 6-well plates or ibidi slides. Cell number was determined using a Neubauer counting chamber and distinct cell numbers were seeded for different culture vessels (Table 1). Unless otherwise specified, transfection of siRNA or DNA was carried out 24 h after cell seeding.

Table 1. Cell seeding densities

Culture vessel	35 mm or 6-well plate	60 mm	100 mm	μ slide (ibidi IV)
Cell number	2-3 x 10 ⁵	4-6 x 10 ⁵	1-3 x 10 ⁶	3 x 10 ⁴ / channel
Volume	2 ml	4 ml	10 ml	60 μl/ channel

3.2.2 siRNA and plasmid Transfection

Transfection of cells with specific siRNAs (sequences listed in section 6.4.1) was carried out using HiPerFect or RNAi Max transfection. For H3.3 depletion, siRNAs against H3.3A and H3.3B were used together in a 1:1 ratio, as previously described¹⁴¹. Experiments were either performed 48 h after transfection or after 72 h with an additional siRNA transfection after 24 h. For HiPerfect, siRNA was mixed with 100 μl serum-free Opti-MEM medium, then 12 μl of HiPerfect were added, vortexed for 10 s and incubated for 10 min at RT. For RNAi Max, siRNA was diluted in 150 μl Opti-MEM and 5 μl of RNAi Max were diluted in 150 μl Opti-MEM in a separate tube. After brief vortexing, both tubes were mixed together by pipetting and the mixture was incubated for 10 min at room temperature (RT). Transfection complexes were gently dropped onto 60-80% confluent cells in 35 mm dishes with slow rotation. Cells were

collected on the day of the experiment to confirm knockdown efficiencies by immunoblotting. Plasmid transfections were carried out 48 h before experiments using Lipofectamine LTX and Effectene according to the manufacturer's instructions. Approximately 1-3 μ l (20- 60 nM) of siRNA and 2.5 μ g DNA were used for 35mm dishes and transfection volumes were doubled for 60 mm dishes.

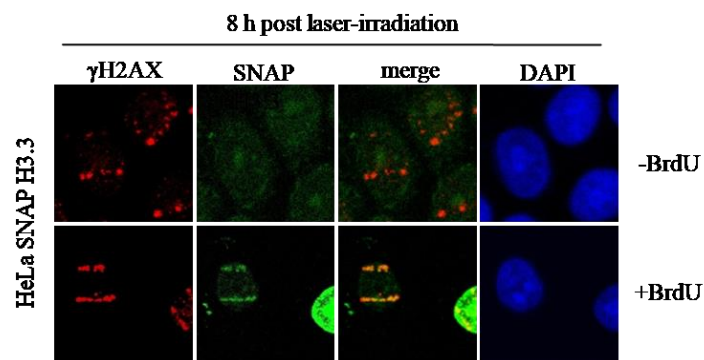
3.2.3 DNA damage induction

X-ray irradiation

Damage by X-rays was performed at 90 kV and 19 mA for all experiments, with a 1 mm aluminum plate serving as a sample holder and a low-energy X-ray filter. The machine used harbors a Philips X-ray tube equipped with a tungsten anode and a thin beryllium window. Irradiation was carried out with consideration of the dose-doubling effect for cells on cover slips¹⁵³, thereby adjusted irradiation durations were used accordingly.

Laser micro-irradiation

For laser micro-irradiation, cells were seeded in a 6-well plate for siRNA transfection as described. After 24 h, the cells were transferred to a μ -slide VI and pre-sensitized with 50 μ M of the thymidine analog 5-bromo-2'-deoxyuridine (BrdU) for 24 h, to enrich for DSBs versus other lesions occurring from the UV laser^{154,155}. Cells irradiated without pre-incubation BrdU showed a lower γ H2AX signal in laser tracks, as well as no SNAP signal (see below). The μ -slide VI was placed in an incubation chamber of an Axio Observer D microscope. A continuous wave diode laser was used for UV-A micro-irradiation (375 nm) coupled to the epifluorescence path of the microscope and focused through a Ph3 63x objective. The laser output was set to 90% (18 mW) and controlled by Omicron PhoxX Controller v.1.2.6 software. The stage speed (0.101 mm per second) was controlled by μ Manager software. For each sample, at least 2 different areas of the slide were irradiated in tandem.



Laser microirradiation using BrdU pre-sensitization

3.2.4 *Cell cycle-specific DSB repair analysis*

To analyze DSB repair in a cell cycle-specific manner, 10 μM of the thymidine analog 5-ethynyl-2'-deoxyuridine (EdU) was added to the cells 30 min prior to irradiation (X-ray and laser microirradiation) and kept throughout the experiment. Cycling cells incorporate EdU in the newly synthesized DNA, therefore cells in S phase during or after irradiation are labeled. After fixation, EdU was stained with a simple chemical reaction and DAPI and EdU intensities were measured and plotted in a diagram using a Zeiss microscope and MetaCyte software. EdU-positive cells were identified as S phase cells, while the EdU-negative cells were categorized as either G1 or G2 based on their DNA content (Figure 3.3.1 A). The EdU-negative G2 population represents cells that have been both irradiated and analyzed in G2, therefore providing a cell cycle phase-specific analysis.

3.2.5 *Immunofluorescence*

Fixation and Staining

Cells grown on glass cover slips or in μ -slide VI were fixed with 3% formaldehyde (FA) in PBS for 10 min at RT. Cells were then washed 3 times with PBS and permeabilized with 0.2% Triton X-100 in PBS for 10 min at RT. Subsequently, cells were washed and blocked for 30-60 min at 4°C with 1x Roti-Block. Incubation with primary antibodies (section 6.6) was carried out over night at 4°C. Cells were then washed 3 times for 5 min with washing buffer and incubated with fluorescently-tagged secondary antibodies (section 6.6) for 1 h at RT then washed 3 times for 5 min. All antibodies were diluted in blocking solution. For cell cycle-specific analysis, EdU was stained using the EdU Click-iT kit, according to the manufacturer's instructions. Cells were washed in PBS and stained with DAPI (0.4 $\mu\text{g}/\text{ml}$) for 10 min at RT then embedded with Vectashield mounting medium. Cover slips mounted on slides were sealed with clear nail varnish.

Microscopic Analysis

Immunofluorescence experiments were analyzed through a semi-automated approach, using a Zeiss microscope and MetaCyte software. For regular foci experiments, cells were scanned for DAPI and EdU intensities for cell-cycle specific analysis. For cells transected with GFP constructs, cells were additionally scanned for GFP and GFP-positive populations were selected for analysis. For each experiment, at least 40 nuclei were analyzed and the foci were enumerated manually¹⁵⁶.

3.2.6 *SNAP-H3.3 detection*

SNAP Labeling

For visualization of newly synthesized histones, pre-existing SNAP-H3.3 histones were quenched with 10 μ M SNAP-block for 30 min, washed twice with fresh medium then incubated for 30 min to allow excess block to diffuse out of the cell. Then, a 1.5 h chase was allowed for the synthesis of new histones. For the pulse step, cells were stained with 5 μ M Oregon Green for 20 min, washed twice with fresh medium then incubated for 30 min to allow excess dye to diffuse out of the cell to reduce background. Immediately after the pulse, cells were pre-extracted with 0.25% Triton-X 100 in CSK buffer for 5 min to wash out soluble histones, and then fixed with 3% FA for 10 min at RT. In all experiments, EdU was added before irradiation and kept on the cells until fixation. To verify the efficiency of SNAP labeling, a pulse step was performed and the cells were fixed directly afterwards to visualize all SNAP-H3.3 histones (Figure 3.4). The efficiency of blocking was verified by a quench-pulse step in which a quench step was followed directly by a pulse then fixed (Figure 3.4).

SNAP signal measurement

To quantify the enrichment of newly synthesized histones in laser tracks, images were acquired with 63x immersion objective and Image J software was used for analysis. The track area was selected and the mean gray value was measured. The mean gray value was also measured for an unirradiated area within the same cell as well as an area with no cells representing the background signal. For calculations, the background intensity was subtracted, and the track intensity was divided by the intensity of the unirradiated area to obtain the enrichment ratio. At least 100 cells were analyzed from 3 independent experiments.

3.2.7 *Reporter assay*

HeLa pGC cells containing a stably-integrated HR substrate were seeded and transfected with siRNA. 24 h later, cells were transfected with I-SceI plasmid to induce targeted DNA damage, and fixed after 48 h to allow for repair and GFP expression. Cells were stained against GFP and with DAPI and signal intensities were measured as described. At least 10,000 cells were analyzed using a Zeiss microscope and MetaCyte software. GFP-positive cells representing HR events were enumerated and normalized to the total cell number.

3.2.8 *BrdU incorporation assay*

Cells were seeded and transfected with siRNA. After 48 h, cells were labeled with 10 μ M EdU for 1 h and then X-irradiated with 4 Gy. Cells were then washed with PBS and incubated with

50 μ M BrdU. G2 cells incorporate BrdU at discrete DNA repair synthesis sites that are dependent on HR factors, as previously shown¹⁵⁶. At different repair times, cells were fixed with FA then treated with 2.5 N HCl for 30 min at RT to denature the DNA and allows access of antibodies to the incorporated BrdU. Cells were then washed thoroughly 10 times with PBS and the staining was performed as described using a specific BrdU antibody.

3.2.9 *Clonogenic survival assay*

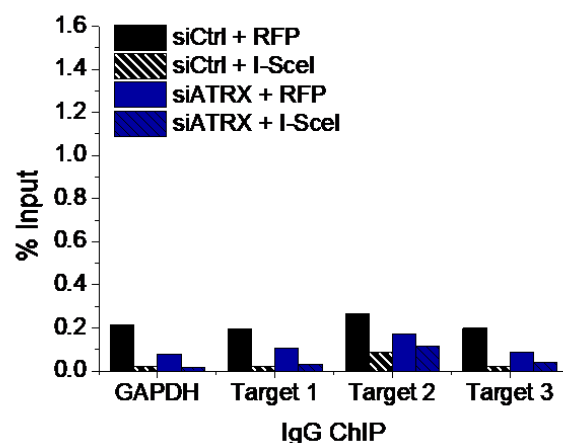
HeLa and ATRX KO cells were transfected with siRNA 48 h prior to DNA damage and seeded in defined numbers in 10 mm dishes 24 h after transfection. DNA damage was induced 24 h later by MMS (0, 0.5, 1, 1.5 mM) or MMC (0, 1.5, 3, 4.5 μ M) treatment for 1 h. Cells were then washed with PBS and incubated for 14 days to obtain single colonies. Fresh medium was added twice a week to maintain growth. Colonies were fixed with ice-cold methanol:acetic acid (3:1) for 20 min at 4°C and stained with 0.1 % crystal violet for 5 min at RT. Cells were washed with distilled water and colonies were scored for each condition and numbers were normalized to the untreated controls.

3.2.10 *Sister chromatid exchanges analysis*

Cells were transfected with siRNAs and incubated with 50 μ M BrdU for 48 h, to allow the incorporation of BrdU for approximately 2 rounds of replication, during which cells will acquire more BrdU in one of the newly synthesized sister chromatids. Cells were washed then treated with EdU 30 min prior to X-irradiation (X-IR) with 2 Gy. To override the G2 checkpoint and arrest the cells in mitosis, 20 μ g/ml caffeine and 10 μ g/ml colcemid were added to the cells 3 h before fixation. Caffeine is a non-specific kinase inhibitor that inhibits checkpoint kinases, while colcemid arrests cell in metaphase by inhibiting spindle formation. For preparation of chromosome spreads, cells were collected by trypsinization and centrifuged at 200 xg for 5 min. Cells were then resuspended in pre-warmed 75 mM KCl for 30 min at 37°C cells then centrifuged at 200 x g and 4°C for 10 min. The hypotonic solution allows the cell to swell up in preparation for subsequent steps. Cells were then fixed with ice-cold methanol:acetic acid (3:1) three times and chromosomes were dropped onto cover slips and left to dry overnight. Slides were washed with PBS and stained for EdU and Acridine Orange (1:10,000). The intercalating dye will bind with differential affinity to chromatid arms with different BrdU content, allowing the detection of sister chromatin exchanges as changes in dye patterns. For each experiment, 40 chromosome spreads were captured and analyzed using a Zeiss microscope with Metafer software. Only EdU-negative (G2-irradiated) spreads were evaluated.

3.2.11 Chromatin Immunoprecipitation (ChIP)

For ChIP experiments, HeLa pGC cells were transfected with siRNA, then 24 h later were transiently transfected with I-Sce-I plasmid to introduce a targeted DNA DSB and were allowed to repair for 24 h. FA was then added drop-wise directly to the medium to a final concentration of 1% for 10 min to form protein-protein and protein-DNA crosslinks. 125 mM Glycine was then added for 5 min to quench unreacted formaldehyde. The medium was then removed and dishes were placed on ice and collected in ice-cold PBS containing protease inhibitors using a cell scraper and processed using EZ-Magna A/G ChIP kit according to manufacturer's instructions. Chromatin sonication was carried out using S220 sonicator controlled by the Sonilab software. Shearing was optimized to yield DNA fragments between 200-500 bp, with a setting of 3 min at continuous cycle duty factor 5. Immunoprecipitation was carried out with an H3.3 antibody (5 μ) and IgG as a control for the pull-down specificity (see below). The extracted DNA was analyzed by qPCR using FastStart Universal SYBR Green Master (Roche) according to manufacturer's instructions and primers targeted against different regions in the HR reporter construct (Figure 3.7) (primer sequences are listed in section 6.4). The amplification program was set to 95°C for 10 min, 40 cycles of 95 °C for 15 s, 60 °C for 60 s, followed by a melting curve stage to confirm primer specificity. All samples were run in triplicates (three technical replicates) for each reaction and qPCR data was normalized using the Percent Input method, in which variability between experiments is accounted for and normalized for both background and input levels. The Percent Input was calculated as $100 \cdot 2^{-(CT_{adj. Input} - CT_{IP})}$.



ChIP IgG control. IgG antibody control showed low signals for all regions assayed (compared to H3.3 pull-down).

3.2.12 *SDS-PAGE and Immunoblotting*

Cell harvest and lysis

Cells were trypsinized and collected in ice-cold PBS in a 2 ml tube and centrifuged for 3 min at 200 x g. The supernatant was removed as not to disrupt the cell pellet and cells were resuspended in 50-100 µl lysis buffer with protease inhibitor cocktail and incubated on ice for 10 min. To shear genomic DNA, the cell lysate was placed in an ultrasound bath with ice cold water for 1 min. Cells were then centrifuged at 4°C and 13000 rpm (maximum speed) for 10 min to pellet cell debris and the supernatant was subsequently transferred to a new tube and kept on ice for protein quantification or stored at -20 °C.

Protein Quantification

Protein quantification was carried out using the Bradford protein assay. Bradford reagent was diluted 1:5 in MilliQ water and for each sample, 1 µl protein was added to 1 ml Bradford reagent, mixed well and incubated for 5 min. Absorption was measured immediately at 595 nm using a Nanophotometer and concentration calculated based on a pre-established standard curve.

SDS-PAGE and Immunoblotting

For SDS-PAGE, the desired protein amounts were mixed with 5x Laemmli buffer and incubated for 10 min at 95°C with rotation for protein denaturation. Samples, along with a protein size marker, were loaded onto 7% or 10% polyacrylamide gel submerged in 1x electrophoresis buffer and run at 90 V until the proteins entered the running gel then the voltage was increase to 130 V until the required resolution of proteins was achieved. To transfer separated proteins to a nitrocellulose membrane, the gel was placed on the membrane and together they were sandwiched between layers of filter paper and sponges, ensuring the exclusion of air bubbles for even transfer. The assembled cassette was placed in a transfer chamber containing cold blotting buffer, while orienting the membrane towards the anode. Blotting was carried out on ice at an applied current of 300 mA for 2-3 h, depending on the size of the proteins. The membrane was then removed, cut for the desired protein size, and blocked with 1x Roti-Block for least 1 h at RT and incubated with the primary antibodies (section 6.6) at 4°C overnight. The membranes were then washed 3 x 10 min times in TBS-T and incubated with HRP-conjugated secondary antibodies diluted in blocking solution (section 6.6) for 1 h at RT. The membrane was washed 3 x 10 min in TBS-T and the blots were developed using WesternBright Quantum chemiluminescent detection system and the signal was captured using Fusion FX image acquisition systems.

3.2.13 *Bacterial transformation*

For plasmid amplification, chemically competent DH5 α *E.coli* were used for transformations. Cells were thawed on ice, gently mixed with 10 ng plasmid DNA and incubated on ice for 30 min. Cells were then subjected to heat shock at 42°C for 90 sec, followed by 5 min on ice. Cells were allowed to recover in 900 μ l LB medium for 1 h at 37°C with rotation at 220 rpm. Cells were then centrifuged for 1 min at 10,000 \times g and ~ 800 μ l of the supernatant were removed and cells were resuspended in the remaining medium. Cells were plated on 30 mg/ml kanamycin or 50 mg/ml ampicillin agar and incubated at 37°C overnight. Single colonies were picked in 5 ml LB medium and grown overnight at 37°C with rotation at 220 rpm. For long term storage, glycerol stocks were generated using 770 μ l 65% glycerol and 230 μ l bacterial culture and kept at -80°C. Plasmid maxi-preparations were done from 150 ml overnight culture using pEqGold Xchange plasmid maxi EF kit and plasmid mini-preparations were done from 5 ml cultures using ZR plasmid mini prep classic according to the manufacturer's instructions. DNA concentration was determined at absorption of 260 nm with a nanophotometer.

3.2.14 *Quantification and statistical analysis*

All data were derived from at least n=3 biological replicates carried out independently and for each experiment at least 40 nuclei or chromosome spreads were analyzed, unless otherwise specified. Background foci were subtracted from the mean values. Column plots show the mean value and the error bars show SEM between the experiments. P values were obtained by a Student's t-test and which compared the mean values of the independent experiments (*, p < 0.05; **, p < 0.01; ***, p < 0.001).

3.3 RESULTS

3.3.1 *The histone variant H3.3 has a role in the repair of X-ray-induced DSBs in S/G2*

The histone variant H3.3 has been implicated in the DNA damage response, especially in response to UVC irradiation, where *de novo* histone deposition is emerging as regulator of various steps of the DNA repair process. Nonetheless, its potential importance to DSB repair pathways, especially HR, is less characterized. To investigate the role of H3.3 in DSB repair, preliminary experiments were carried out to characterize the DSB repair kinetics after damage induction by X-rays in different cell cycle phases. To this end, the γ H2AX foci assay was employed as a sensitive approach for the detection of DSBs in response to physiological levels of irradiation, as previously described¹⁵⁷. One advantage of this approach is the ability to characterize repair in a cell-cycle specific manner when combined with an EdU labeling approach (see methods, Figure 3.1 A), as it is established that different repair pathways have distinct kinetics throughout the cell cycle. Cells repair IR-induced DSBs in G1 by a fast resection-independent NHEJ sub-pathway in the first 2 h, followed by a slow component comprising of resection-dependent c-NHEJ^{158,159}. In G2, cells utilize the fast c-NHEJ to repair the majority of breaks, with HR operating at late time points, observed as elevated γ H2AX foci in HR mutants 6-8 h post IR^{44,156}. Studying cells irradiated in G2 has the additional advantage of avoiding detection of lesions arising from S phase-related replication errors and provides a simpler setting for a more specific analysis. siRNA-mediated knockdown of both copies of H3.3 (H3.3A and H3.3B) resulted in similar γ H2AX foci numbers at early time points (1 h and 3 h) post 2 Gy X-IR in G2 HeLa cells compared to siCtrl-treated cells (Figure 3.1 B), suggesting that the induction of DSBs and formation of γ H2AX foci are unaffected. However, at late time points, H3.3-depleted cells showed elevated γ H2AX foci numbers compared to control cells, similar to repair defects seen in cells deficient in HR¹⁵⁶. Analysis of the G1 cell population in the same sample showed no difference between siH3.3- and siCtrl-treated cells, while EdU-positive cells showed a repair defect similar to G2 cells (Figure 3.1 C).

To gain further insight into the potential HR role of H3.3, the formation and resolution of Rad51 foci, as a more HR-specific marker, were analyzed. Cells lacking BRCA1 or BRCA2, which promote resection and Rad51 loading, respectively, fail to form Rad51 filaments, observed as peak of Rad51 foci approximately 2 h after IR¹⁶⁰. Alternatively, cells deficient in Rad54, which removes Rad51 from the DNA, show normal Rad51 foci formation, but fail to resolve these foci at late hours in G2⁴⁴. Unlike these factors, depletion of H3.3 did not affect Rad51 foci formation compared to control cells, and despite a delay in foci resolution, exhibited only

slightly higher foci levels at 8 h post IR (Figure 3.1 D). Together, these data preliminarily suggest that H3.3 is important for DSB repair in S/G2 phase cells in a manner independent of Rad51 loading or removal.

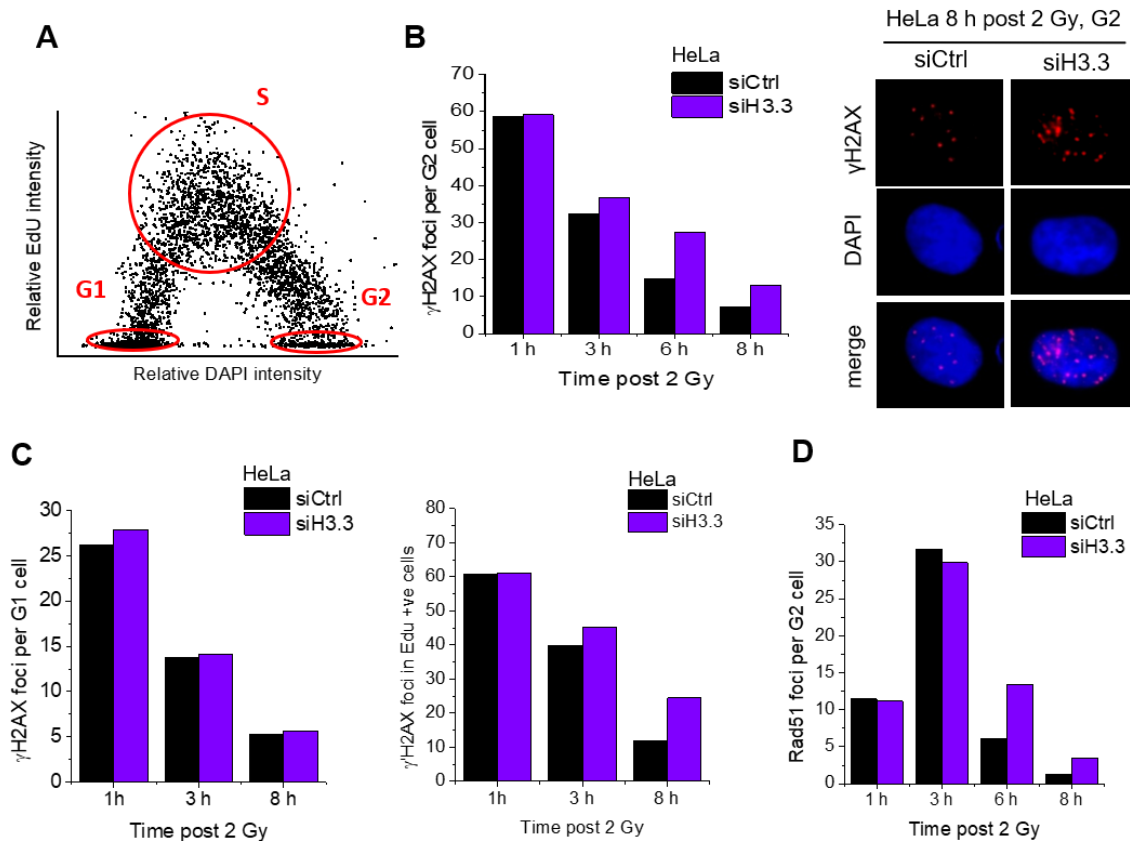


Figure 3.1 The histone variant H3.3 has a role in the repair of X-ray-induced DSBs in G2 cells

- (A) Cell cycle phase-specific analysis using a semi-automated microscopy approach. Asynchronously growing cells were treated with EdU 30 min prior to DNA damage, and maintained throughout the experiment. After immunostaining, the slides are scanned and the EdU and DAPI intensities of individual cells (at least 2000) were measured and plotted in a diagram showing a horseshoe pattern. EdU-positive cells represent the S phase population and EdU-negative cells are sub-classified into G1 or G2 based on their DNA content (DAPI signal). Cells transitioning from G1 and S phase to G2 incorporate EdU and are excluded from analysis.
- (B) HeLa cells were transfected with siCtrl or siH3.3; 48 hours later, EdU was added for 30 min and cells were X-irradiated with 2 Gy and fixed at multiple time points. γ H2AX foci, as a marker for DSBs, were enumerated in EdU-negative G2 cells.
- (C) HeLa cells as in panel B, where γ H2AX foci were enumerated in EdU-negative G1 cells and EdU-positive S phase cells and
- (D) HeLa cells, as in panel A; Rad51 foci, as a marker for resected breaks, were enumerated in EdU-negative G2 cells.

Data show the mean of 2 experiments.

3.3.2 H3.3 is required for HR in a manner epistatic to the chromatin remodeler ATRX

Since the data indicated a role of H3.3 in late S/G2 cells, and not in G1, a likely pathway regulated by the histone variant is HR. To consolidate this potential function, a GFP-based

gene conversion (GC) reporter assay was employed. The system is comprised of HeLa cells with an integrated reporter cassette carrying two non-functional copies of the GFP gene sharing a 520-bp region of homology: one copy carries an 18-bp recognition site for the endonuclease enzyme I-SceI that disrupts the coding sequence and the other copy is truncated on the 3' end (Figure 3.2 A) ¹⁵¹. Transient expression of I-SceI generates a DSB in one of two GFP genes and only HR-mediated repair using the second gene copy as a template restores the correct sequence and results in the expression of a functional GFP protein. HR frequencies were assessed by enumerating GFP-positive cells after I-SceI expression relative to control cells, which corrects for differences in transfection efficiencies of I-SceI between experiments (assuming similar ones between samples in the same experiment). Depletion of the HR factor BRCA2 expectedly resulted in a significant reduction of GFP-positive cells, thereby confirming the validity of the system. Additionally, cells treated with siATRX and siH3.3 also exhibited a reduction in HR frequencies, albeit to a lesser extent than BRCA2 depletion (Figure 3.2 B). To confirm that the HR defects seen in H3.3-depleted cells pertain to the ATRX chromatin remodeling axis (versus other remodelers/chaperons), γ H2AX foci levels were assessed in G2-irradiated HeLa and ATRX KO cells depleted for H3.3 (Figure 3.2 C, left panel). HeLa cells treated with two different siRNA pairs for H3.3 resulted in elevated foci levels at 8 h post IR compared to control cells, corroborating the specificity of the observed phenotype (i.e. excluding off-target effects of the siRNA). The elevated γ H2AX foci levels were similar to those observed (previously and herein) in ATRX KO cells, where additional depletion of H3.3 did not lead to a further increase, indicating that ATRX and H3.3 operate in the same repair pathway. This observation was extended to Rad51 foci which, as described earlier, remain only slightly elevated in H3.3-depleted cells and are at a similar level as observed in ATRX KO cells treated with siCtrl and siH3.3 (Figure. 3.2 C, right panel). To confirm and expand these results using alternate DSB inducers, the topoisomerase I (Top1) inhibitor camptothecin (CPT) was used (Figure 3.2 D). Top1 functions to overcome topological stress ahead of the replication fork by introducing a single-stranded break (SSB) in the DNA backbone, allowing DNA unwinding followed by re-ligation of the broken strands ¹⁶¹. CPT stabilizes the Topo1-DNA complex and prevents the re-ligation step, resulting in a persistent SSB that is converted into a DSB upon encountering replication forks, whose repair is known to require HR ¹⁶². CPT was added together with EdU for 1 h to label replicating cells and only EdU-positive cells, where replication-associated damage was induced, were analyzed. γ H2AX foci levels assessed 2 h post treatment were comparable in all samples, indicating a similar level of damage induction (Figure 3.2 D). However, 8 h after treatment H3.3-depleted HeLa

cells, ATRX KO and H3.3-depleted ATRX KO cells exhibited a marked elevation in γ H2AX foci compared to control HeLa cells, showing the requirement for these factors in the repair of CPT-induced DSBs and further evidencing their cooperative role in HR. Furthermore, clonogenic survival assays showed an enhanced, but comparable, sensitivity of ATRX KO cells, H3.3-depleted cells and H3.3-depleted ATRX KO cells to methyl methanesulfonate (MMS) and mitomycin C (MMC), a DNA-alkylating and a crosslinking agent, respectively (Figure 3.2 E). While these are distinct lesions, both require HR for their repair and sensitivity to these agents indicates HR deficiency¹⁶³. Collectively, these data provide evidence that H3.3 is essential to HR-mediated DSB repair in a process requiring the remodeler ATRX and whose repair foci kinetics suggest that it occurs late during HR.

3.3.3 *H3.3 is required during the late steps of HR*

Since Rad51 foci formation and resolution was largely unaffected in ATRX KO and/or H3.3-depleted cells, downstream stages of HR were investigated. Following D-loop formation and Rad51 removal by Rad54, DNA repair synthesis takes place to recover sequences lost during resection. To investigate this process, the incorporation of the nucleoside analog BrdU following IR of G2 cells was assessed. DNA repair synthesis can be visualized as nuclear BrdU foci that arise in control cells 4-8 h post IR in a manner dependent on HR factors but is unaffected by depletion of c-NHEJ factors¹⁵⁶. The visibility of these repair foci microscopically suggests that this process involves extended repair synthesis (~1-2 kbp)¹⁵⁰. Remarkably, HeLa cells treated with siH3.3 failed to show the accumulation of BrdU foci up to 8 h post 4 Gy irradiation, compared to control cells (Figure 3.3 A), showing that this variant is indeed essential for DNA repair synthesis during HR. Additionally, the formation of IR-induced SCEs was analyzed as a further downstream process occurring after repair synthesis completion as a result of HJ resolution. SCEs have been previously described to arise in G2-irradiated cells in a manner dependent on BRCA2, Rad51 and Rad54 and could be detected as changes in nucleic acid staining of mitotic chromosomes^{44,164}. Unirradiated HeLa cells showed a basal level of SCEs, likely arising during S phase, and exhibited a robust increase in SCEs in response to X-IR. (Figure 3.3 B). In contrast, H3.3-depleted cells did not exhibit such an increase, showing that this process is impaired in the absence of this histone variant. Since ATRX KO cells also fail to form BrdU repair foci and IR-induced SCEs¹⁵⁰, these findings provide evidence that chromatin remodeling, possibly involving histone variant exchange, is required for the late steps of HR.

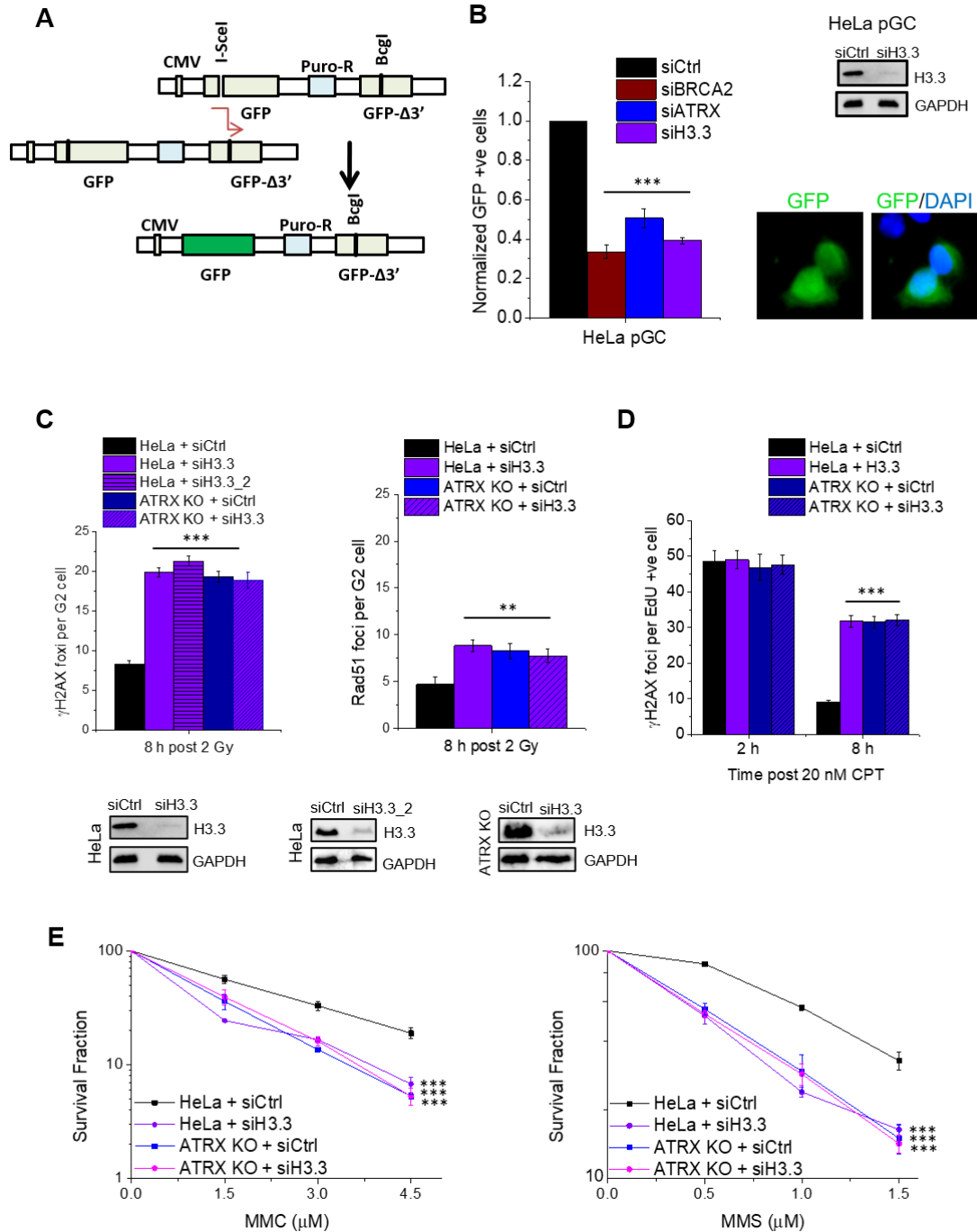


Figure 3.2. H3.3 is required for HR in a manner epistatic to the chromatin remodeler ATRX.

- (A) Schematic representation of the HR reporter cassette. I-SceI-induced breaks drive homology-mediated repair based on a 520-bp shared homology with the second, truncated copy of the GFP gene that is used as a template for repair synthesis. Successful HR leads to the restoration of the GFP sequence and expression of a functional GFP protein. HeLa pGC carrying an HR reporter cassette were transfected with indicated siRNAs followed by I-SceI plasmid transfection 24 h later then fixed after 48 h. GFP-positive cells were enumerated and normalized to siCtrl samples. Mean \pm SEM (n=3). Knockdown efficiencies were confirmed by immunoblotting (also see Juhász et al. 2018).
- (B) HeLa and ATRX KO cells were transfected with **H3.3 is required for HR in a manner epistatic to the chromatin remodeler ATRX** siCtrl, siH3.3 or siH3.3_2; 48 hours later, EdU was added for 30 min and cells were X-irradiated with 2 Gy and fixed after 8 h. γ H2AX and Rad51 foci were

- enumerated in EdU-negative G2 cells. Mean \pm SEM (n=3); spontaneous foci were subtracted. Knockdown efficiencies were confirmed by immunoblotting.
- (C) HeLa and ATRX KO cells were transfected with siCtrl or siH3.3. After 48 hours, cells were pulse-treated with EdU and 20 nM CPT for 1 hr and fixed after 2 h and 8 h. γ H2AX foci were enumerated in EdU-positive cells. Mean \pm SEM (n=3); spontaneous foci were subtracted.
- (D) Clonogenic survival of HeLa and ATRX KO cells transfected with siCtrl or siH3.3. DNA damage was induced by MMS or MMC at the indicated concentrations for 1 h and single colonies were fixed 14 days later, enumerated and normalized to mock-treated cells. Mean \pm SEM (n=3).

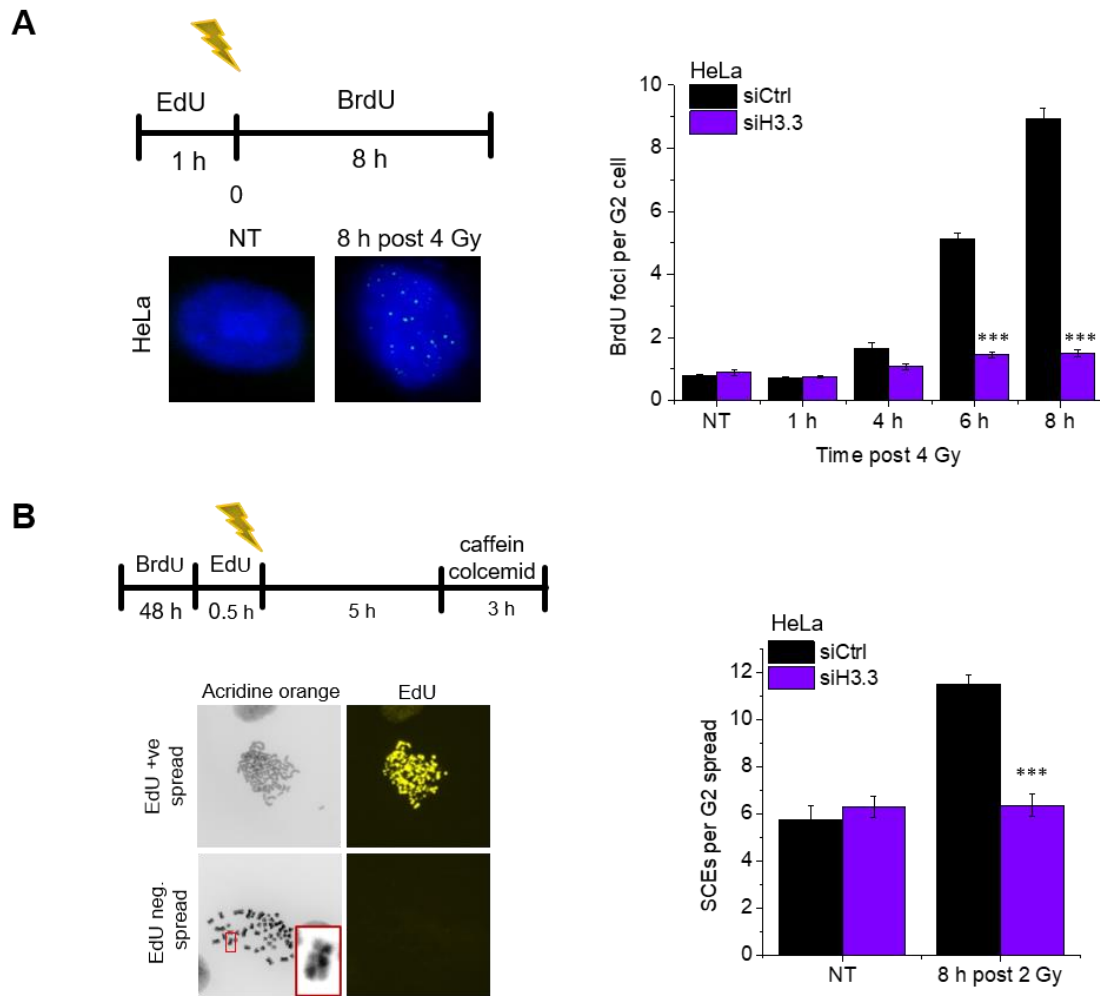


Figure 3.3. H3.3 is required during the late steps of HR.

- (A) HeLa cells were transfected with siCtrl and siH3.3 and 48 later, cells were treated with EdU for 1 h then X-irradiated with 4 Gy. Cells were then washed, labeled with BrdU and fixed at the indicated time points. BrdU foci (see image), corresponding to DNA repair synthesis, were enumerated in EdU-negative G2 cells. Mean \pm SEM (n=3). Image is extracted from Juhász *et al.* 2018.
- (B) HeLa cells were transfected with siCtrl and siH3.3 and incubated with BrdU for 48 h. Cells were then labeled with EdU for 30 min and X-irradiated with 2 Gy. Cells were treated with caffeine and colcemid for 3 h and collected at 8 h post IR. SCEs were counted in EdU-negative mitotic spreads from G2-irradiated cells. Mean \pm SEM (n=3). Image is extracted from Juhász *et al.* 2018.

3.3.4 *Newly synthesized H3.3 is deposited early at sites of damage independently of ATRX*

To investigate if H3.3 exchange is taking place during DNA repair synthesis and to better characterize the deposition kinetics of H3.3 *in vivo*, a HeLa cell system stably expressing SNAP-tagged H3.3 was employed to monitor H3.3 incorporation dynamics, as previously shown¹⁵². The SNAP polypeptide is a 20 kDa self-tagging protein derived from the DNA repair enzyme O⁶-alkylguanine-DNA alkyltransferase and can react with benzylguanine derivatives irreversibly to form covalent linkages to synthetic substrates¹⁶⁵. Non-fluorescent and fluorescent SNAP substrates are cell-permeable which allows *in vivo* labeling of proteins in live cells, irrespective of cellular compartmentalization. The expression of SNAP-H3.3 was verified via western blot, which was detected with an H3.3 antibody at the expected size of 37 kDa, while the endogenous H3.3 was detected at 17 kDa (Figure 3.4 A). To verify this system *in vivo*, a pulse-quench-chase sequence was carried out. A pulse of fluorescent substrate (Oregon green) effectively labeled pre-existing H3.3 in the cell, while a quench-pulse with a non-fluorescent substrate preceding the pulse blocked all SNAP-tags and gave only background signal, confirming the efficiency of the quenching reaction (Figure 3.4 A). A quench-chase-pulse sequence introduced a chase period to allow for *de novo* histone synthesis. An additional triton-X pre-extraction step prior to fixation removed soluble histones and allowed the labeling of incorporated histones only, thereby giving a lower signal than the pulse alone. To confirm that H3.3 can be detected at damage sites, the previously described rapid deposition of H3.3 at laser-induced damage was assessed¹⁴³. In these experiments, UVA laser was used to introduce DNA damage, where the cells were pre-sensitized with BrdU to enrich for DSBs, versus other UV-induced lesions (see methods section 3.2.3). Cells were subjected to a quench-chase sequence, followed by micro-irradiation, a pulse step then fixation after a total of 1 h post irradiation (see scheme in Figure 3.4 B). In agreement with previous findings, SNAP-H3.3 signal was detected at laser tracks marked with γ H2AX 1 h post irradiation in G2 cells (Figure 3.4 B). Depletion of Rad51, ATRX and DAXX did not affect the observed enrichment, indicating that this deposition involves a process distinct to HR.

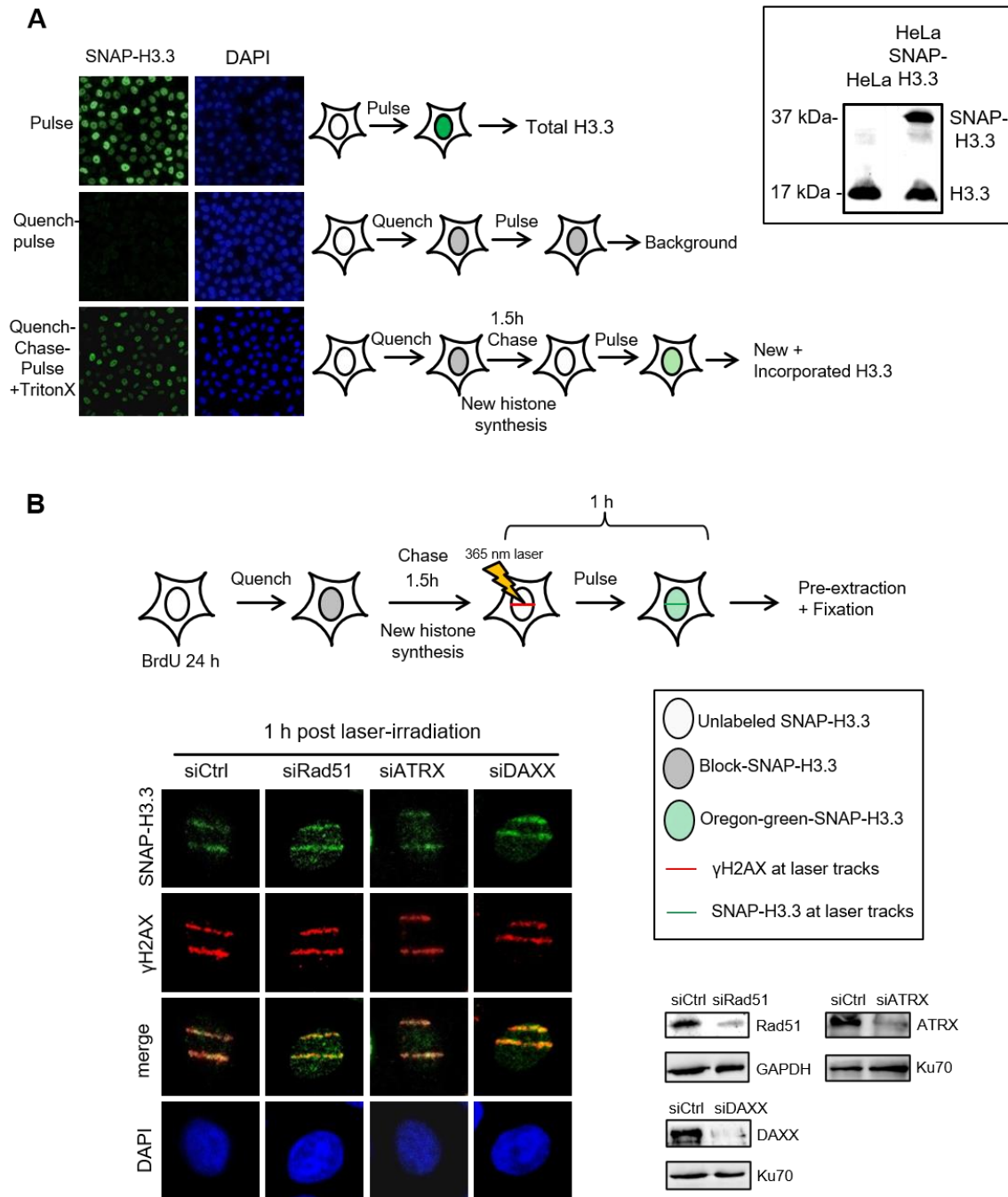


Figure 3.4 Newly synthesized H3.3 is deposited early at sites of damage independently of ATRX

(A) SNAP-H3.3 expression was confirmed by immunoblotting. Validation of the SNAP system was carried out through a quench-chase-pulse succession. In the pulse step, the SNAP substrate (Oregon green) was added for 20 min and cells were fixed directly after to label total SNAP-H3.3 protein. In the quench-pulse sequence, the SNAP block is added, washed and then a pulse step followed directly to confirm the efficiency of the blocking step and represents the background. In the quench-chase-pulse sequence, a 1.5 h chase period was introduced between the quench and pulse steps, and was followed by pre-extraction step prior to fixation. This allowed the visualization of the newly synthesized and incorporated SNAP-H3.3.

(B) SNAP-H3.3 HeLa cells were transfected with siCtrl, siRad51, siATRX and siDAXX and after 24 h, cells were pre-sensitized with BrdU for 24 h. A quench-chase sequence was performed with the addition of EdU prior to laser-irradiation, followed by a pulse step and fixation. Knockdown efficiencies were confirmed by immunoblotting.

3.3.5 *Late deposition of newly synthesized H3.3 at sites of damage is dependent on Rad51, ATRX and DAXX*

In order to monitor H3.3 incorporation specifically at later times (8 h) following DNA damage, the experimental setup was modified such that quenching of the tagged histones was performed several hours after laser irradiation. This blocks the signal from early H3.3 deposition and allows the detection of histones incorporated in the last 2.5 hours of the repair period (see scheme in Figure 3.5 A). Strikingly, using this modified setup, H3.3 enrichment in laser tracks was also observed at laser-induced DNA damage in G2 cells at late times (Figure 3.5 A). However, this deposition was strictly dependent on Rad51, as Rad51 depletion almost abolished all SNAP-H3.3 signal in γ H2AX-positive tracks. This shows that this is an independent process from the early deposition events and suggests that it occurs downstream of the Rad51-mediated strand invasion and D-loop formation steps of HR. Additionally, depletion of ATRX or DAXX also diminished late H3.3 laser track signal, indicating that these factors are required for histone deposition at this late stage of HR (Figure 3.5 A).

To confirm the results obtained with the SNAP system with a different approach, chromatin immunoprecipitation (ChIP) of H3.3 was carried out in HeLa pGC cells carrying an HR reporter cassette, described in section 3.3.2. Cells were transfected with RFP (as a control) or I-SceI to introduce a targeted DSB at a defined genomic locus and ChIP was carried out against H3.3, and IgG was used as a control for the pull-down. Primers for qPCR were designed at 3 different sites in or near the GFP donor site spanning an area of 1 kbp, where extended DNA repair synthesis and histone deposition is expected to occur. HeLa cells expressing I-SceI, but not those expressing RFP, showed a 2-3 fold increase in H3.3 signal at all three target sites, indicating an enrichment of H3.3 at sites of DSBs which likely extend beyond the donor site, and suggesting that this assay monitors events that would not necessarily give rise to a functional GFP protein (Figure 3.5 B). The signal detected in the control GAPDH showed no increase in response to DSB induction, indicating the specificity of the PCR primers. However, since the overall H3.3 enrichment was much lower than the other PCR target loci, it is possible that the HR cassette locus is generally enriched in H3.3. Moreover, this enrichment in H3.3 was reduced to control levels in ATRX-depleted cells, consistent with the SNAP-tag results supporting ATRX-dependent H3.3 deposition at sites of DSBs (Figure 3.5 B). Furthermore, ChIP using the IgG antibody also gave negligible signal for all conditions, confirming the specificity of the pull-down (see methods section 3.2.11).

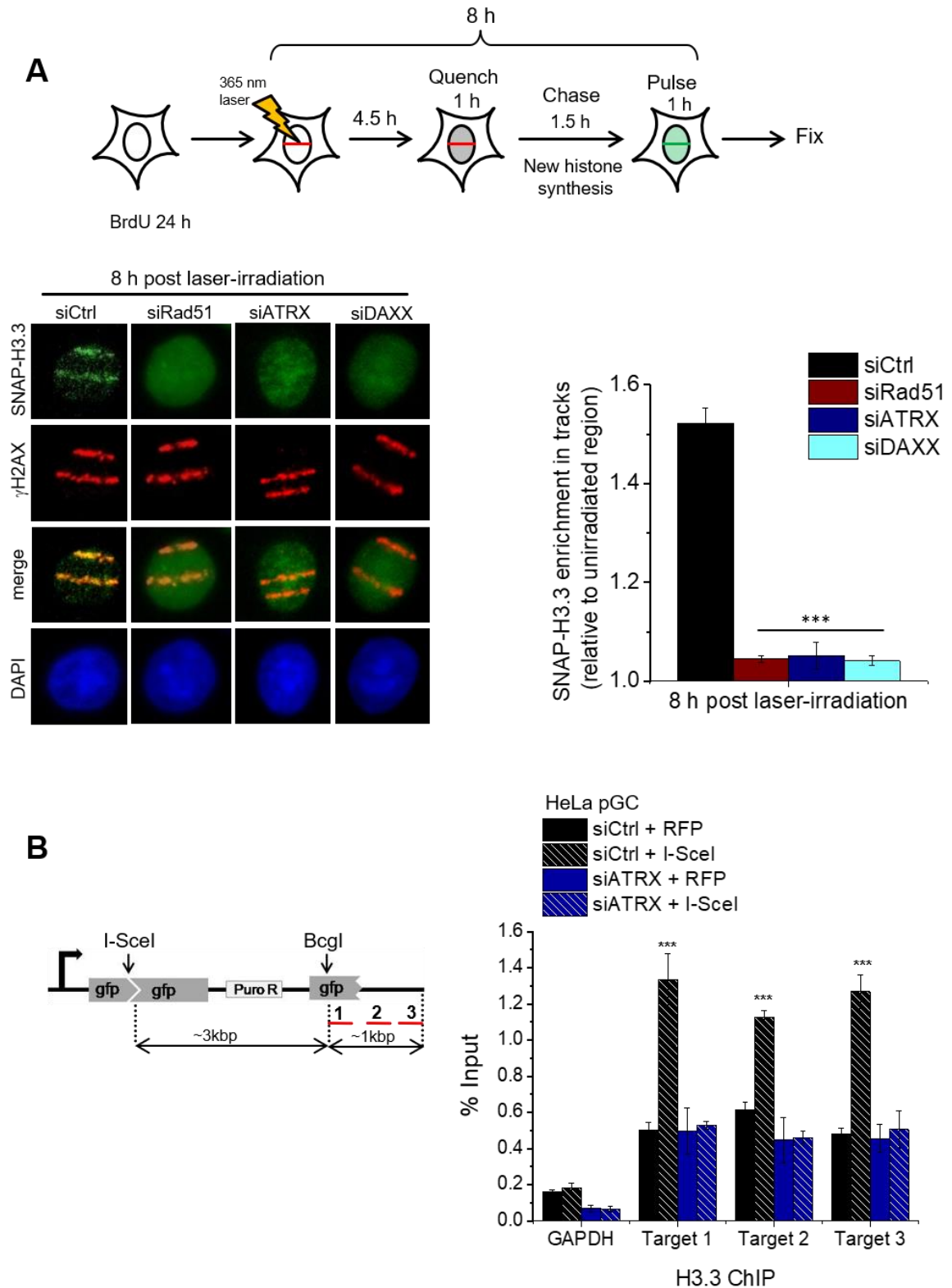


Figure 3.5 Late deposition of newly synthesized H3.3 at sites of damage is dependent on Rad51, ATRX and DAXX

(A) SNAP-H3.3 HeLa cells were transfected with siCtrl, siRad51, siATRX and siDAXX and after 24 h, cells were pre-sensitized with BrdU for 24 h. EdU was added for 30 min prior to laser-irradiation and a quench-chase-pulse sequence was performed 4.5 h later. SNAP-H3.3 signal enrichment in tracks was measured in EdU-negative G2 cells. Mean \pm SEM (n=3).

- (B) HeLa pGC cells transfected with siCtrl or siATRX were transfected with I-SceI or RFP plasmids 24 h later. Cells were collected after 24 h, ChIP was performed against H3.3 and purified DNA was analyzed by qPCR using 3 different primer pairs up to 1 kbp away from the GFP donor site and the GAPDH locus as a control. The qPCR signal normalized to the input via the Percent Input method is shown. Use of a non-specific IgG antibody provided negligible qPCR signals (see methods section 3.2.11). Mean \pm SEM (n=3).

3.3.6 *Histone H3.3 deposition and DNA repair synthesis are interlinked*

Building on evidence for H3.3 requirement for DNA repair synthesis and deposition as sites of DNA damage, the dependence on DNA synthesis factors was then investigated. The processivity clamp PCNA and its loader complex RFC are key factors during replication and also are required for Pol δ -mediated processive DNA synthesis following Rad51 strand invasion *in vitro*^{45,166,167}. RFC-1 is the largest subunit of the clamp loader complex RFC that is required to load PCNA onto DNA. To evaluate the localization of the RFC-1 to DNA damage, HeLa cells were irradiated with 4 Gy and fixed at multiple time points. RFC-1 foci were detected in G2 HeLa cells and localized to DSBs 6-8 h post damage, with kinetics reminiscent of BrdU repair foci formation (Figure 3.6 A). RFC-1 foci formation was dependent on Rad54, which is consistent with *in vitro* results showing the requirement of Rad54 for the formation of free 3' suitable for DNA synthesis¹⁶⁶. Interestingly, depletion of PCNA and ATRX also abolished RFC-1 foci formation, possibly due to decreased stability of the DNA synthesis complex. Furthermore, depletion of RFC-1 caused elevated γ H2AX foci levels at 8 h post X-IR in G2 HeLa cells compared to control cells, with no difference at 2 h, supporting the requirement for the clamp loader, and likely PCNA as well, in HR-mediated DBS repair (Figure 3.6 B). To understand how these factors influence histone deposition at DNA damage sites, PCNA and RFC-1 were depleted in HeLa SNAP-H3.3 and both early and late incorporation events were monitored. PCNA and RFC-1 depletion did not affect the early enrichment of H3.3 at laser tracks, suggesting that this process is uncoupled from DNA synthesis (Figure 3.6 C). In contrast, H3.3 enrichment at late times was significantly reduced in siPCNA and siRFC-1 treated cells compared to control cells, indicating that this incorporation process is coupled to DNA synthesis. Together, these results provide a link between DNA repair synthesis and H3.3 deposition during HR, with implications that the two processes could be interdependent or occur simultaneously.

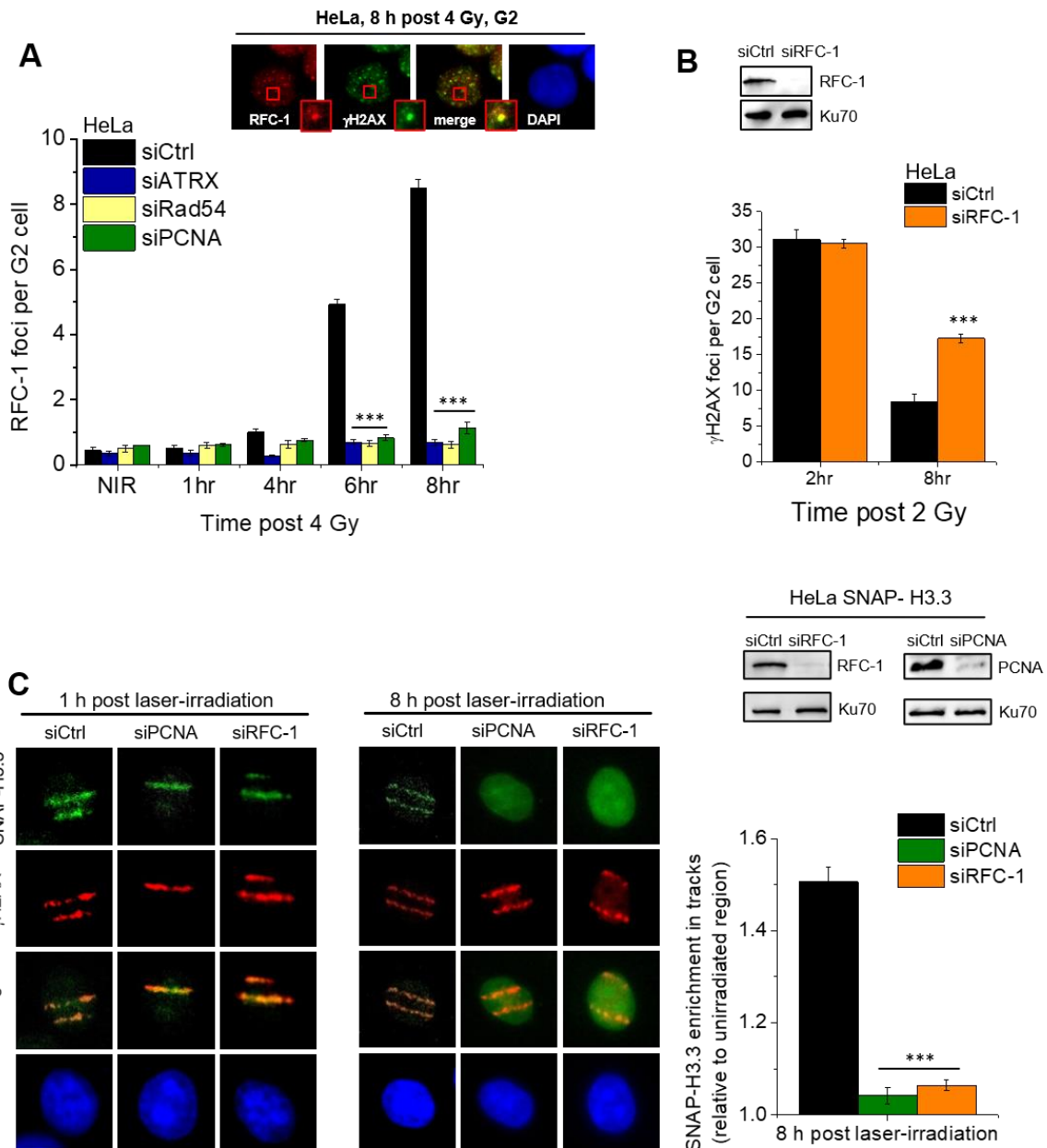


Figure 3.6 Histone H3.3 deposition and DNA repair synthesis are interlinked

- (A) HeLa cells were transfected with the indicated siRNAs and 48 h later EdU was added for 30 min and cells were X-irradiated with 4 Gy and fixed at different time points. RFC-1 foci, visualized as shown (image from Juhász *et al.* 2018), were enumerated in EdU-negative G2 cells. Mean \pm SEM (n=3). Knockdown efficiencies were confirmed by immunoblotting (see Juhász *et al.* 2018).
- (B) HeLa cells were transfected with siCtrl or siRFC-1 and 48 h later EdU was added for 30 min and cells were X-irradiated with 2 Gy and fixed after 2 h and 8 h. γ H2AX foci were enumerated in EdU-negative G2 cells. Mean \pm SEM (n=3); spontaneous foci were subtracted. Knockdown efficiency was confirmed by immunoblotting.
- (C) SNAP-H3.3 HeLa cells were transfected with siCtrl, siRFC-1 or siPCNA and after 24 h, cells were pre-sensitized with BrdU for 24 h. Early (1 h post irradiation) and late (8 h post irradiation) H3.3 incorporation was assessed as described in the schemes depicted in Figures 3.3.4 and 3.3.5 respectively. SNAP-H3.3 enrichment in tracks at late times was quantified in EdU-negative G2 cells. Knockdown efficiencies were confirmed by immunoblotting.

3.3.7 *Histone H3.3 deposition by other chromatin remodelers and chaperons*

Since histone deposition is an important process for many repair events, the involvement of other histone chaperones was investigated to understand the specificity of this process. H3.3 deposition can be mediated by the variant-specific chaperon HIRA, typically during transcription, but also in response to UVC damage¹⁴¹. Additionally, CAF-1 mediates H3.1 deposition during replication in a process coupled to DNA synthesis as well as post-repair of UV lesions¹⁶⁸⁻¹⁷⁰. Notably, depletion of HIRA but not the p60 subunit of CAF-1 resulted in a reduced, but still detectable, H3.3 signal in laser tracks at early times (Figure 3.7 A). Since fast DSB repair in G2 involves c-NHEJ¹⁵⁶, this result is consistent with a role of H3.3 in this pathway¹⁴³, albeit involving the chaperon HIRA. Whether this is required for pathway choice or for repair factor recruitment is not clear. Furthermore, HIRA depletion partially reduces late (8 h) H3.3 incorporation, suggesting a possible cross-talk between early H3.3 deposition and downstream events (Figure 3.7 A). Alternatively, HIRA could have a genuine role in the HR repair process that is secondary to ATRX. Consistent with this notion, HeLa cells treated with siHIRA exhibited a moderate increase of γ H2AX foci numbers in G2 cells at 8 h post IR compared to control cells, although foci levels were also elevated slightly at 2 h (Figure 3.7 B). The lack of observable phenotype of CAF-1 p60 depletion on neither H3.3 deposition dynamics nor γ H2AX foci levels counter a role for CAF-1 in HR-mediated repair involving H3.3 deposition (Figure 3.7 A & B). However, a role for its associated histone H3.1 cannot be excluded and would require further investigation.

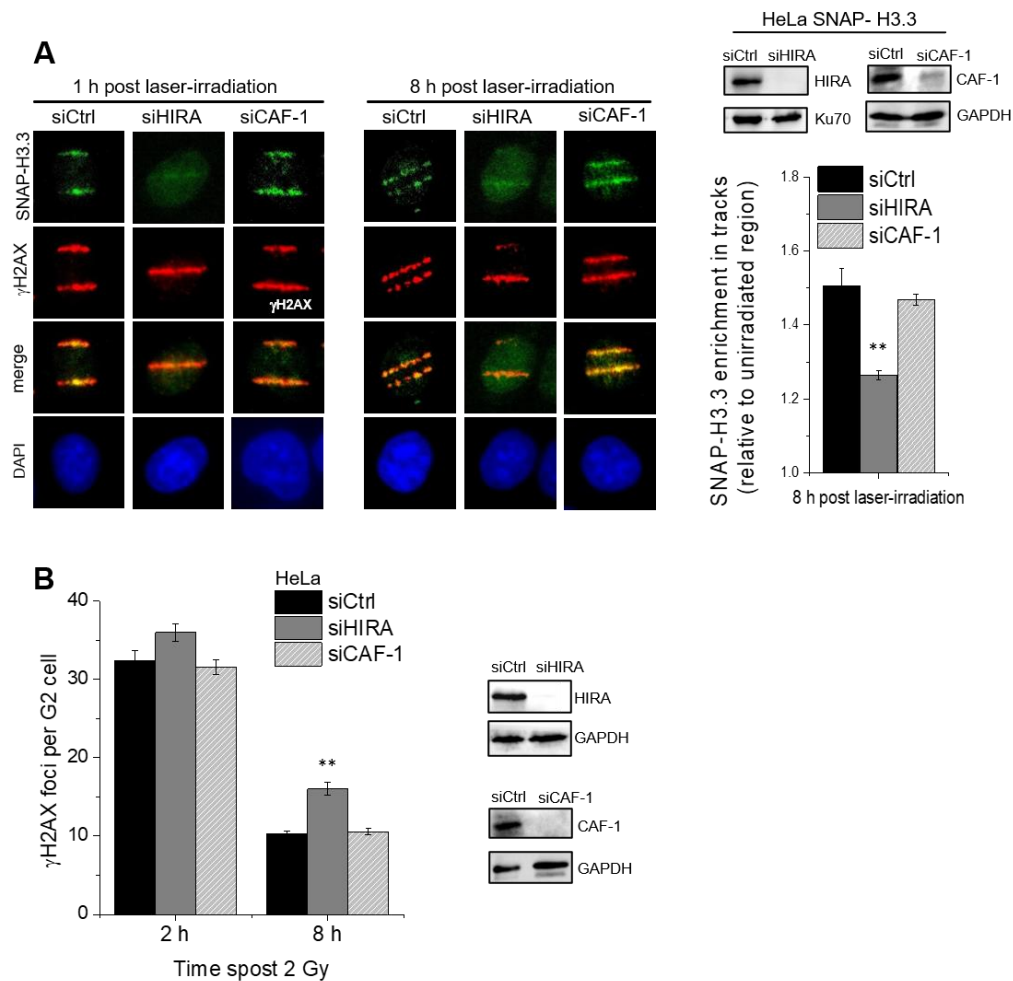


Figure 3.7. Histone H3.3 deposition by other chromatin remodelers and chaperons.

- (A) SNAP-H3.3 HeLa cells were transfected with siCtrl, siCAF-1 p60 or siHIRA and after 24 h, cells were pre-sensitized with BrdU for 24 h. Early (1 h post irradiation) and late (8 h post irradiation) H3.3 incorporation was assessed using the protocols depicted in Figures 3.3.4 and 3.3.5 respectively. SNAP-H3.3 enrichment in tracks at late times was quantified in EdU-negative G2 cells. Knockdown efficiencies were confirmed by immunoblotting as shown.
- (B) HeLa cells were transfected with siCtrl, siCAF-1 p60 or siHIRA and 48 h later EdU was added for 30 min and cells were X-irradiated with 2 Gy and fixed after 2 h and 8 h. γ H2AX foci were enumerated in EdU-negative G2 cells. Mean \pm SEM (n=3); spontaneous foci were subtracted. Knockdown efficiency was confirmed by immunoblotting as shown.

3.4 DISCUSSION

Chromatin undergoes extensive modifications and remodelling in response to DNA damage, which allow the repair proteins to access the DNA, and also strongly influence the DDR¹³². Chromatin dynamics in response to DSBs involve multiple histone modifications, as well as the disassembly and reassembly of nucleosomes before and after DNA repair, respectively. Additionally, the exchange of canonical histones for specific histone variants plays an important role in regulating repair factor recruitment and pathway choice^{131,132}. Previous reports have shown the rapid incorporation of the histone variant H3.3 at sites of DNA damage to promote c-NHEJ, as well as during post-repair chromatin reassembly^{117,118}. Here, we present evidence for a role for the histone variant H3.3 during HR-mediated repair of DSBs in G2 phase cells. Interestingly, H3.3 is required for repair at late stages during HR where it is essential for DNA repair synthesis and the subsequent formation of SCEs, which the chromatin remodeling-chaperone complex ATRX-DAXX was also shown to promote¹⁵⁰. Consistent with these observations and published data, the *in vivo* visualization of H3.3 dynamics revealed the incorporation of newly synthesized H3.3 at sites of DNA damage at both early and late time points. However, only late incorporation was ATRX dependent and was associated with DNA synthesis, revealing distinct, temporally regulated functions for H3.3 deposition. DNA synthesis is integral to various repair mechanisms, such as nucleotide excision repair (NER), where it has been shown to proceed concomitant with chromatin reconstitution through CAF-1^{168,169}. However, CAF-1-mediated histone deposition is not a prerequisite for repair and is considered part of post-repair chromatin assembly. Nevertheless, this association between DNA synthesis and repair synthesis can be applied to the findings here to suggest a model in which extended DNA synthesis during HR is tightly coupled to H3.3 deposition and nucleosome assembly facilitated by a direct, IR-induced interaction between PCNA and ATRX (Figure 3.8 A)¹⁵⁰. In contrast to NER, this is a prerequisite for repair completion as the disruption of this process impedes repair and results in an excess of unrepaired breaks. A possible explanation for this discrepancy is the range of repair synthesis, which is much longer during HR versus NER where nucleosome reassembly could have a more profound impact on the progression of the DNA synthesis machinery. This is analogous to the long-range DNA synthesis during replication, where CAF-1 interacts with PCNA to deposit the histone H3.1 behind the replication fork¹³⁵. This coordination of nucleosome assembly and DNA synthesis is important for the regulation of fork progression and elongation rate although the exact mechanism is not clear¹⁷¹. Furthermore, H3.3 is known to be deposited in actively transcribed

regions where H3.3 exchange promotes transcription initiation and elongation and regulates transcription rate ^{152,172}. Therefore, histone exchange and nucleosome reassembly play an important role during long-range nucleic acid synthesis that regulates various processes including replication, transcription, and repair (Figure 3.8 B). This is not unexpected; protection of long stretches of naked DNA in such processes is imperative for genomic integrity, a notion in agreement with the gap-filling role described for H3.3 during transcription ¹⁵². In our model, H3.3 deposition is required for DNA repair synthesis, which could safeguard chromatin integrity over long repair patches and provide structural stability facilitating the progression of the D-loop. A similar mechanism has been described in fission yeast, where CAF-1-mediated deposition of H3.1 is important for recombination-dependent replication restart at stalled forks ^{173,174}. In this context, histone deposition stabilizes the D-loop and prevents its disassembly by RecQ-type helicase Rqh1 to promote template switching events ¹⁷³. Additional structural support could be generated from regulating the 3-D architecture of the DNA. The unwinding of the DNA, as in transcription, generates torsional stress, manifesting as positive and negative supercoiling ahead of and behind the moving synthesis complex, respectively. Positive stress can destabilize nucleosomes and cause histone eviction, whilst negative supercoiling promotes nucleosome assembly (Figure 3.8 A) ^{175,176}. Studies show that nucleosome arrays accommodate more torsional stress than naked DNA and higher order chromatin structure provide structural plasticity under torsion, therefore histone deposition would function to increase torsional resilience of the region around the break ^{177,178}. The reason for a specific need for H3.3 is not clear, especially given the structural similarity to H3.1. A histone-variant specific function is supported by the observation that CAF-1 does not influence repair synthesis, with a small role for the H3.3 chaperon HIRA. While a simple explanation could be the abundance of H3.3 throughout the cell cycle versus an S phase-restricted H3.1 expression, it is unlikely to be sufficient as replication-independent H3.1 deposition outside S phase was reported ^{168,179}. Furthermore, while H3.3 deposition can compensate for impairment of H3.1 incorporation during replication, the opposite is not valid, indicating that H3.3 serves additional functions that cannot be compensated by H3.1 ¹⁵². It is also plausible that H3.3 can provide a scaffold for post-translation modifications serving as epigenetic marks for DNA damage sites. This is consistent with observations that H3 histone variants harbor distinct PTMs and therefore can provide signatures for different genomic regions, such as damaged DNA ¹⁸⁰. H3.3 is known to be actively methylated at lysine 9 at

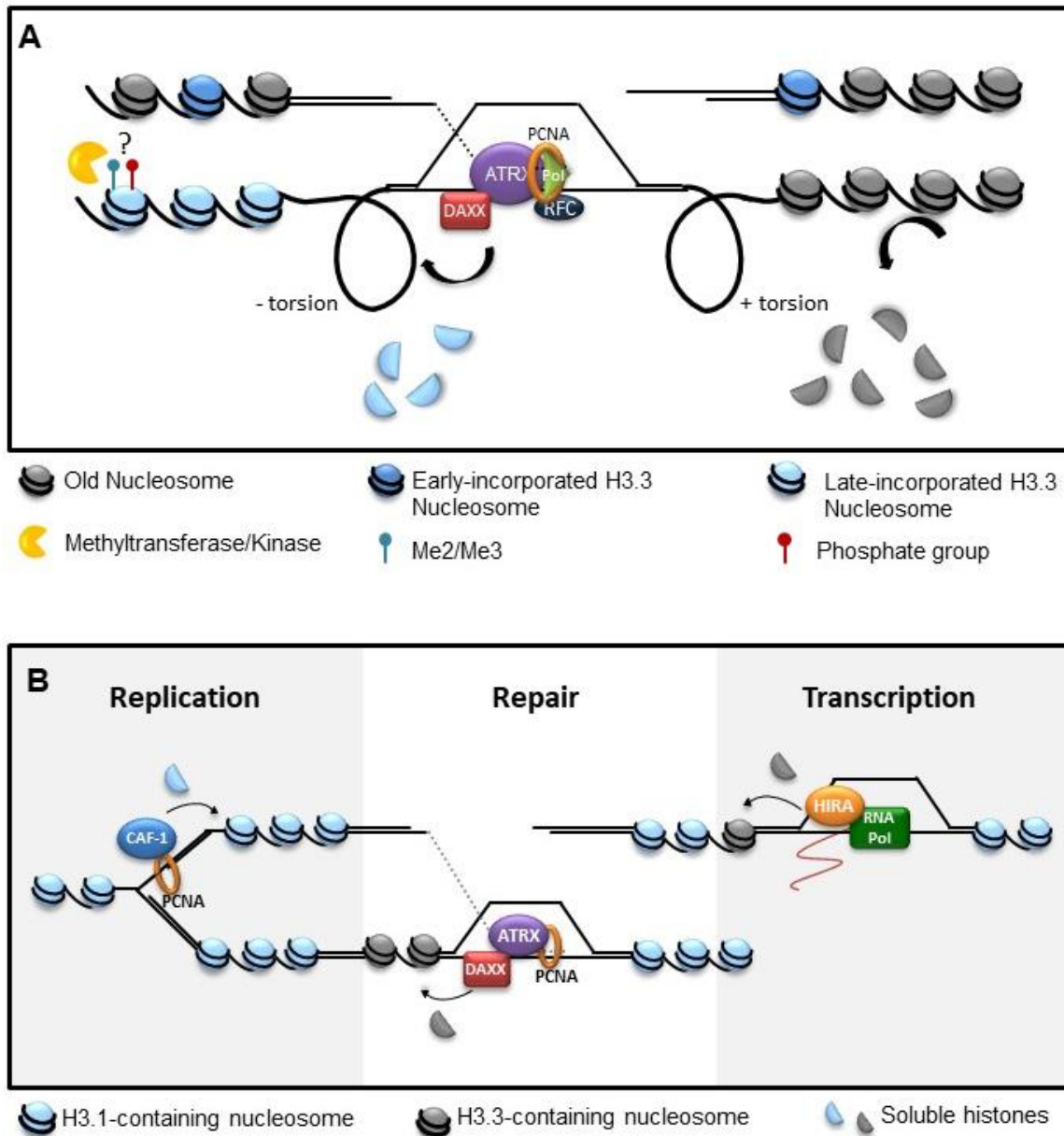



Figure 3.8. Model for histone deposition during homologous recombination.

- (A) ATRX interacts with PCNA and together with chaperone DAXX, deposits newly synthesized H3.3 behind the complex in a step that promotes the progression of DNA synthesis. Chromatin around the DSB may still contain H3.3 incorporated during earlier events. In a migrating D-loop model, DNA unwinding generates positive torsional stress ahead of the polymerase to destabilize nucleosomes and evict histones while negative torsional stress accumulates behind the complex, a conformation that favours nucleosome assembly and stabilizes the DNA. It is unclear where this histone turnover dynamic includes histone recycling. Possible histone H3.3-specific modifications like methylation or phosphorylation could add another layer of regulation or act as epigenetic damage markers.
- (B) Chromatin remodeling is a common requirement for the regulation of DNA and RNA synthesis. Distinct chromatin remodelers and chaperons direct the deposition of histones during replication (CAF-1), repair synthesis in homologous recombination (ATR and DAXX) and transcription (HIRA), in a highly coordinated, tightly coupled process.



telomeric regions by methyltransferases that are also active during the DNA damage response, but a link between them has not been established^{181,182}. Similarly, H3.3 can be uniquely phosphorylated at serine 31 which is linked to DNA damage at telomeres, but not internal breaks¹⁸³.

3.5 CONCLUSION

Taken together, these findings inspire a model in which HR-mediated DSB repair synthesis is coupled to histone deposition, where a high histone turnover manifests as a balanced process of nucleosome disassembly ahead of the progressing D-loop and reassembly behind it using newly synthesized histone variants. The timely coordination of these processes provides topological and structural stability that allows DNA synthesis progression and genomic protection and possibly generates epigenetic signatures for damaged regions.

4. ATRX AND RECQ5 DEFINE DISTINCT SUB-PATHWAYS OF HOMOLOGOUS RECOMBINATION

4.1 INTRODUCTION

HR is an essential process for the maintenance of genomic integrity and shown to be vital for diverse cellular processes, such as replication, as well as DSB repair during meiosis and in somatic cells. HR relies on the use of a homologous template for repair to ensure the faithful restoration of genetic information and is restricted to the S/G2 phase of the cell cycle in somatic cells. DSB repair is channeled to HR by the extensive 5'-to-3' resection of break ends to generate 3' ssDNA overhangs. The recombinase RAD51 is then loaded to ssDNA to direct the homology search for complementary sequences and the formation of a D-loop to allow DNA repair synthesis and the recovery of the lost sequences^{39,44}. Repair of two-ended breaks requires the annealing and sealing of the break ends, which can proceed in two known sub-pathways. During SDSA, the extended break end is displaced from the D-loop followed by annealing to the complementary sequence at the non-invading break end. In the other sub-pathway, the non-invading end anneals to the displaced strand of the extending D-loop in a second-end capture step, leading to the formation of a dHJ. To complete the repair process, this structure can be resolved by the structure-specific nucleases SLX4-SLX1, Mus81-EME1 and Gen1 which induce asymmetrical or symmetrical incisions in the two strands at each HJ, giving rise to both CO and non-CO products⁶⁴. Alternatively, dHJs can be dissolved by the BTR complex in a decatenation reaction, thus separating the two molecules without exchange of genetic material.

Pathways leading to COs are often viewed as mutagenic, as exchanges between homologous chromosomes can cause LOH, a contributing factor to carcinogenesis. Therefore, cells harbor multiple mechanisms of CO-suppression, where non-meiotic cells employ the sister chromatid instead of the homologous chromosome in both yeast and mammalian systems^{2,3}. Additionally, as SDSA is inherently refractory to CO formation, it is believed to be the predominant HR sub-pathway in the repair of DSBs^{48,184,185}. Furthermore, the preferential usage of BLM-mediated dissolution of dHJs limits COs, with resolution acting as a last-resort back up to handle these intermediates. Results from HR reporter systems, where COs are rarely observed, and the lower rate of dHJ formation per DSB in somatic versus meiotic cells support a general CO-avoidance tendency during HR in somatic cells^{2,58}. This notion appears also consistent with historic studies suggesting that DSB-inducing agents, including IR, are poor inducers of SCEs^{186,187}.

However, it is now known that most IR-induced two-ended DSBs are repaired in mammalian cells by c-NHEJ with HR accounting for only about 20% of all repair events even in G2 phase, thereby explaining the relative scarcity of SCEs compared to the number of induced breaks^{156,188}. Moreover, the sister chromatid represents the natural substrate for HR and COs might not be readily monitored in reporter systems which rely on unequal recombination events between the damaged loci and the provided substrates. Thus, it is unclear how often COs arise during HR in somatic cells.

Recently, it has been shown that the chromatin remodeler ATRX promotes extended DNA repair synthesis and SCE formation during HR-mediated DSB repair¹⁵⁰. In this process, ATRX and the chaperone DAXX deposit the histone variant H3.3 during HR in a step downstream of Rad51 removal¹⁵⁰. Interestingly, the ATRX/DAXX complex interacts with the polymerase processivity factor PCNA after DSB induction, suggesting that histone deposition is tightly coupled to DNA repair synthesis¹⁸⁹. The observation that SCE formation after IR is strictly dependent on ATRX further suggests that extended repair synthesis leads the generation of HR intermediates that give rise to COs¹⁵⁰. This notion is consistent with findings showing that gene conversion tracts for CO forming pathways are substantially larger than for SDSA^{190,191}. However, the frequency in CO formation versus the use of SDSA in this system has not been investigated and would present an opportunity to quantitatively compare HR sub-pathway usage and choice, but an SDSA-specific factor is required for this comparison.

Multiple helicases in yeast and mammals have been implicated to facilitate the strand displacement step in SDSA, including the yeast RECQ helicase Sgs1 and its human homolog BLM, which have been shown to be able to disrupt D-loops *in vitro*, as well as suppress COs in *in vivo*¹⁹². This CO-counteracting mechanism is dependent on TOPOIII α -RMI1 and functions by dissolving intermediates of the dHJ pathway, rather than D-loop dissolution¹⁹³. Human and yeast Rad54 are also capable of dismantling D-loops *in vitro*, although the *in vivo* function of Rad54 is indicated to be pro-recombination and is required for HR pathways resulting in COs^{42,44,150}. The yeast Srs2 helicase is also known to dissociate RAD51 from ssDNA and to promote non-CO products via SDSA exerting seemingly paradoxical anti- and pro-recombinogenic effects^{50,194,195}. Further evidence showed the ability of Srs2 to dismantle extended D-loops post DNA repair synthesis in a manner enhanced by SUMO-PCNA, thereby allowing strand annealing and CO avoidance⁵¹. A plausible pro-recombination role of the RAD51-filament disruption function could be freeing the second end to allow strand annealing. While Srs2 does not have a known homolog in human cells, multiple helicases have analogous

functions. A prominent example is RECQ5, which has multiple roles in the DNA damage response. RECQ5 is recruited to sites of DNA damage in an MRN-dependent manner, resolves replication-transcription conflicts and promotes processing of stalled forks¹⁹⁶⁻¹⁹⁸. RECQ5 has been shown to interact with and remove Rad51 from ssDNA using an RPA-dependent ATPase activity, identifying it as an anti-recombination factor^{199,200}. However, further studies suggested that this function serves to promote SDSA by preventing aberrant Rad51 filament formation post strand displacement and possible dHJ formation⁵³. Additionally, RECQ5 depletion leads to increased Rad51 occupancy around breaks and elevated SCE formation in response to DNA damage, further corroborating its role in promoting SDSA^{53,194}.

This prompted the investigation of the interplay between RECQ5 and ATRX and their relative contributions to HR-mediated DSB repair. Here, we show that ATRX-deficient U2OS and Saos-2 cells are dependent on RECQ5 for the repair of IR-induced DSBs in G2, indicating the use of SDSA instead of the dHJ pathway. We also show that the ATRX-dependent dHJ is dominant over the SDSA pathway, and in contrast to previous reports, leads to a high CO frequency, amounting to 50% of HR events. We propose a model in which ATRX-mediated chromatin remodeling during repair synthesis likely promotes the formation of joint molecules that are refractory to both strand displacement and dissolution in favor of resolution. This unexpected pathway choice could be unique to DSBs induced in G2 phase and are distinct from how HR intermediates generated in S phase.

4.2 METHODS

4.2.1 Cell culture

Cell culture was carried out as described in section 2.2.1. Additionally, U2OS were cultured in DMEM supplemented with 10% FBS and 1% NEAA. Saos-2 cells were cultured in McCoy's 5A with 15% FBS. U2OS^{ATRX} cells with inducible ATRX expression were a gift from David Clynes²⁰¹ and were grown in DMEM with 10% tetracycline-free FBS, 700 µg/ml G418 sulfate, 0.5 µg/ml Puromycin and 1x glutamate. ATRX expression was induced by addition of 0.4 µg/ml doxycycline for 4 days. Immortalized human primary fibroblasts 82-6 hTert²⁰² cells were cultured in MEM supplemented with 20% FCS and 1% NEAA.

4.2.2 *siRNA, plasmid Transfection and inhibitors*

Transfections were carried out as described in section 2.2.2. For Rad51 inhibition, 60 μ M B02 were added 30 min prior to irradiation and maintained throughout the experiment. B02 interacts with Rad51 and prevents DNA binding and thereby the formation of Rad51 filaments, as confirmed by the reduction of Rad51 foci observed at 2 h post IR.

4.2.3 *X-ray irradiation*

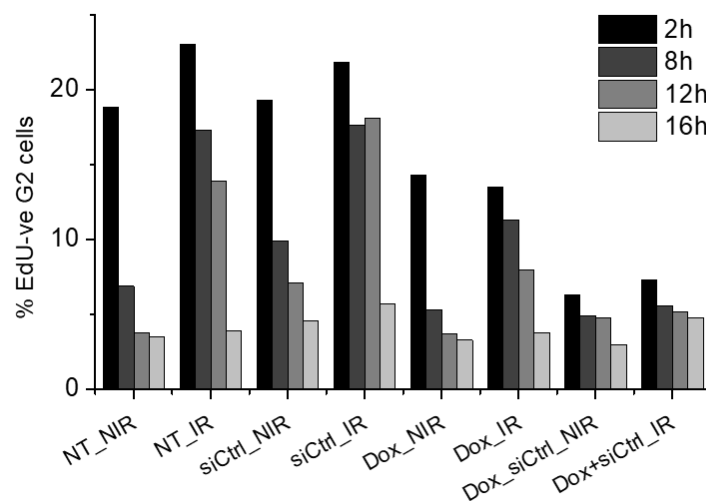
Damage by X-rays was performed as described in section 2.3.3.

4.2.4 *Immunofluorescence*

Immunostaining was carried out as described in section 2.2.5. Additionally, for mitotic cells analyses (UFB and Mus81 foci), cells were fixed with PTEMF buffer for 10 min and then permeabilized with 0.2% Triton X-100 in PBS for 5 min. For Mus81 foci colocalization studies, Z-stacks (Z-stack distance 0.3 μ M, 10 stacks per image) were acquired using 100x immersion objective and images were analyzed using Image J software.

4.2.5 *Sister chromatid exchanges analysis*

The SCE assay was carried out as previously described (section 2.2.10), with some modification. After irradiation, HeLa cells were collected after 8 hours while U2OS^{ATR_X} cells were collected after 16 hours due to slower exit from G2 into M phase (see below). 82-6 cells



U2OS^{ATR_X} cells with and without doxycycline-induced ATRX expression and/or siRNA transfection were labelled with EdU for 30 mins then irradiated with 2 Gy and incubated for distinct time points. Cells were stained for DAPI and EdU and scanned using Metapher system and the percentage of G2 cells was calculated for each sample. Reduction of G2 cells after IR indicates the release of the check point and progression into mitosis.

were treated with 100 nM of the Chk1 inhibitor UCN-01 for 3 hours instead of caffeine and collected at 9 h post irradiation to obtain sufficient mitotic cells. After fixation, to obtain the differential staining between the two sister chromatids, slides were then washed, incubated with 5 ug/ml bisbenzimid (Hoechst 33258) for 1 hour and then covered with 200 mM Na₂HPO₄ and 4 mM citric acid (pH 7.1-7.2) buffer and irradiated with UVC at 9 joule/cm². Slides were then washed in 2x SSC buffer at 50°C for 30 min then stained with geimsa. Chromosome spreads were captured and analyzed using a Zeiss microscope with Metafer software.

4.2.6 Ultra-fine bridges analysis

For the detection of UFBs, cells were transfected twice with siMus81 and siGen1 on two consecutive days to ensure optimal knockdown of both proteins. 48 h after the second transfection, cells were irradiated with 4 Gy and fixed with cold PTEMF buffer. Non-irradiated samples were fixed at 2 h and 8 h after EdU addition. After immunostaining, cells were scanned for DAPI intensities (mean and total intensities) and gated for anaphase cells. Cells in late anaphase were selected and DAPI-negative UFBs were counted and categorized as positive for RPA only, BLM only or both and plotted as an average of all cells analyzed.

4.2.7 SDS-PAGE and Immunoblotting

Immunoblotting was carried out as described in section 2.2.12

4.2.8 Bacterial transformation

Plasmid amplification and preparation was carried out as described in section 2.2.13

4.2.9 Quantification and statistical analysis

Data collection and analysis were carried out as described in section 2.2.14.

4.3 RESULTS

4.3.1 *ATRX and RECQ5 define two distinct sub-pathways of HR*

The requirement for ATRX in HR prompted the investigation of DSB repair in cells naturally lacking ATRX. Approximately 10-15% of all tumors rely on telomerase-independent pathway for telomere maintenance, known as ALT, and are strongly associated with inactivating mutations of the ATRX/DAXX/H3.3 complex, with the majority exhibiting loss of expression of the ATRX protein^{147,203}. To investigate how these cells perform HR, two known ALT cell line were used to characterize their DSB repair dependency: U2OS and Saos-2, both of which lack ATRX expression as previously shown^{147,150}. Assessment of γ H2AX foci in G2 phase U2OS cells 8 h post X-IR revealed levels similar to those previously observed in ATRX-positive HeLa cells (Figure 4.1 A, left panel). Depletion Rad51 resulted in significantly higher levels of γ H2AX compared to control cells, showing that these cells perform HR in an ATRX-independent manner. Depletion of the SDSA factor RECQ5 also resulted in elevated γ H2AX levels similar to those in siRad51-treated cells and inhibition of Rad51 in U2OS cells lacking RECQ5 did not result in a further increase, indicating that these cells rely on SDSA for all HR events (Figure 4.1 A, right panel). Transient expression of GFP-ATRX did not significantly affect γ H2AX foci levels in control U2OS, but rescued the repair defect in RECQ5-depleted cells, showing that ATRX can compensate for the loss of RECQ5-mediated SDSA. However, ATRX expression did not rescue the elevated γ H2AX levels observed in Rad51-depleted cells, consistent with Rad51 being upstream of two sub-pathways of HR defined by the factors ATRX and RECQ5. On the other hand, Saos-2 cells showed higher γ H2AX foci levels 8 h post X-IR than U2OS cells, suggesting delayed or impaired repair possibly due to ATRX deficiency (Figure 4.1 B). However, Rad51 and RECQ5 depletion further increased the number of γ H2AX foci to similar levels, indicating that these cells also employ SDSA but to a lesser extent than U2OS cells. Transient expression of GFP-ATRX rescued the elevated break levels seen in Saos-2 cells, confirming that those indeed reflected an impaired repair and that RECQ5 is not sufficient to compensate for ATRX deficiency. However, similar to U2OS cells, ATRX expression in Saos-2 cells rescued the repair defect observed after RECQ5, but not Rad51, depletion (Figure 4.1 B). Collectively, these results show that Rad51-mediated HR of IR-induced DSBs can proceed in two distinct sub-pathways that rely on ATRX and RECQ5 and their contributions vary in different cell lines, but ATRX seemingly can compensate for the loss of RECQ5 and could have a dominant role in this pathway choice.

To further characterize the HR sub-pathway used by cells lacking ATRX, several HR-related factors were depleted in U2OS and Saos-2 cells and γ H2AX foci levels were assessed in G2 cells 8 h post X-IR. Consistent with previous results, Rad51 depletion caused elevated γ H2AX foci numbers compared to control cells in both cell lines (Figure 4.1 C). Depletion of the SSA factor Rad52 and the histone variant H3.3 had no effect on foci levels, excluding a role for this pathway in G2 DSB repair and confirming that the histone variant H3.3 does not play an ATRX-independent function in these cells. Depletion of DNA synthesis factors RFC-1 and PCNA resulted in elevated foci levels albeit not to the same level as Rad51-depleted cells, suggesting a requirement for these factors in most, but not all SDSA events (Figure 4.1 C). Interestingly, depletion of the HR factor Rad54, shown to be required for the ATRX pathway¹⁵⁰, did not result in additional unrepaired DSBs in either cell line, indicating an independent mechanism for Rad51 removal. Strikingly, transient expression of ATRX in U2OS cells depleted for Rad54 resulted in the restoration of a repair defect similar to that reported in HeLa cells lacking Rad54⁴⁴ (Figure 4.1 D), suggesting a less hierarchical structure between the different stages of HR and perhaps a more planar, interconnected regulation. Finally, to compare these findings to the pathway choice in HeLa cells, γ H2AX foci were analyzed in control and RECQ5-depleted cells. HeLa cells treated with siRECQ5 showed only a slight elevation in unrepaired DSBs, considerably less than that observed ATRX KO cells (Figure 4.1 E). RECQ5 depletion in ATRX KO cells led to unrepaired DSBs similar to inhibition of Rad51, suggesting that ATRX- and RECQ5-dependent HR together account for the majority of all IR-induced HR events (Figure 4.1 E). Taken together, these findings point to the presence of two discrete HR sub-pathways that, despite sharing common upstream processes, seem to progress differently and utilize distinct factors. While it could be tempting to speculate a simple regulatory node of pathway choice downstream of Rad51 removal, it seems likely that a more complicated, interlinked system of regulation combining heteroduplex formation, Rad51 removal, DNA synthesis and chromatin remodeling is in place.

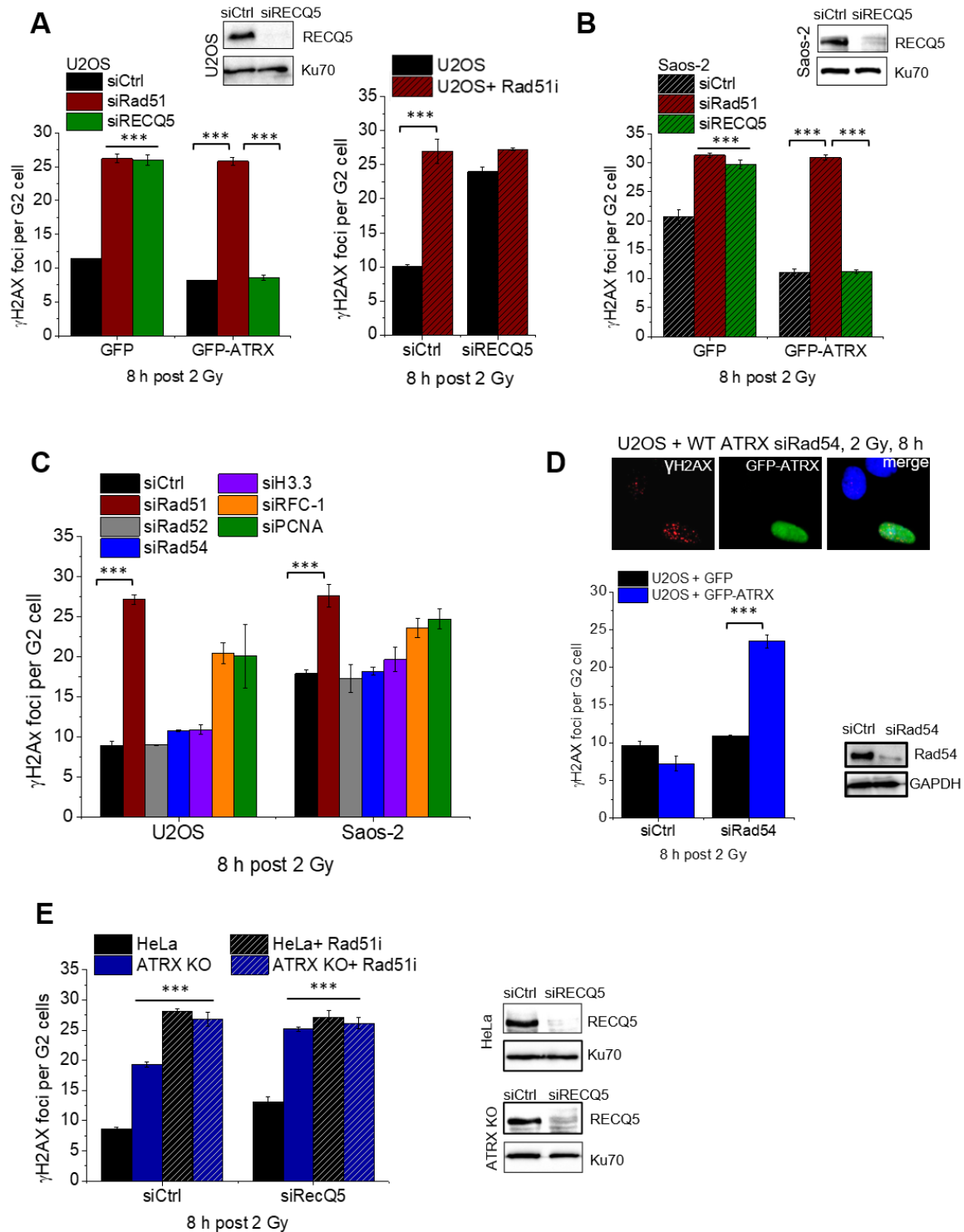


Figure 4.1. ATRX and RECQ5 define two distinct sub-pathways of HR.

(A) Left: U2OS were transfected with siCtrl, siRECQ5 or siRad51 and 24 h later were transfected with GFP-empty or GFP-ATRAX. After 24 h EdU was added for 30 min and cells were X-irradiated with 2 Gy and fixed after 8 h. γ H2AX foci were enumerated in GFP-positive, EdU-negative G2 cells. Right: Cells were treated with Rad51i prior to irradiation and throughout repair incubation. γ H2AX foci were enumerated in EdU-negative G2 cells. Mean \pm SEM (n=3); spontaneous foci were subtracted. Knockdown and plasmid transfection were confirmed by immunoblotting (also see Juhász *et al.* 2018).

- (B) Saos-2 cells were transfected with siCtrl, siRECQ5 or siRad51 and 24 h later were transfected with GFP-empty or GFP-ATRAX. After 24 h EdU was added for 30 min and cells were X-irradiated with 2 Gy and fixed after 8 h. γ H2AX foci were enumerated in GFP-positive, EdU-negative G2 cells. Mean \pm SEM (n=3); spontaneous foci were subtracted. Knockdown and plasmid transfection were confirmed by immunoblotting (also see Juhász *et al.* 2018).
- (C) U2OS and Saos-2 cells were transfected with the indicated siRNAs and after 48 h EdU was added for 30 min and cells were X-irradiated with 2 Gy and fixed after 8 h. Mean \pm SEM (n=3, except U2OS siPCNA and siRFC n=2, mean \pm SD); spontaneous foci were subtracted.
- (D) U2OS were transfected with siCtrl or siRad54 and 24 h later were transfected with GFP-empty or GFP-ATRAX. After 24 h EdU was added for 30 min and cells were X-irradiated with 2 Gy and fixed after 8 h. γ H2AX foci were enumerated in GFP-positive, EdU-negative G2 cells. Mean \pm SEM (n=3); spontaneous foci were subtracted. Knockdown was confirmed by immunoblotting.
- (E) HeLa and ATRX KO cells transfected with siCtrl or and after 48 h EdU was added for 30 min and cells were X-irradiated with 2 Gy and fixed after 8 h. Additionally, cells were treated with Rad51i prior to irradiation and throughout repair incubation. γ H2AX foci were enumerated in EdU-negative G2 cells. Mean \pm SEM (n=3); spontaneous foci were subtracted. Knockdown was confirmed by immunoblotting.

4.3.2 *ATRAX dominates over RECQ5 to promote high SCE frequency*

To further dissect how the sub-pathways interact, SCEs were analyzed, as a known product of the ATRAX pathway¹⁵⁰. To quantify the formation of SCEs that arise in response to G2-induced damage, U2OS cells that express ATRAX upon induction with doxycycline (U2OS^{ATRAX}) were used. This system was chosen to ensure that most cells expressed ATRAX, as transient transfections with the ATRAX construct have low efficiency and ATRAX-expressing cells cannot be specifically analyzed as in immunofluorescence studies. However, these cells showed a slower cell cycle progression, therefore the analysis was carried out 16 h post IR (see section 4.2.6). To this end, the DSB repair capacity of these cells was first confirmed. U2OS^{ATRAX} cells showed comparable repair profiles as in WT U2OS cells, as RECQ5 depletion caused a high number of residual γ H2AX foci in G2-irradiated cells, similar to Rad51 depletion (Figure 4.2 A). Likewise, ATRAX expression rescued the repair defect observed in RECQ5- but not Rad51-depleted cells. In agreement with previous findings, U2OS^{ATRAX} cells did not show IR-induced SCEs in the absence of ATRAX (Figure 4.2B, left panel). RECQ5 depletion only caused a slightly higher basal SCE levels but no IR-induced SCE formation. However, ATRAX expression resulted in a robust IR-induced increase in SCEs to the levels observed in HeLa cells, an effect which was enhanced after RECQ5 depletion. Similarly, elevated levels of IR-induced SCEs were observed in HeLa cells after depletion of RECQ5 (Fig 4.2B, right panel), which failed to form in ATRAX KO cells, indicating that all these events are ATRAX dependent. These results show that the ATRAX sub-pathway dominates over RECQ5-dependent SDSA, as cells form IR-induced SCEs even in the presence of RECQ5 and RECQ5 depletion has only a mild effect on SCE formation.

The seemingly high frequency of SCEs warranted a more quantitative comparison between the number of HR events promoted by each sub-pathway and the consequent formation of COs. For this, Rad51 foci were used as a more specific marker for HR. Total HR events were considered to be the net difference between the maximum number of Rad51 foci formed and the residual foci level at the end of the repair time, measured in ATRX-proficient HeLa and U2OS^{ATRX} cells. While the two cell lines had different kinetics, both showed similar numbers of Rad51 foci being maximally formed in the presence and absence of ATRX and/or RECQ5 (Figure 4.2 C). Residual Rad51 foci also did not vary in response to RECQ5 depletion in ATRX-proficient cells. HeLa cells showed slightly higher Rad51 foci levels, but the net number of 18-20 events is almost identical in the two cell lines. This estimate is in agreement with the increase in γ H2AX foci numbers after Rad51 depletion, assessed at 8 h in ATRX-proficient HeLa (Figure 4.1 C) or at 16 h post IR in U2OS^{ATRX} cells (Figure 4.2 A).

Since these results were derived from cancer cells and could be non-representative of 'normal' cells, similar analyses were carried out in 82-6 non-transformed human fibroblasts immortalized by the expression of human telomerase. γ H2AX foci assessment showed a dependence on Rad51 and ATRX, but not RECQ5, for the repair of G2-induced DSBs, consistent with results obtained in HeLa cells (Figure 4.2 D). IR-induced SCEs were observed in 82-6 cells (Figure 4.2 E) and represented a considerable number of HR events, as measured by Rad51 foci analysis (Figure 4.2 F).

Collectively, these analyses demonstrate that ATRX and RECQ5 define the two major HR sub-pathways for IR-induced DSBs with a more dominant role of ATRX compared with RECQ5 in cells proficient for both factors, with CO formation being a frequent event in G2-irradiated cells.

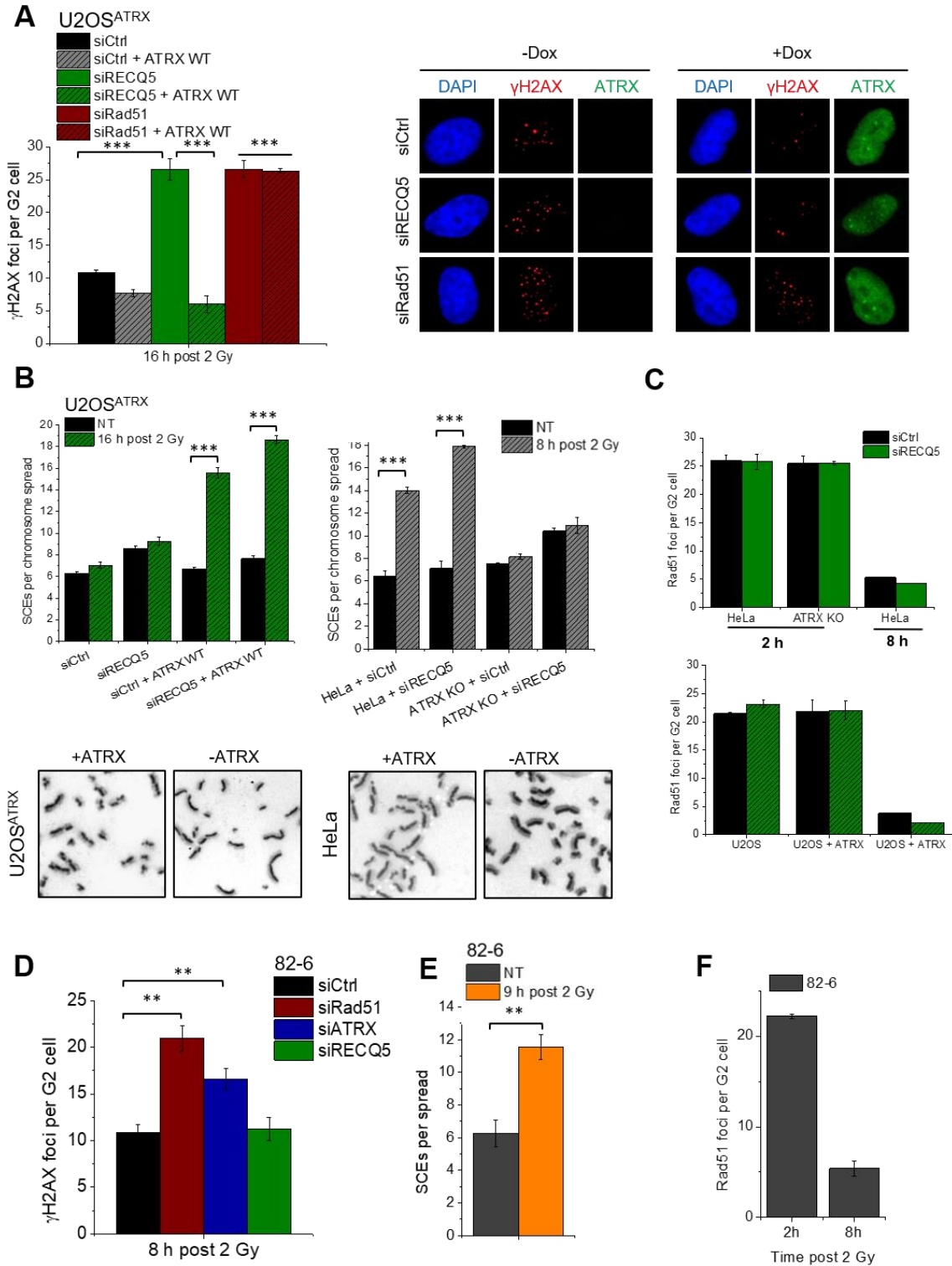


Figure 4.2. ATRX dominates over RECQ5 to promote high SCE frequency.

(A) U2OS^{ATRX} cells, with and without doxycycline-inducible ATRX expression, were transfected with siCtrl, siRECQ5 or siRad51. After 48 h, EdU was added for 30 min, cells were X-irradiated with 2 Gy and fixed after 16 h to reflect repair times of the SCEs measured in this system (Figure 4.3.2 B). γH2AX foci were enumerated in ATRX-positive, EdU-negative G2 cells and irradiated with 2 Gy. Mean ± SEM (n=3); spontaneous foci were subtracted.

- (B) Left panel: U2OS^{ATR_X} cells, with and without doxycycline-inducible ATRX expression, were transfected with siCtrl or siRECQ5 and incubated with BrdU for 48 hrs. Cells were then irradiated with 2 Gy, collected after 16 h and processed to obtain mitotic spreads and sister chromatid exchanges (SCEs) were quantified per spread. Right Panel: HeLa and ATRX KO cells transfected with siCtrl or siRECQ5 and incubated with BrdU for 48 hrs. Cells were then irradiated with 2 Gy, collected after 8 h and processed to obtain mitotic spreads SCEs were quantified per spread. Mean \pm SEM (n=3).
- (C) HeLa and induced U2OS^{ATR_X} cells were transfected with siCtrl or siRECQ5 and after 48 h EdU was added for 30 min and cells were X-irradiated with 2 Gy and fixed at early and late time points. Rad51 foci were enumerated in EdU-negative G2 cells. Mean \pm SEM (n=3); spontaneous foci were subtracted.
- (D) 82-6 cells were incubated with BrdU for 48 hrs then cells were then irradiated with 2 Gy, collected after 9 h and processed to obtain mitotic spreads. SCEs were quantified per spread. Mean \pm SEM (n=3).
- (E) 82-6 cells were incubated with EdU for 30 min and cells were X-irradiated with 2 Gy and fixed at 2 h and 8 h. Rad51 foci were enumerated in EdU-negative G2 cells. Mean \pm SEM (n=3); spontaneous foci were subtracted.
- (F) 82-6 cells were transfected with the indicated siRNAs and after 48 h EdU was added for 30 min and cells were X-irradiated with 2 Gy and fixed after 8 h. γ H2AX foci were enumerated in EdU-negative G2 cells. Mean \pm SEM (n=3); spontaneous foci were subtracted.

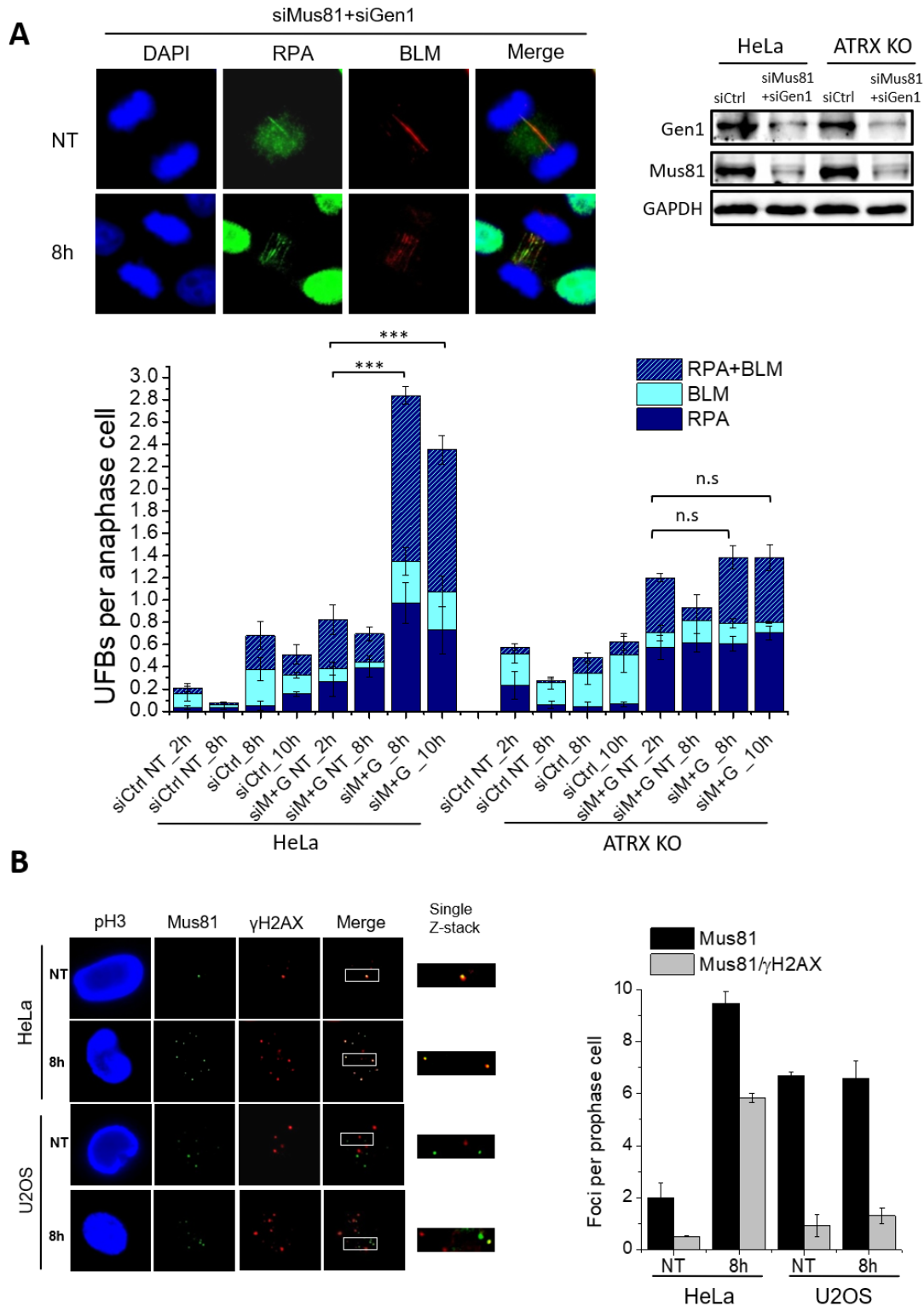
4.3.3 *ATR_X-dependent HR leads to the formation of IR-induced Mus81-dependent HR intermediates*

The high SCE frequency observed in the ATRX sub-pathway suggested a strong reliance on nuclease-dependent resolution of JMs formed after the completion of DNA synthesis. To further dissect these mechanisms characteristic of the ATRX pathway, the formation of HR intermediates in response to IR was analyzed. Several types of JMs can be visualized in anaphase/telophase cells as DAPI-negative ultra-fine bridges (UFBs) that immunostain positive for RPA and/or BLM²⁰⁴. Recently, HR-specific intermediates were shown to arise in cells depleted of Mus81 and Gen1, and increase following DNA damage that is repaired by HR²⁰⁵. To assess if such intermediates also arise in response to X-IR, HeLa and ATRX KO cells were treated with siMus81 and siGen1, irradiated with 4 Gy and analyzed for UFB formation (Figure 4.3 A). EdU was added to the cells before IR and maintained throughout the repair time, and only EdU-negative anaphase cells were analyzed to ensure the observed UFBs are specific to HR events in G2. HeLa cells treated with siCtrl exhibited a modest increase in UFBs 8-10 h post IR, indicating that joint molecules are indeed formed in response to DSB induction in G2 cells that manifest as UFBs in anaphase cells (Figure 4.3 A). Resolvase-depleted, unirradiated HeLa and ATRX KO cells showed an increase in UFBs compared to unirradiated siCtrl-treated cells, likely arising from S phase-generated joint structures and consistent with published data²⁰⁵. However, irradiated resolvase-depleted HeLa cells exhibited approximately a 4-fold increase in UFBs, demonstrating that IR-induced joint molecules are processed by

resolvases that can give rise to CO products (Figure 4.3 A). This increase was due to both a higher frequency of UFB-positive cells and more UFBs per UFB-positive cell (data not shown) and persisted until 10 h post IR. In contrast, ATRX KO cells failed to show such an IR-induced increase, in either siCtrl-treated or resolvase-depleted cells, indicating IR-induced UFBs require ATRX-mediated HR (Figure 4.3 A). Most bridges stained for RPA only or RPA plus BLM and a small fraction was positive for BLM only, with no considerable differences in staining patterns between the samples.

After establishing a primary role for Mus81 in resolving these HR structures arising in G2-irradiated cells, Mus81 localization to DSBs in response to irradiation was also analyzed. HeLa and U2OS cells were assessed for the recruitment of Mus81 to γ H2AX foci 8 h after X-IR (Figure 4.3 B). Since discreet Mus81 foci were difficult to visualize in G2 cells, mitotic prophase cells were analyzed, consistent with a peak of Mus81 nuclear localization at G2/M entry⁶⁴. HeLa cells exhibited a significant increase in Mus81 foci in response to irradiation, with approximately 60% co-localizing with γ H2AX foci (Figure 4.3 B). In contrast, U2OS cells did not show an IR-induced elevation of Mus81 foci levels, despite having significantly more foci than unirradiated HeLa cells. Furthermore, most Mus81 foci in both irradiated and unirradiated U2OS cells did not localize to γ H2AX (Figure 4.3 B), indicating their recruitment to structures other than DSB-derived intermediates, likely 3' flaps or other structures from replication-associated events.

Collectively, these data show that the ATRX sub-pathway promotes the formation of joint molecules whose structure requires resolution by structure-specific nucleases, resulting in the observed high CO frequency.



4.3. ATRX-dependent HR leads to the formation of IR-induced Mus81-dependent HR intermediates

(A) HeLa and ATRX KO cells were transfected twice on consecutive days with siCtrl or siMus81+siGen1. 48 h after the second transfection, EdU was added for 30 min and cells were X-irradiated at 4 Gy and fixed at 8 or 10 h. Non-irradiated cells were incubated with EdU for either 2 h or 8 h. Ultra-fine bridges (UFBs) were enumerated in EdU-negative late anaphase cells, and categorized as positive for: RPA-only, BLM-only or RPA+BLM. Mean \pm SEM (n=3).

Knockdown was confirmed by immunoblotting. Due to lack of sufficient cell numbers in some samples, statistical analysis was carried out for samples that had at least 30 cells per experiment.

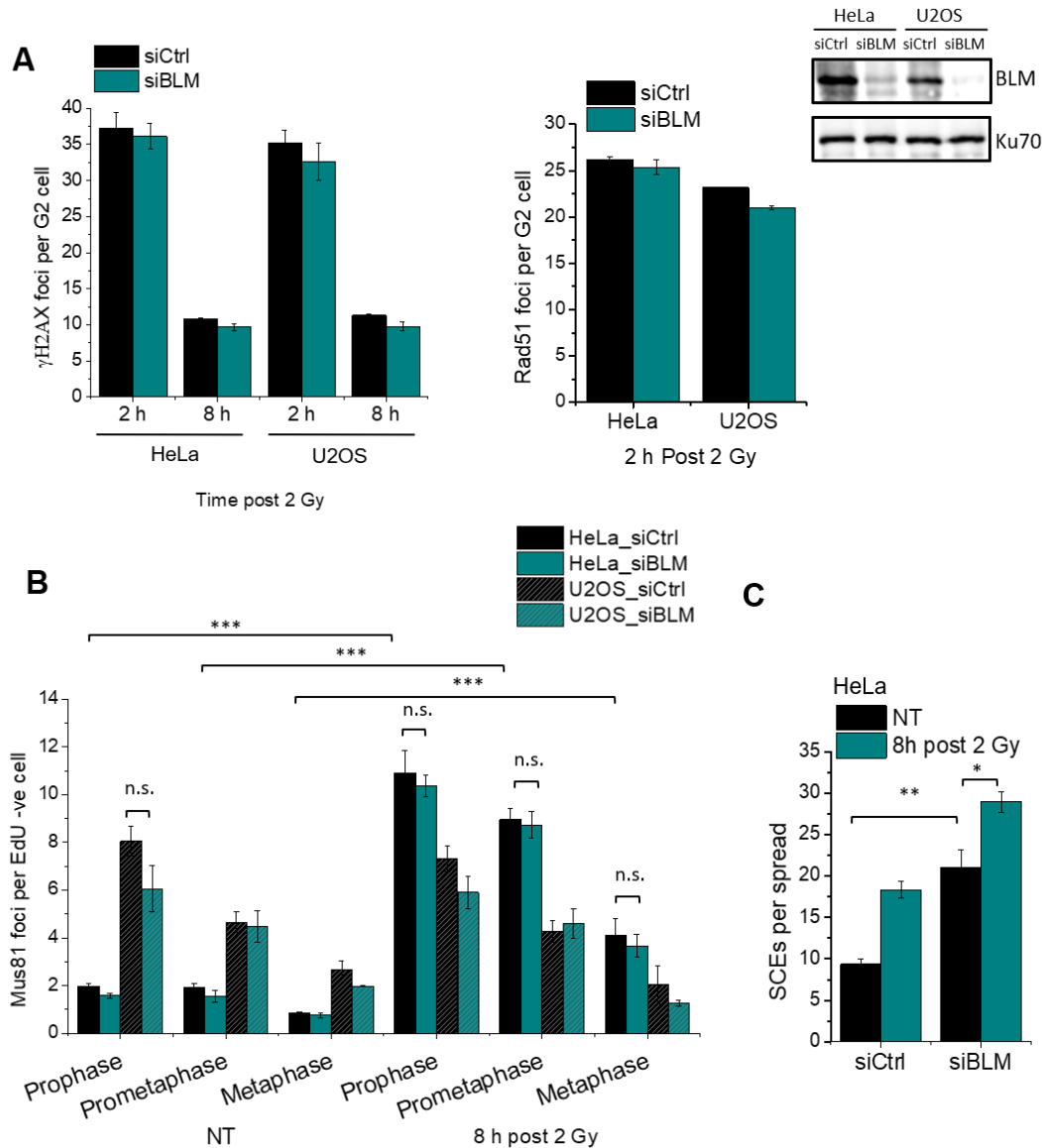
(B) HeLa and U2OS cells were incubated with EdU for 30 mins, X-irradiated with 2 Gy and fixed after 8 h. Prophase cells positive for the mitotic marker pH3 were selected and Z-stack images were captured and analyzed for Mus81 foci numbers and colocalization with γ H2AX foci.

4.3.4 *Processing of ATRX-dependent HR intermediates is BLM-independent*

Since HR intermediates can also be targeted by dissolution that prevents COs, the involvement of this pathway was investigated by targeting the BLM helicase. Since BLM has been reported to also be involved in resection¹⁵, the proficiency of HR was first tested in BLM-depleted cells. HeLa and U2OS cells treated with siBLM showed normal peak formation of Rad51 foci at 2 h post IR and similar γ H2AX foci levels at 2 and 8 h compared to controls cells, confirming that resection in G2 was unaffected and that repair could take place via HR (Figure 4.4 A). As BLM deficiency prevents UFB visualization using BLM or RPA immunofluorescence, this assay could not be used for the analysis of HR intermediate formation²⁰⁵. Instead, Mus81 foci formation was assessed in the absence of BLM, with increased levels expected to compensate for loss of the BLM function under investigation. Mus81 foci were enumerated in prophase, pro-metaphase and metaphase cells 8 h post 2 Gy in both HeLa and U2OS cells. As described above, HeLa cells exhibited a significant IR-induced increase in Mus81 foci in all mitotic stages, with the peak appearing in prophase cells, followed by a gradual decrease to metaphase (Figure 4.4 B). BLM depletion did not have an impact on Mus81 foci levels in any of the mitotic stages analyzed, suggesting that the resolvase already occupy all cleavable structures even in the presence of BLM. U2OS cells had similar numbers of Mus81 foci in both unirradiated and irradiated samples in all mitotic stages, which also decreased from prophase to metaphase (Figure 4.4 B). Depletion of BLM slightly decreased Mus81 foci in prophase cells, after which they stayed similar to control levels in prometaphase and metaphase cells. Therefore, in both cell lines, BLM depletion did not affect Mus81 foci localization, suggesting that these resolvases localize to distinct structures than the BLM dissolution complex.

Next, SCEs were assessed to test if the knockdown of BLM would lead to more IR-induced exchanges, as the unprocessed structures would then be resolved by nucleases. Consistent with literature, BLM depletion significantly increased SCE levels in unirradiated cells, which are known to be caused by the resolution of intermediates arising during S phase that are normally dissolved by the BTR complex (Figure 4.4 C)^{64,72}. BLM-depleted cells also exhibited an increase in SCEs in response to irradiation, but to an extent similar to BLM-proficient cells, indicating that BLM normally does not process G2-specific HR intermediates (Figure 4.4 C). These findings corroborate a model in which ATRX-dependent HR involves the formation of

HR intermediates that are exclusively processed by the resolution pathway and are refractory to dissolution by BLM, thereby giving rise to a high frequency of SCEs. This pathway is likely specific to the repair of DSBs, as BLM seems to maintain its S phase-related dissolution function.



4.4. Processing of ATRX-dependent HR intermediates is BLM-independent.

- (A) HeLa and U2OS cells were transfected with siCtrl or siBLM and after 48 h EdU was added for 30 min and cells were X-irradiated with 2 Gy and fixed at early and late time points. γ H2AX (left panel) Rad51 (right panel) foci were enumerated in EdU-negative G2 cells. Mean \pm SEM (n=3); spontaneous foci were subtracted. Knockdown was confirmed by immunoblotting.
- (B) HeLa and U2OS cells were transfected with siCtrl or siBLM and after 48 h EdU was added for 30 min and cells were X-irradiated with 2 Gy and fixed at 8h. Mus81 foci were enumerated in pH3-positive, EdU-negative mitotic cells. Mean \pm SEM (n=3).
- (C) HeLa cells were transfected with siCtrl or siBLM and incubated with BrdU for 48 h. Cells were then irradiated with 2 Gy, collected after 8 h and processed to obtain mitotic spreads and SCEs were quantified per spread. Mean \pm SEM (n=3).

4.4 DISCUSSION

4.4.1 *HR by SDSA and the dHJ pathway*

HR of two-ended DSBs can proceed by SDSA or the dHJ junction pathway. Key distinguishing features between the two sub-pathways are the extent of DNA repair synthesis and the potential for CO formation. SDSA is believed to involve only limited DNA repair synthesis prior to the strand displacement step that prevents COs. In contrast, following extended DNA repair synthesis, second end capture leads to the formation of a dHJ junction that can be dissolved or resolved with the potential for CO formation. RECQ5 has previously been implicated in SDSA while ATRX has been shown to promote extended DNA repair synthesis and CO formation^{53,150}. Analysis of cells with and without ATRX expression showed that RECQ5 and ATRX define distinct, competing HR sub-pathways which together account for the majority, if not all, HR events at two-ended DSBs. Furthermore, while these two sub-pathways rely on common essential factors, like Rad51, PCNA and RFC, only ATRX-dependent HR requires the histone variant H3.3, as expected. Surprisingly, the essential HR factor Rad54 was dispensable for HR in ATRX-deficient U2OS cells, showing that the regulation of pathway choice could be further upstream, before the DNA repair synthesis step. Rad54 is involved in the formation of the presynaptic filament, as well as homology search and D-loop formation, all of which could affect the final choice of sub-pathway. Interestingly, evidence from yeast studies suggests the formation of different species of D-loops that affect the repair outcome, regulated by distinct Rad54 paralogs, a situation that could be paralleled in mammalian cells, although specific assays to address this are still not available²⁰⁶.

4.4.2 *SCEs frequently arise in G2-irradiated mammalian cells*

Here, a quantitative comparison of Rad51-dependent HR events and SCE frequency was carried out in HeLa and U2OS^{ATRX} under the same conditions. γ H2AX foci analysis showed that Rad51 inactivation causes about 18-20 additional unrepaired DSBs compared with control cells, which was also confirmed by Rad51 foci analysis showing similar number of HR events in both cell lines (Figures 4.1 E and 4.2 A). Strikingly, both cell lines show an increase of approximately 8 SCEs above background level, which rise upon RECQ5 depletion to about 10 IR-induced SCEs (Figure 4.3 B). However, SCE formation is strictly dependent on ATRX as it is neither observed in ATRX KO nor in U2OS^{ATRX} cells without ATRX induction. Furthermore, ATRX-dependent HR seems to dominate over RECQ5-mediated SDSA, as evidenced by the robust formation of SCEs in cells where both factors are present.

Collectively, these data suggest that every second ATRX-dependent HR event leads to an SCE, a considerably higher frequency than previously thought, while RECQ5-dependent SDSA does not lead to SCEs, a notion consistent with published data^{53,194}. The most likely explanation for this observation is that ATRX promotes extended DNA repair synthesis which leads to second-end capture and the formation of a dHJ with a 50% likelihood to be resolved into an SCE. Thus, CO formation appears to be a frequent event in mammalian cells but necessitates the presence of ATRX. It is, therefore, not readily detected in ALT cells (e.g. U2OS cells) which are often used for cellular studies. Furthermore, HR reporter assays are typically restricted to the analysis of unequal recombination events, which are only a subset of total HR thereby potentially introducing a bias in sub-pathway choice. Therefore, since sister chromatids represent the natural substrates for HR events, SCE measurements arguably assess CO frequencies more reliably.

4.4.3 *ATRX-dependent HR intermediates are exclusively channeled into the resolution pathway*

The above analysis raises the question about the primary pathway used to deal with the ATRX-dependent HR intermediates and suggests that resolution strongly competes with dissolution. This idea was addressed by analyzing the formation of IR-induced UFBs that were shown to accumulate in resolvase-deficient cells and whose formation is dependent on ATRX. Additionally, the IR-induced recruitment of Mus81 to DSBs was only observed in ATRX-expressing HeLa cells, further corroborating the notion that the Mus81 and Gen1 resolvases play a major role in processing these HR intermediates. Furthermore, the SCE assay was employed to investigate the involvement of the BTR complex and showed no increase in IR-induced SCEs in the absence of BLM, precluding its function in processing these HR intermediates. Of note, in contrast to IR-induced SCEs, the spontaneous SCE level increases drastically upon BLM depletion, suggesting that they arise from different substrates, such as dHJs formed at single stranded gaps, or template switches after fork regression that are specifically handled by the BTR complex^{59,207}. Therefore, the regulation of how these substrates are handled could be more than just the temporally restricted activity of the enzymes, but through substrate specificity/affinity. This would be consistent with reports showing Mus81 being active in S phase, with roles in replication fork progression and stability^{63,72}. This also raises the intriguing possibility of the HR intermediates arising during DSB repair being distinct from the classical dHJ structure, such as nicked HJs or other substrates that are more suitable for resolution reactions (Figure 4.5 B).

4.4.4 *A role for chromatin in HR sub-pathway choice*

The above findings could be explained in light of the chromatin-remodeling function of ATRX, suggesting a novel consequence for *de novo* histone deposition during repair synthesis. It is possible that instead of histone deposition behind a moving D-loop, as initially proposed, this actually occurs within the D-loop and serves to 'chromatinize' the dsDNA regions consisting of the two single strands from both sister chromatids (Figure 4.4 A). Such a step would likely preclude strand displacement for SDSA and promote the dHJ pathway. This is reminiscent of the antagonistic effect of the chromatin remodeler CAF-1 on the RecQ-type helicase Rqh1 during repair synthesis observed in fission yeast, where chromatin assembly on the D-loop counteracts strand displacement and favors D-loop stability¹⁷⁴. This model could also explain the preferential use of JM resolution versus dissolution where ATRX-dependent histone deposition within an expanding D-loop would likely impede the merger of the two HJs that is a necessity for the decatenation reaction during dissolution. It is interesting to note in this context that the SDSA pathway often encompasses gene conversion tracts of less than 50 bp, while CO-forming pathways exhibit gene conversion tracts on the order of 500 bp^{190,191}. Thus, a single histone deposition event corresponding to about 200 bp of DNA might represent a commitment step to proceed with extended DNA repair synthesis and JM formation. A prediction of this second model is that the D-loop would grow in size when repair synthesis proceeds while it would likely remain constant when histone deposition occurs behind the migrating D-loop.

4.4.5 *Conclusion*

The data presented here show that ATRX and RECQ5 define two distinct HR sub-pathways for repairing two-ended DSBs, with ATRX being essential for the dHJ pathway and RECQ5 promoting SDSA. A quantitative comparison between the relative usages of ATRX- and RECQ5-dependent HR at DSBs suggests that the dHJ pathway outcompetes SDSA for the majority of HR events and leads to the formation of COs in approximately half of these events. The more extended DNA repair synthesis promoted by ATRX likely results in second-end capture and the formation of HR intermediates that are exclusively processed by resolvases, and are not subject to dissolution by BLM, and therefore constitute distinct substrates than those formed spontaneously during S phase. This highlights a potential role for chromatin remodeling in determining DSB repair outcomes. Furthermore, this work challenges the current belief that CO formation is largely suppressed in mammalian cells and the nature of HR intermediates formed during HR-mediated repair of DSBs and warrants reconsideration of

studies which addressed the question of HR sub-pathway usage by investigating ATRX-deficient cell lines.

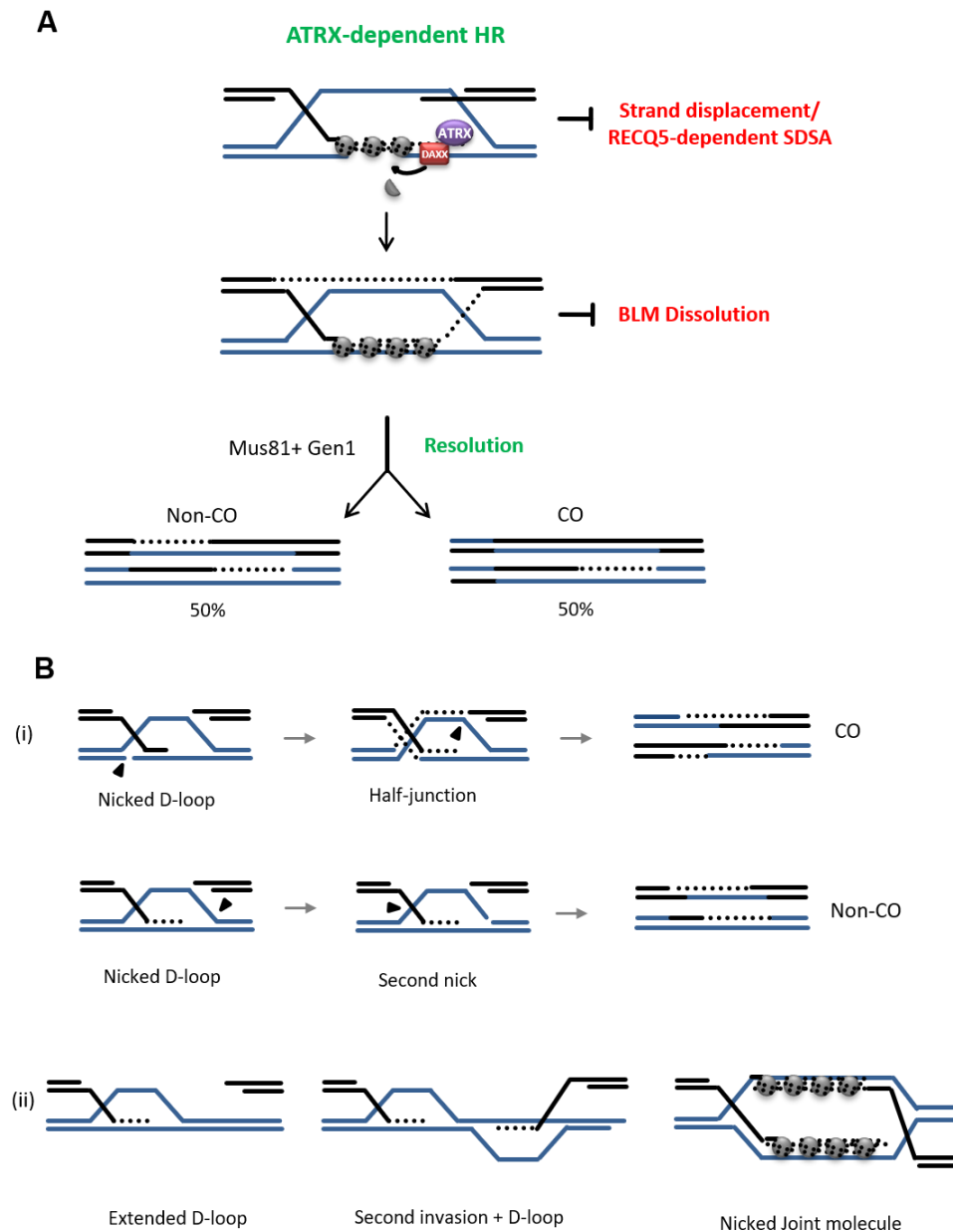


Figure 4.5. Model depicting the interplay between ATRX and RECQ5 to regulate distinct sub-pathways of HR.

(A) ATRX-mediated HR leads to chromatinized HR intermediates, which could preclude the action of helicases leading to strand displacement and thereby preventing SDSA. Upon the completion of DNA repair synthesis, the resulting dHJ is refractory to dissolution by BLM, thereby is subject to resolution by Mus81 and Gen1, leading to equal probability of CO and non-CO products.

(B) Alternative HR intermediates have been previously suggested³⁹ and could include (i) nicked D-loops, which upon cleavage by nucleases can result in CO and non-CO products. (ii) Alternatively, both ends can undergo strand invasion reactions leading to two D-loops that initiate DNA repair synthesis that can merge into a dHJ-like structure or can be processed independently by nucleases, where also the presence of histones could inhibit the action of helicases.

5. DISCUSSION

5.1 HR SUB-PATHWAYS AND THE FREQUENCY OF COs

The findings presented here provide new insights into the mechanisms of HR-mediated DSB repair and how sub-pathway choice is regulated. HR is vital for genomic stability and survival in proliferating cells, ensuring the faithful repair of DSBs, replication fork protection and restart as well as proper chromosome segregation in meiosis. Extensive research has focused on the initial step of end resection, which regulates the pathway choice between c-NHEJ and HR at DSBs and also plays an important role in replication fork recovery. In contrast, less is known about later steps during HR, and specifically the choice between SDSA and the dHJ sub-pathways. One reason for this could be the lack of assays that monitor specific stages in mammalian cells *in vivo*, such as homology search, D-loop formation and HJs, leading to most knowledge being generated from yeast or *in vitro* systems. Perhaps more importantly, it is generally believed that SDSA is the main HR pathway in somatic cells, a conclusion derived from the lack of CO detection in cell systems. This is consistent with the notion that CO are mutagenic, and therefore should be avoided, as strand exchange with a homologous chromosome leads to LOH, a cancer-driving event. The historical model of DSB repair was first introduced based on meiotic recombination, a process that is inherently skewed towards crossing over and therefore COs were subsequently viewed as meiosis-specific events ²⁰⁸. However, just as they were detected in meiotic cells, dHJs were also detected during recombination repair in somatic cells, albeit to a much lesser extent, thereby showing they are not exclusive to meiosis and supporting their relative scarcity compared to SDSA ⁵⁸. These observations were derived from yeast cells, and a comparable analysis in mammalian cells has not been carried out, making it difficult to draw conclusions of similarity. Studies in mammalian cells, however, rely mainly on reporter assays, in which unequal sister chromatid recombination is measured, since equal exchanges with the sister chromatid are genetically indistinguishable ^{2,184}. Although these studies provided essential information, such as the preference of the sister chromatid during HR repair of DSBs, they also have shortcomings. First, only “successful” clones, i.e. those expressing the selection gene (antibiotic resistance or GFP), are analyzed thereby ignoring other events on the genetic level that may not give rise to a positive clone. Second, the analysis of events that rely on unequal exchanges also skews the observations to a minor subset of events, as the majority of SCE events have been shown to be equal exchanges ²⁰⁹. Third, the introduction of an artificial construct could disrupt the

chromatin organization surrounding the DSB thereby influencing repair dynamics, a notion supported by multiple studies showing that the pre-existing chromatin state surrounding a DSB, especially enzyme-induced ones, can influence pathway choice^{106,132}. Additionally, many of the cell reporter assays were established in U2OS cells, which the current study argues have already an HR-defective background, thus further skewing the results. An alternative method to measure SCEs is through the cytological visualization of differential staining on chromosome spreads and therefore detect COs with the genetically identical sister chromatid that represents the natural recombination partner²¹⁰. This approach was used to show that SCEs arise consequent to the irradiation of G2 cells, in a manner dependent on HR factors and extended DNA synthesis^{44,150,164}. These IR-induced SCEs arise differently from spontaneous SCEs, which can still be detected in the absence of some HR factors, and have been also been suggested arise from non-DSB lesions^{211–214}. These observed SCEs, which increase dramatically in the absence of the helicase BLM, are likely to arise from HR intermediates arising in S phase-related lesions such as post-replicative ssDNA gaps^{212,213}. Therefore, it is becoming clear that distinct mechanisms of HR operate at DSBs in somatic cells, at replication-associated lesions, and during meiosis, and therefore a generalized pathway cannot be assumed.

5.2 CHROMATIN REMODELING AND REGULATION OF REPAIR OUTCOME

In the model proposed here, chromatin remodeling and histone deposition play an important, previously unappreciated, role in HR. In this model, the chromatin remodeler ATRX promotes DNA synthesis after D-loop formation by directing simultaneous *de novo* histone H3.3 deposition. This pathway leads to the formation of COs in approximately 50% of HR events in G2, a high frequency caused by the suppression of two CO-counteracting pathways. ATRX-mediated HR dominates over RECQ5-dependent SDSA and channels repair towards the formation of JMs that are exclusively cleaved by Mus81 and Gen1 and seem to be refractory to dissolution by BLM. One explanation for these observations is that nucleosome assembly takes place inside an expanding D-loop where the wrapping of DNA around histones could physically impede helicase activity, thereby suppressing the action of both RECQ5 and BLM. However, a growing D-loop, in contrast to a migrating one, would cause an increasing buildup of positive torsional stress necessitating topoisomerase activity to allow extended DNA synthesis. This possibility has not been explored yet although there are reports of Sgs1-independent functions of the yeast top3 at this stage of HR, but in the context of D-loop disruption^{49,215}. Alternatively, these JMs could represent structures distinct to HJs, which would not be appropriate substrates for BLM, and thereby require cleavage by nucleases. These

could include nicked D-loops or HJs, or simply extended D-loops where both ends of the break engage in invasion and synthesis steps, which would also preclude the need for an independent second-end capture, for which a promoting factor has not been identified. How these structures would suppress SDSA, however, is not clear. While RECQ5 is shown to remove Rad51 from ssDNA, whether it can also dismantle D-loops in mammalian cells, like yeast Srs2, and if this function is necessary for its SDSA role, have not been shown. It would be interesting to understand how RECQ5 promotes SDSA in a manner that is counter-acted by ATRX. The finding that the two sub-pathways employ different factors, including Rad54, raises the intriguing possibility that the pathway choice is determined earlier than the DNA synthesis step. Recent evidence from yeast studies using an *in vivo* D-loop assay showed the formation of two distinct and non-overlapping species of D-loops that are targeted specifically by distinct helicases, Srs2 on one type and Mph1 and STR on the other²⁰⁶. These helicases disrupt nascent D-loops as a part of a “quality control” mechanism to ensure recombination with the correct template, and delay the formation of extended D-loops. However, this process is regulated by the Rad54 paralog Rdh54, that functions to promote the formation of one type of Mph1-specific substrates at the expense of Srs2-specific targets. This role seems to be in part imposed by influencing the length of the homology used for D-loop formation, a proposed distinguishing feature between the two species. A competition between Rad54 and Rdh54 is also possible, as Rdh54 has been shown to block Rad54-mediated hDNA formation³⁶. While carrying this model over to human cells is not straightforward, a possible scenario is one where Rad54 and its paralog Rad54B can mediate the formation of distinct D-loops that give rise to different outcomes mediated by sub-pathway-specific factors. Although Rad54B is similar to Rad54 in structure and biochemical properties, they have non-overlapping roles *in vivo*²¹⁶. While the upstream effectors of this choice, like homology length, are unknown, the presence of ATRX seems to be important and could pertain to two separate functions, one in possibly stabilizing Rad54-mediated D-loops and excluding disrupting helicases, and another in promoting DNA synthesis through histone deposition. Delineating these functions in details requires *in vivo* assays that are not yet available to allow separate analysis of D-loop formation, maturation and extension. Alternatively, ATRX and Rad54 could cooperate in a DNA synthesis-dependent regulation of Rad51 removal, where ATRX-PCNA interaction could necessitate Rad54-mediated completion of D-loop processing to finish repair. Interaction with PCNA would then be an important node of regulation, which is an interesting possibility given that RECQ5 has been shown to interact with PCNA during replication-transcription conflicts²¹⁷, an interaction that has not yet been explored in its SDSA function. This would be analogous to the SUMO-

regulated Srs2-PCNA interaction observed in yeast in this process, and could shed some light as to how pathway choice is regulated in human cells ⁵¹.

5.3 PATHWAY CHOICE AND THE FIDELITY OF HR

The dominance of a CO-promoting sub-pathway raises questions regarding the fidelity of HR and why this pathway is preferred. One point of consideration is the view that COs harbor the risk of LOH and chromosomal rearrangements. These would occur in the case of recombination with a homologous chromosome, where a genetic exchange would lead to loss of genetic information or with a non-allelic locus leading to a translocation. However, HR in somatic cells is primarily restricted to the sister chromatid, which requires cohesion formation between the two molecules. This process is normally regulated during S phase by the loading of cohesin molecules that ensure the association of sister chromatids in close proximity and is important for proper chromosome segregation ²¹⁸. However, an independent post-replicative loading of cohesin has been shown in response to DNA damage as part of recombinational DNA repair, highlighting the importance of correct sister chromatid alignment in this process ^{219,220}. Interestingly, ATRX has been linked to the maintenance of cohesion at both telomeric and internal DBSs, as its depletion leads to misalignment of chromosomes and mitotic defects ^{221,222}. However, it remains unknown if this role is related to its chromatin remodeling activity and the maintenance of chromatin structure and epigenetic marks, or to an additional function related to cohesin protein loading. If ATRX assumes a similar role in internal DSB repair in G2 cells, this would intricately link this CO pathway to sister chromatid HR, minimizing the risk for inter-homolog recombination and thereby LOH; however, this possibility is yet to be investigated. While ensuring the use of the sister chromatid during HR reduces the mutagenic effects of this sub-pathway, it does not eliminate them, as the formation of joint molecules confers the risk of chromosomal aberrations if they are not resolved in a timely manner ²⁰⁵. Therefore, it would be reasonable to expect that the usage of SDSA might harbor an intrinsic higher risk for incorrect repair if an alternate pathway is preferred. An interesting perspective to consider is the evolution of HR as a pathway to repair one-ended breaks arising in S phase, when replication forks encounter SSBs and collapse ²²³. The repair of these breaks requires HR, as described earlier, through the error-prone BIR process. However, one-ended DSBs can be converted into two-ended DSBs by the convergence of an opposite fork, generating the second end. In this case the second end serves as flag mark for the presence of compatible break ends for faithful repair. Therefore, processes that require the capture of the second end for completion, such as the dHJ pathway, could be preferred. Since SDSA does require the

presence of a second end and the generation of a joint structure, the invading strand can be displaced before the proper annealing partner is generated. Thereby there is a risk that two non-compatible ends, i.e. from different one-ended breaks, are used to complete repair, leading to chromosomal rearrangements (Figure 5.1). Therefore, the synchronization of the HR pathway usage together with the generation of the second end of a DSB serves to limit these aberrations and is compatible with the temporal overlap between late stages of HR and the completion of the replication. With this model in consideration, the formation of largely genetically-neutral CO could actually be less mutagenic than non-CO events that harbor a higher risk of

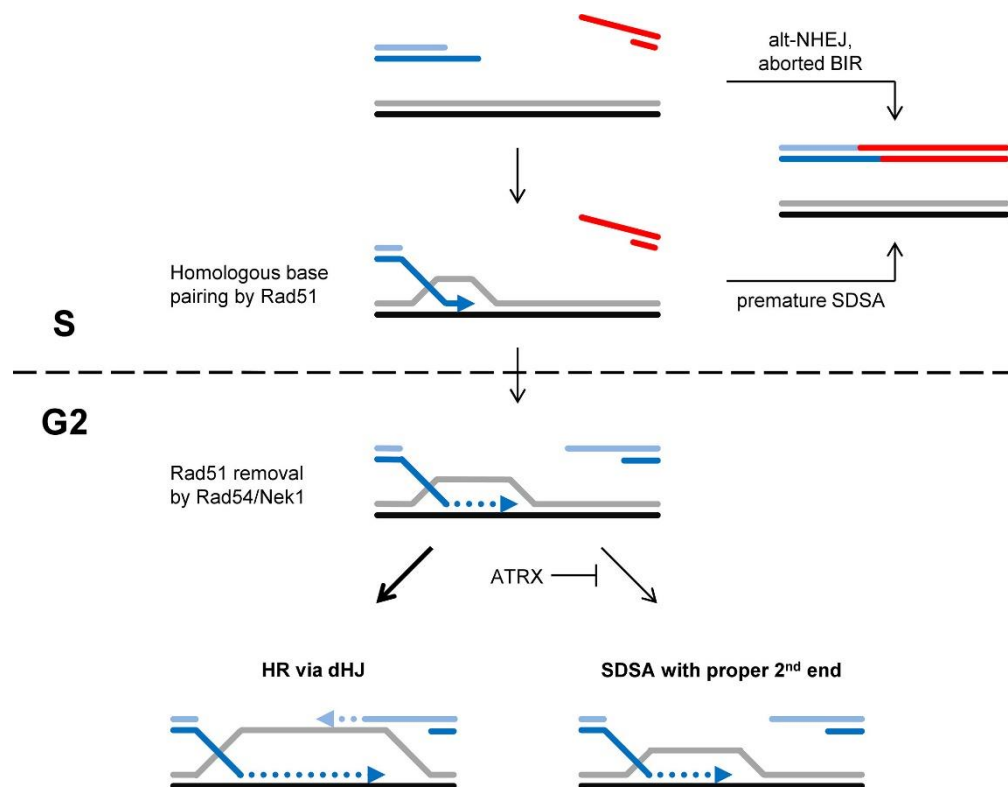


Figure 5.1. Repair of one-ended breaks and formation of chromosomal rearrangements. Repair of one-ended breaks by BIR or premature SDSA (prior to formation of the second end) can lead to the formation of chromosomal rearrangements if annealing occurs with the non-compatible end. Generation of the second end by a converging fork allows for more accurate repair by either of the sub-pathways of HR, where the dHJ sub-pathway inherently controls for the presence of the second end, reducing the risk of rearrangements. (Figure extracted and modified from *Ensminger and Löbrich, 2020*).

chromosomal rearrangement. In this context also, SDSA could be viewed to have evolved as a quality control pathway to displace incorrectly formed or harmful HR intermediates, as shown for Srs2-mediated removal of BIR-mediated toxic joint molecules²²⁴. It is worth noting that processes involving one break end seem to be inherently error-prone, exemplified by BIR, which is known to induce genomic rearrangements due to frequent template switching and

unchecked extensive DNA synthesis. BIR is also usually suppressed and is out-competed by DSB repair in the presence of a second end. Another more recently-described process that is the basis of large-scale genomic alterations involves the simultaneous invasion of two intact molecules by a third broken end, to cause what is termed multi-invasion-induced rearrangements (MIR) ²²⁵. Resolution of these JMs could lead to the formation of two additional DSBs that, with the potential to initiate more MIRs, would result in the propagation of chromosomal rearrangements or insertions. These processes also result from one-ended breaks, a subset of which could be BIR intermediates and have been proposed to explain the occurrence of clusters of large-scale genomic rearrangements, formation of genomic structural variants through non-allelic recombination in repeat regions as well as specific unexpected features of meiotic and mitotic DSB repair ²²⁶. Taken together, emerging evidence challenges long-standing views of HR as a strictly error-free pathway of DNA break repair where the original black and white picture develops more shades of grey. The presence of multiple sub-pathways of HR indicates the need for different context-specific mechanisms that deal with lesions according to nature of the break, cell cycle phase, chromatin structure and probably damage load with a general propensity of minimizing errors and maximizing repair, in a system that is not fail-safe. Delineating the regulation of HR pathways choice and the mutagenic risk associated is needed to refine our understating of the processes governing genome stability and would provide a blueprint for mapping out associated disease risk, diagnostics and therapeutic strategies.

5.4 HR SUB-PATHWAY CHOICE: CLINICAL RELEVANCE

The findings described here could have important clinical implications for diseases associated with mutations in the ATRX/H3.3 axis. As described above, H3.3 is mutated in a variety of neurological and endocrine tumors and is associated with high-risk cancers ²²⁷. Additionally, ATRX is mutated in the majority of ALT tumors that rely on an HR-based mechanism of telomere elongation instead of telomerase reactivation. In fact, re-expression of ATRX in ALT cells is sufficient to suppress the ALT phenotype in a manner dependent on DAXX and H3.3, highlighting the importance for the histone deposition aspect in this function ²⁰¹. While the finding that ATRX is required for HR, but is also almost exclusively deficient in cells that rely on HR for survival seems paradoxical, considering that in light of HR sub-pathway choice and outcome may provide a better understanding of the process. ALT recombination is initiated by telomeric DSBs resulting from the structural instability of telomers, shown to be exacerbated in the absence of ATRX, which normally functions to maintain a heterochromatic state in these

repetitive regions ²²⁸. These one-ended breaks would then initiate recombinational repair through a BIR-like mechanism, where the template used can be the same telomere, the sister telomere, a telomere on another chromosome or extra chromosomal telomeric sequences, necessitating high telomeric mobility ^{83,229}. Therefore, it was believed that ATRX loss leads to the initiating events for telomeric recombination and elongation. However, since the inactivation of ATRX alone is not sufficient to initiate ALT, there seems to be an additional function that contributes to ALT suppression observed upon ATRX re-expression. In light of findings described here, one potential role could be the repair of these breaks, where ATRX would be promoting a pathway choice switch towards a less promiscuous DNA repair mechanism that would not support telomere elongation and/or suppress BIR. Indeed, a recent study showed that ATRX is involved in the repair of enzyme-induced telomeric breaks, where this function, together with the maintenance of telomeric sister cohesion is needed to suppress ALT ²²². The model proposes that ATRX mediates “in-register” DNA repair by restricting the template to a properly-aligned sister, and suppressing ectopic BIR with misaligned and/or non-sister telomeres and therefore no net gain of telomere length is achieved. How or if this telomeric DSB repair resembles repair at internal breaks is not clear, but it likely involves a similar mechanism of histone deposition, since H3.3 is required for suppressing the ALT pathways as well. Therefore, it is clear that HR sub-pathway choice has wider implications in understanding the initiation and progression of tumors that have mutations or are deficient in these factors which can be utilized for therapeutic purposes. For example, the reliance on alternative pathways for repair of radiation-induced DSBs can provide a therapeutic window for selectively targeting cancer cells. Additionally, understanding of how these pathways are regulated in the repair of other lesions, such one ended-breaks induced by agents often used in chemotherapy would also provide a wider, more detailed frame for therapeutic targeting.

5.5 CONCLUSION AND OUTLOOK

The findings presented above provide insights into the regulation of the late stages of HR at DSBs and sub-pathway choice. HR can proceed via RECQ5-dependent SDSA or a dHJ pathway promoted by ATRX, which are distinct in the extent of DNA repair synthesis and the propensity for CO formation. ATRX promotes extended DNA repair synthesis through the simultaneous deposition of H3.3 at sites of damage, which is necessary for repair completion. This involves the formation of HR intermediates that are exclusively resolved by the structure-specific nucleases Mus81 and Gen1, resulting in CO formation at a 50% frequency. These JMs are not subject to dissolution by BLM, which could be explained by histone deposition within an expanding D-loop that would physically hinder BLM-mediated strand separation. These JMs could be dHJs or alternative structures that are more suitable substrates for resolution. Histone deposition could also prevent strand displacement at earlier steps that would otherwise promote SDSA and CO suppression and would explain the dominance of ATRX-mediated HR over RECQ5-dependent SDSA for repair of DSBs. However, the high frequency of observed SCEs in the ATRX sub-pathway challenges established views that COs are generally suppressed in mammalian cells and calls for further investigation of how this process is regulated to minimize mutagenic events. Although SDSA harbors a smaller risk of genetic exchange with a homologous chromosome, and possible LOH, premature strand displacement, e.g. during S phase and before a matching second end is generated, carries a great risk for chromosomal rearrangements. Therefore, the fidelity of both sub-pathways is in questions and the regulation of this choice is critical for the fate of the cell. The choice between HR sub-pathways seems to require distinct factors and may occur earlier than the DNA synthesis step is completed. Multiple questions still stand, such as how does ATRX dominate over RECQ5 and if there is a role for Rad54 in this process. An intriguing possibility is a possible PCNA interaction node, as both proteins have been shown to interact with the clamp. It is also interesting to unravel the JM formed by the ATRX pathway, if it is a distinct structure to a dHJ and if there are additional factors required for its processing. Furthermore, the exact role of histone deposition at breaks and if PTMs play additional functions in sub-pathway choice, epigenetic marking or factor recruitment is still unclear. If such a node of regulation also exists during the repair of one-ended breaks, or other replication-associated lesions remain to be determined and could be critical to extend these findings to a clinically-applied setting.

6. MATERIALS

6.1 CONSUMABLES

Item	Vendor
Blotting paper, 703	VWR
Cell culture dishes (35x10 mm, 60x20 mm, 100x20 mm)	nunc™ VWR
Cell culture flasks (25 cm ² , 75 cm ²)	TPP
Cell Culture 6-well plates	TPP
Cover slips	Roth
Centrifuge tubes (15 ml, 50 ml)	Greiner
Kim Wipes	NeoLab
Micro tubes (1.5 and 2 ml)	Roth
PCR tubes	Greiner
qPCR 96-well plates	ABI
Microscope slides superfrost	Roth
Parafilm	Bemis
Pasteur pipettes, Plastic and glass	Roth
Plastic Pipettes (5 ml, 10ml, 25ml)	Sarstedt
Pipette tips	Sarstedt
Pipette tips, filtered	Roth
PVDF membrane	Thermo Scientific
Nitrocellulose membrane	GE Healthcaere
μ-slide IV	Ibid
microTUBE AFA Fiber Pre-Slit Snap-Cap	Covaris

6.2 LAB EQUIPMENT AND SOFTWARE

Item	Instruments	
	Model	Vendor
Agarose gel electrophoresis set	Horizon 58; 11-14	Life Technologies
Camera system (microscope)		AxioCamMRm Zeiss
Cell counting chamber	Neubauer improved	Marienfeld Superior
Centrifuge	Biofuge pico	Heraeus
Centrifuge	5451 R/5804 R	Eppendorf
Chemiluminescence detection	Fusion FX Vilber	Lourmat
Laser	LuxXdiodelaser	Omicron
Microscope	Axiovert 200M	Zeiss
Microscope	Observer.D1	Zeiss
Microscope	Imager.Z2	Zeiss

Microscope (cell culture)	Eclipse TS100	Nikon
Nano Photometer	P-Class	Implen
Nanophotometer	P-Class	Implen
pH Meter	pMX2000	WTW
Power supply	PowerPac™HC	BIO-RAD
Real Time PCR system	StepOnePlus	Applied Biosystems
Scale	TE 1502S/TE 153S-DS	Sartorius
Shaker	3011	GFL
Sonicator	S220 Focused Ultra Sonicator	Covaris
Thermal Cycler	Thermocycler	PeqLab
Thermomix	Comfort	Eppendorf
Vortex	Vortex genie2	Scientific Industries
Water bath	1083	GFL
Western blotting system	Mini Trans-Blot® Cell	BIO-RAD
X-Ray tube	MCN 165/796704	Philips

Software

Item	Vendor
Metafer4	MetaSystems
PhoxX Controller Software	Omicron
Micro-Manager	Open Source
AxioVision V4.6.3.0	Zeiss Imaging Solutions
ImageJ	Open Source
OriginPro 8.6	OriginLab
ChemiCapt	VilberLourmat
FusionCaptAdvance FX7	VilberLourmat
SonoLab 7.2	Covaris
StepOne™ and StepOnePlus™ Software v2.3	Applied Biosystems
Serial Cloner 2.6.1	SerialBasics

6.3 CHEMICALS

Chemical	Vendor
Acridine orange	Sigma-Aldrich
Agar	Roth
Agarose	Roth
APS	Roth
Bisbenzimid (hoechst 33258)	Roth
Blasticidin S Hydrochlorid	Thermo Fischer
BrdU (1 mM)	BD Bioscience
Bromophenol blue	Roth
BSA	AppliChem

CaCl ₂	Roth
Caffeine	Roth
Crystal violet	Sigma-Aldrich
10x Cell lysis buffer	Cell signalling
DAPI	Sigma-Aldrich
DMSO	Sigma-Aldrich
EDTA	Roth
EdU (10 mM)	Invitrogen
EGTA	Roth
Ethanol	Roth
G418 (Geneticin)	Sigma-Aldrich
Geimsa	Sigma-Aldrich
Glacial acetic acid	Sigma-Aldrich
Glycerin	Roth
Glycine	Roth
37% HCl	Roth
Immersion oil	Zeiss
Isopropanol	Roth
Kanamycin	Sigma-Aldrich
KaryoMAX Colcemid	Thermo Fischer
KCl	Roth
KH ₂ PO ₄	Roth
MEM	Sigma-Aldrich
Methanol	Roth
MgCl ₂	Roth
MMC	Roth
MMS	Merck
Mounting medium Vectashield®	Axxora Alexis
Na ₂ HPO ₄	Roth
NaCl	Roth
NaOH	Roth
NEAA (Non-essential amino acids)	Biochrom
Opti-MEM (Reduced serum MEM)	Life Technologies
10% FA (Formaldehyde)	Roth
PIPES	Roth
Protease inhibitor 25x Complete	Roche
Puromycin	Sigma-Aldrich
Roti Block for IF	Roth
Roti Block for WB	Roth
Roti-Safe GelStain	Roth
SDS	Roth
SNAP- Cell Block	New England Biolabs
SNAP-Cell- Oregon Green	New England Biolabs
β-Mercaptoethanol	Sigma-Aldrich
Sucrose	Roth
TEMED	Roth

tetracyclin-free FBS	Takara
Tris	Roth
TritonX-100	Roth
Trypsin	Roth
Tween®20	Roth

6.4 OLIGONUCLEOTIDES (siRNA AND PRIMERS)

siRNA

Target	Target Sequence	Concentration	Vendor
ATRX	5'-GAGGAAACCTTCAATTGTATT-3'	30 nM	QIAGEN
BLM	5'-AAGCTAGGAGTCTGCGTGCGA-3'	25 nM	QIAGEN
BRCA2	5'-TTGGAGGAATATCGTAGGTAA-3'	30 nM	QIAGEN
CAF-1 (p60)	5'-AAGCGTGTGGCTTTAATGTT-3'	25 nM	QIAGEN
DAXX	5'-AAGCCAAGCTCTATGTCTACA-3'	30 nM	QIAGEN
Gen1	5'-AAGCGTAATCTTGGTGGGAAA-3'	25 nM	QIAGEN
H3.3A	5'-AACTACAAAAGCCGCTCGCAA-3'	30 nM	QIAGEN
H3.3A_2	5'-GAGAAATTGCTCAGGACTT-3'	30 nM	QIAGEN
H3.3B	5'-AAGCTAAGAGAGTCACCATCA-3'	30 nM	QIAGEN
H3.3B_2	5'-CAGAGGTTGGTGAGGGAGA-3'	30 nM	QIAGEN
HIRA	5'-AAGGAGATGACAAACTGATTA-3'	20 nM	QIAGEN
Mus81	5'-AACAGCCCTGGTGGATCGATA-3'	25 nM	QIAGEN
Negative control	5'-AATTCTCCGAACGTGTCACGT-3'	20 nM	QIAGEN
PCNA	5'-CGGTGACACTCAGTATGTC-3'	25 nM	QIAGEN
Rad51	5'-AAGGGAATTAGTGAAGCCAAA-3'	25 nM	QIAGEN
Rad52	M-011760-01-0020	20 nM	Dharmacon
Rad52_2	5'-CCAACGCACAACAGGAAACTT-3'	20 nM	QIAGEN
Rad54	5'-GAACTCCCATCCAGAATGATT-3'	25 nM	QIAGEN
RFC-1	L-009290-00	25 nM	Dharmacon
RECQ5	E-019338-00-0010	30 nM	Dharmacon

PCR primers

Target	Sequence	Vendor
DNA oligo for H3.3 ChIP Target1 fwd	5'-CGATGCCACCTACGGCAAG-3'	Eurofins
DNA oligo for H3.3 ChIP Target1 rev	5'-GTAGGTCAGGGTGGTCACG-3'	Eurofins
DNA oligo for H3.3 ChIP Target2 fwd	5'-CGTCCCATTTCGCCATTCAG-3'	Eurofins
DNA oligo for H3.3 ChIP Target2 rev	5'-TAATCGCCTTGCAGCACATC-3'	Eurofins
DNA oligo for H3.3 ChIP Target3 fwd	5'-CTCTTCGCTATTACGCCAGC-3'	Eurofins
DNA oligo for H3.3 ChIP Target3 rev	5'-TACAACGTCGTGACTGGGAA-3'	Eurofins

6.5 DNA CONSTRUCTS

Construct	Description
pEGFP_C1	Vector for the mammalian expression of EGFP, purchased from Clontech
pRFP_N1	Vector for the mammalian expression of RFP, purchased from SnapGene
GFP-ATRX WT	Vector for the mammalian expression of EGFP-tagged WT ATRX, isoform 2, purchased from Addgene
Myc-ATRX WT	Vector for the mammalian expression of Myc-tagged WT ATRX, isoform 2, purchased from Origene

6.6 ANTIBODIES

Antibodies	Vendor	ID	Application	dilution
Mouse-anti-ATRX	Santa Cruz	sc-55584	IF/WB	1:300/ 1:1000
Rabbit-anti-ATRX	Santa Cruz	sc-15408	WB	1: 1000
Rabbit-anti-Rad51	Abcam	ab63801	IF/WB	1:10,000/ 1:1000
Mouse-anti-Rad51	Abcam	ab213	IF/WB	1:10,000/ 1:1000
Mouse-anti-PCNA	Santa Cruz	sc-56	WB	1:1000
Rabbit-anti-RFC-1 (H-300)	Santa Cruz	sc-20993	WB	1:1000
Mouse-anti-BrdU (3D4)	BD Pharmingen	555627	IF	1:1000
Rabbit-anti-DAXX	Santa Cruz	sc-7152	WB	1:1000
Mouse-anti-HIRA WC119	Merck	04-1488	WB	1:1000
Rabbit-anti-CAF-1 (p60)	Abcam	ab109442	WB	1:1000
Rabbit-anti-H3.3	Abcam	ab176840	WB/IP	1:1000/ 5 μ g
Mouse-anti-GAPDH	Santa Cruz	sc-47724	WB	1:2000

Mouse-anti-Mus81 (MTA30)	Santa Cruz	sc-53382	IF/WB	1:200/1:1000
Mouse-anti-GFP	Roche	11814460001	IF	1:1000
Mouse-anti-phospho-Histone H2A.X (Ser139)	Merck	05-636	IF	1:2000
Rabbit-anti-phospho-Histone H2A.X (Ser139)	Abcam	ab81299	IF	1:2000
Chicken-anti-phospho-Histone H2A.X (Ser139)	Biozol	BRD-0675MZ	IF	1:2000
Mouse-anti-Ku70 (A-9)	Santa Cruz	sc-5309	WB	1:2000
Mouse-anti-alpha-Tubulin (TU-02)	Santa Cruz	sc- 8035	WB	1:2000
Rabbit-anti-RECQ5	Abcam	ab91422	WB	1:1000
Rabbit-anti-Rad54 (H-152)	Santa Cruz	sc-11428	WB	1:1000
Goat-anti-BLM (C-18)	Santa Cruz	sc-7790	IF/WB	1:200/1:500
Mouse-anti-BLM (B4)	Santa Cruz	sc-365753	IF/WB	1:200/1:500
Mouse-anti-RPA2 (9H8)	Abcam	ab2175	IF	1:700
Rabbit anti-Gen1	Abgent	AP9493a	WB	1:1000
Rabbit-anti-phospho-Histone 3	Millipore	06-570	IF	1:1000

Secondary antibodies	Vendor	ID	Application	dilution
Goat-anti-mouse IgG-HRP	Santa Cruz	c-2031	WB	1:10000
Goat-anti-rabbit IgG-HRP	Santa Cruz	sc-2030	WB	1:10000
Goat-anti-mouse AlexaFluor 488	Molecular Probes	A11001	IF	1:1000
Goat-anti-mouse AlexaFluor 594	Molecular Probes	A11005	IF	1:1000
Goat-anti-rabbit AlexaFluor 488	Molecular Probes	A11008	IF	1:1000
Goat-anti-rabbit AlexaFluor 594	Molecular Probes	A11012	IF	1:1000
Donkey-anti-mouse AlexaFluor 488	Molecular Probes	R37114	IF	1:1000
Donkey-anti-mouse AlexaFluor 594	Molecular Probes	R37115	IF	1:1000
Donkey-anti-rabbit DyLight 405	Dianova	711-475-152	IF	1:500
Chicken-anti-goat AlexaFluor 594	Molecular Probes	A-21468	IF	1:1000

6.7 KITS, ENZYMES AND LADDERS

Reagent	Vendor
Transfection	
Effectene Transfection Reagent	QIAGEN
HiPerFect Transfection Reagent	QIAGEN
Lipofectamine LTX	Thermo Fisher
RNAi Max	Thermo Fisher

Kits

EdU-Click Kit	Baseclick
peqGOLD Xchange Plasmid maxi-EF Kit	Peqlab
ZR Plasmid Miniprep Classic	Zymo research
WesternBright™ Quantum	Advansta
WesternBright™ Sirius	Advansta
DNAeasy DNA extraction Kit	QIAGEN
PCR Clean-up Kit	QIAGEN
EZ Magna ChIP A/G Kit	Merck
FastStart Universal SYBR Green Master (Rox)	Merck

Ladders

PageRuler plus prestained protein ladder	Fermentas
ProSieve quad color protein ladder	Biozym

Inhibitors

Rad51 inhibitor B02	Calbiochem
Chk1 inhibitor UCN-01	Sigma-Aldrich

6.8 BUFFERS, SOLUTIONS AND MEDIA

Buffer/reagent	Composition
Phosphate-Buffered Saline (PBS)	137 mM NaCl 2.7 mM KCl 8 mM Na ₂ HPO ₄ 1.5 mM KH ₄ PO ₄ pH 7.4
Tris-Buffered Saline (TBS)	20 mM Tris/HCl 137 mM NaCl pH 7.6

Cell culture

Dulbecco's Modified Eagle's Medium (DMEM)	Sigma-Aldrich
Minimum Essential Medium Eagle (MEM)	Sigma-Aldrich
Fetal calf serum (FCS)	Biochrom
Tetracycline-free FBS	Takara
Non-essential amino acids (NEAA)	Biochrom
Trypsin/EDTA	0.5 M EDTA pH 8
L-Glutamine	Sigma-Aldrich

Immunofluorescence

Fixation	3% Formaldehyde in PBS
Washing	0.1 TritonX-100 in PBS
Permeabilization	0.2%-0.5% TritonX-100 in PBS

Blocking	1 X RotiBlock in MilliQ	
DAPI	0.4 µg/ml DAPI in PBS	
2.5 N HCL	37% HCL diluted in MilliQ	
CSK buffer	10 mM PIPES	pH 7
	100 mM NaCl	
	300 mM sucrose	
	3 mM MgCl ₂	
PTEMF Buffer	20 mM PIPES	pH 6.8
	0.2% Triton X-100	
	1 mM MgCl ₂	
	10 mM EGTA	
	4% Formaldehyde	

Chromosome staining

Bisbenzimid (Hoechst 33258)	5 µg/ml in MilliQ	
UVC irradiation buffer	200 mM Na ₂ HPO ₄	
	4 mM citric acid	pH 7.1-7.2
Giemsa	6% in distilled H ₂ O	
Clonogenic Survival		
Crystal Violet solution	0.1% Crystal Violet	
	25% Methanol	
	MilliQ	

Bacteria

Kanamycin	20 mg/ml in MilliQ	
LB broth	10 g/l Tryptone	
	2% Yeast extract	
	5 g/l NaCl	
LB Agar plates	1.5% Agar in LB broth	

SDS-PAGE

Cell lysis buffer	1X Cell lysis buffer (Cell signalling)	
	1x Complete protease inhibitor	
5x Loading buffer (Laemmli)	60 mM Tris/HCl	pH 6.8
	2% (w/v) SDS	
	5% (v/v) β-Mercaptoethanol	
	10% (v/v) Glycerin	
	0.01% Bromophenol blue	
Electrophoresis buffer	25 mM Tris/HCl	pH 8.8
	0.2 M Glycine	
	0.5% (w/v) SDS	
Stacking gel buffer	0.5 M Tris/HCl	pH 6.8
	14 mM SDS	
Running gel buffer	1.5 M Tris/HCl	pH 8.8

14 mM SDS

Western Blot

Transfer buffer	20 mM Tris/HCl pH 8.3 150 mM Glycine
Washing	0.1% Tween20 in TBS
Blocking	1x RotiBlock in MilliQ

6.9 CELL LINES AND BACTERIA

Cells	Description
HeLa-S3	Human epithelial cancer cell line derived from adenocarcinoma of the cervix. Cells were cultivated in DMEM supplemented with 10% FCS and 1% NEAA and passaged twice per week at a dilution of 1:8 to 1:10. Source: ATCC.
HeLa ATRX KO	HeLa S3 cells with a loss-of-function deletion in the ATRX gene leading to loss of protein expression, generated by CRISPR/Cas9. Cells were cultivated in DMEM supplemented with 10% FCS and 1% NEAA and passaged twice per week at a dilution of 1:8 to 1:10. Source: Markus Löbrich lab ¹⁵⁰ .
HeLa pGC	HeLa S3 cells with an integrated HR reporter cassette. Cells were cultivated in DMEM supplemented with 10% FCS, 1% NEAA and 0.6 µg/ml puromycin and passaged twice per week at a dilution of 1:8 to 1:10. Source: Kind gift from Jochen Dahm-Daphi ¹⁵¹ .
HeLa SNAP-H3.3	HeLa S3 cells stably expressing SNAP-H.3. cells were cultured with DMEM with 10% FCS and 1x NEAA and blasticidin (1 µg/ml) and passaged twice per week at a dilution of 1:8 to 1:10. Source: kind gift from Geneviève Almouzni ¹⁵² .
U2OS	Human epithelial cancer cell line derived from osteosarcoma. Cells were cultivated in DMEM supplemented with 10% FCS and 1% NEAA and passaged twice per week at a dilution of 1:8 to 1:10. Source: ATCC.
U2OS ^{ATRX}	U2OS stable cell line with a doxycyclin-inducible expression of ATRX. Cells were cultured in DMEM supplemented with 10% tetracycline-free Serum, 1x glutamine, G418 sulphite (0.7 mg/ml) and puromycin (0.5ug/ml). Source: kind gift from David Clynes ²⁰¹ .
Saos-2	Human epithelial cancer cell line derived from osteosarcoma. Cells were cultivated in McCoy's 5A medium supplemented with 15% FCS and passaged once a week at a dilution of 1:10. Source: ATCC.
82-6 hTert	Human fibroblast cell line immortalized through the expression of human telomerase. Cells were cultivated in MEM supplemented with 20% FCS and 1% NEAA and passaged once a week at a dilution of 1:10. Source: Kind gift from Penny Jeggo ²⁰² .
<i>Escherichia coli</i> DH5α	<i>E. coli</i> strain suitable for high efficiency transformation.

7. REFERENCES

1. O’Kane, G. M., Connor, A. A. & Gallinger, S. Characterization, Detection, and Treatment Approaches for Homologous Recombination Deficiency in Cancer. *Trends Mol. Med.* **23**, 1121–1137 (2017).
2. Johnson, R. D. & Jasin, M. Sister chromatid gene conversion is a prominent double-strand break repair pathway in mammalian cells. *EMBO J.* **19**, 3398–3407 (2000).
3. Kadyk, L. C. & Hartwell, L. H. Sister chromatids are preferred over homologs as substrates for recombinational repair in *Saccharomyces cerevisiae*. *Genetics* **132**, 387 LP – 402 (1992).
4. Hunter, N. Meiotic recombination: The essence of heredity. *Cold Spring Harb. Perspect. Biol.* **7**, 1–36 (2015).
5. Beijersbergen, R. L., Wessels, L. F. A. & Bernards, R. Synthetic Lethality in Cancer Therapeutics. *Annu. Rev. Cancer Biol.* **1**, 141–161 (2017).
6. Richardson, C. D., Ray, G. J., DeWitt, M. A., Curie, G. L. & Corn, J. E. Enhancing homology-directed genome editing by catalytically active and inactive CRISPR-Cas9 using asymmetric donor DNA. *Nat. Biotechnol.* **34**, 339–344 (2016).
7. Hustedt, N. & Durocher, D. The control of DNA repair by the cell cycle. *Nat. Cell Biol.* **19**, 1–9 (2017).
8. Nakamura, K. *et al.* H4K20me0 recognition by BRCA1–BARD1 directs homologous recombination to sister chromatids. *Nat. Cell Biol.* **21**, 311–318 (2019).
9. Shibata, A., Jeggo, P. & Löbrich, M. The pendulum of the Ku-Ku clock. *DNA Repair (Amst)*. **71**, 164–171 (2018).
10. Aymard, F. *et al.* Transcriptionally active chromatin recruits homologous recombination at DNA double-strand breaks. *Nat. Struct. Mol. Biol.* **21**, 366–374 (2014).
11. Symington, L. S. & Gautier, J. Double-Strand Break End Resection and Repair Pathway Choice. *Annu. Rev. Genet.* **45**, 247–271 (2011).
12. Ceccaldi, R., Rondinelli, B. & D’Andrea, A. D. Repair Pathway Choices and Consequences at the Double-Strand Break. *Trends Cell Biol.* **26**, 52–64 (2016).
13. Sartori, A. A. *et al.* Human CtIP promotes DNA end resection. *Nature* **450**, 509–514 (2007).
14. Shibata, A. *et al.* DNA Double-Strand Break Repair Pathway Choice Is Directed by Distinct MRE11 Nuclease Activities. *Mol. Cell* **53**, 7–18 (2014).
15. Nimonkar, A. V. *et al.* BLM–DNA2–RPA–MRN and EXO1–BLM–RPA–MRN constitute two DNA end resection machineries for human DNA break repair. *Genes Dev.* **25**, 350–362 (2011).
16. Huertas, P. & Jackson, S. P. Human CtIP Mediates Cell Cycle Control of DNA End Resection and Double Strand Break Repair. *J. Biol. Chem.* **284**, 9558–9565 (2009).
17. Reczek, C. R., Szabolcs, M., Stark, J. M., Ludwig, T. & Baer, R. The interaction between CtIP and BRCA1 is not essential for resection-mediated DNA repair or tumor suppression. *J. Cell Biol.* **201**, 693–707 (2013).
18. Bunting, S. F. *et al.* 53BP1 inhibits homologous recombination in *Brc1*-deficient cells by blocking resection of DNA breaks. *Cell* **141**, 243–254 (2010).
19. Escribano-Díaz, C. *et al.* A Cell Cycle-Dependent Regulatory Circuit Composed of

- 53BP1-RIF1 and BRCA1-CtIP Controls DNA Repair Pathway Choice. *Mol. Cell* **49**, 872–883 (2013).
20. Tomimatsu, N. *et al.* Phosphorylation of EXO1 by CDKs 1 and 2 regulates DNA end resection and repair pathway choice. *Nat. Commun.* **5**, 3561 (2014).
 21. Falck, J. *et al.* CDK targeting of NBS1 promotes DNA-end resection, replication restart and homologous recombination. *EMBO Rep.* **13**, 561–568 (2012).
 22. Chen, H., Lisby, M. & Symington, L. S. RPA Coordinates DNA End Resection and Prevents Formation of DNA Hairpins. *Mol. Cell* **50**, 589–600 (2013).
 23. Sugiyama, T., Zaitseva, E. M. & Kowalczykowski, S. C. A Single-stranded DNA-binding Protein Is Needed for Efficient Presynaptic Complex Formation by the *Saccharomyces cerevisiae* Rad51 Protein. *J. Biol. Chem.* **272**, 7940–7945 (1997).
 24. Deng, S. K., Gibb, B., de Almeida, M. J., Greene, E. C. & Symington, L. S. RPA antagonizes microhomology-mediated repair of DNA double-strand breaks. *Nat. Struct. Mol. Biol.* **21**, 405–412 (2014).
 25. Ma, C. J., Gibb, B., Kwon, Y., Sung, P. & Greene, E. C. Protein dynamics of human RPA and RAD51 on ssDNA during assembly and disassembly of the RAD51 filament. *Nucleic Acids Res.* **45**, 749–761 (2016).
 26. Carreira, A. & Kowalczykowski, S. C. Two classes of BRC repeats in BRCA2 promote RAD51 nucleoprotein filament function by distinct mechanisms. *Proc. Natl. Acad. Sci. U. S. A.* **108**, 10448–10453 (2011).
 27. Liu, J., Doty, T., Gibson, B. & Heyer, W.-D. Human BRCA2 protein promotes RAD51 filament formation on RPA-covered single-stranded DNA. *Nat. Struct. Mol. Biol.* **17**, 1260–1262 (2010).
 28. Jensen, R. B., Carreira, A. & Kowalczykowski, S. C. Purified human BRCA2 stimulates RAD51-mediated recombination. *Nature* **467**, 678–683 (2010).
 29. Shahid, T. *et al.* Structure and mechanism of action of the BRCA2 breast cancer tumor suppressor. *Nat. Struct. Mol. Biol.* **21**, 962–968 (2014).
 30. Jensen, R. B., Ozes, A., Kim, T., Estep, A. & Kowalczykowski, S. C. BRCA2 is epistatic to the RAD51 paralogs in response to DNA damage. *DNA Repair (Amst)*. **12**, 306–311 (2013).
 31. Prakash, R., Zhang, Y., Feng, W. & Jasin, M. Homologous Recombination and Human Health: The Roles of BRCA1, BRCA2, and Associated Proteins. *Cold Spring Harb. Perspect. Biol.* **7**, (2015).
 32. Xu, J. *et al.* Cryo-EM structures of human RAD51 recombinase filaments during catalysis of DNA-strand exchange. *Nat. Struct. Mol. Biol.* **24**, 40–46 (2017).
 33. Gupta, R. C., Folta-Stogniew, E., O'Malley, S., Takahashi, M. & Radding, C. M. Rapid Exchange of A:T Base Pairs Is Essential for Recognition of DNA Homology by Human Rad51 Recombination Protein. *Mol. Cell* **4**, 705–714 (1999).
 34. Qi, Z. *et al.* DNA Sequence Alignment by Microhomology Sampling during Homologous Recombination. *Cell* **160**, 856–869 (2015).
 35. Lee, J. Y. *et al.* DNA RECOMBINATION. Base triplet stepping by the Rad51/RecA family of recombinases. *Science* **349**, 977–981 (2015).
 36. Wright, W. D. & Heyer, W.-D. Rad54 functions as a heteroduplex DNA pump modulated by its DNA substrates and Rad51 during D loop formation. *Mol. Cell* **53**,

- 420–432 (2014).
37. Ristic, D., Kanaar, R. & Wyman, C. Visualizing RAD51-mediated joint molecules: implications for recombination mechanism and the effect of sequence heterology. *Nucleic Acids Res.* **39**, 155–167 (2010).
 38. Christiansen, G. & Griffith, J. Visualization of the paranemic joining of homologous DNA molecules catalyzed by the RecA protein of *Escherichia coli*. *Proc. Natl. Acad. Sci.* **83**, 2066 LP – 2070 (1986).
 39. Wright, W. D., Shah, S. S. & Heyer, W. D. Homologous recombination and the repair of DNA double-strand breaks. *J. Biol. Chem.* **293**, 10524–10535 (2018).
 40. Sanchez, H., Kertokalio, A., van Rossum-Fikkert, S., Kanaar, R. & Wyman, C. Combined optical and topographic imaging reveals different arrangements of human RAD54 with presynaptic and postsynaptic RAD51–DNA filaments. *Proc. Natl. Acad. Sci.* **110**, 11385 LP – 11390 (2013).
 41. Mazina, O. M. & Mazin, A. V. Human Rad54 Protein Stimulates DNA Strand Exchange Activity of hRad51 Protein in the Presence of Ca²⁺. *J. Biol. Chem.* **279**, 52042–52051 (2004).
 42. Tavares, E. M., Wright, W. D., Heyer, W.-D., Le Cam, E. & Dupaigne, P. In vitro role of Rad54 in Rad51-ssDNA filament-dependent homology search and synaptic complexes formation. *Nat. Commun.* **10**, 4058 (2019).
 43. Solinger, J. A., Kiianitsa, K. & Heyer, W.-D. Rad54, a Swi2/Snf2-like Recombinational Repair Protein, Disassembles Rad51:dsDNA Filaments. *Mol. Cell* **10**, 1175–1188 (2002).
 44. Spies, J. *et al.* Nek1 Regulates Rad54 to Orchestrate Homologous Recombination and Replication Fork Stability. *Mol. Cell* **62**, 903–917 (2016).
 45. Sneed, J. L., Grossi, S. M., Tappin, I., Hurwitz, J. & Heyer, W. D. Reconstitution of recombination-associated DNA synthesis with human proteins. *Nucleic Acids Res.* **41**, 4913–4925 (2013).
 46. Wilson, M. A. *et al.* Pif1 helicase and Pol δ promote recombination-coupled DNA synthesis via bubble migration. *Nature* **502**, 393–396 (2013).
 47. Hustedt, N. *et al.* Control of homologous recombination by the HROB-MCM8-MCM9 pathway. *Genes Dev.* **33**, 1397–1415 (2019).
 48. Verma, P. & Greenberg, R. A. Noncanonical views of homology-directed DNA repair. *Genes Dev.* **30**, 1138–1154 (2016).
 49. Fasching, C. L., Cejka, P., Kowalczykowski, S. C. & Heyer, W.-D. Top3-Rmi1 dissolve Rad51-mediated D loops by a topoisomerase-based mechanism. *Mol. Cell* **57**, 595–606 (2015).
 50. Krejci, L. *et al.* DNA helicase Srs2 disrupts the Rad51 presynaptic filament. *Nature* **423**, 305–309 (2003).
 51. Liu, J. *et al.* Srs2 promotes synthesis-dependent strand annealing by disrupting DNA polymerase δ -extending D-loops. 1–24 (2017) doi:10.7554/eLife.22195.
 52. Prakash, R. *et al.* Yeast Mph1 helicase dissociates Rad51-made D-loops: implications for crossover control in mitotic recombination. *Genes Dev.* **23**, 67–79 (2009).
 53. Paliwal, S., Kanagaraj, R., Sturzenegger, A., Burdova, K. & Janscak, P. Human RECQ5 helicase promotes repair of DNA double-strand breaks by synthesis-dependent strand

- annealing. *Nucleic Acids Res.* **42**, 2380–2390 (2014).
54. Adelman, C. A. & Boulton, S. J. Metabolism of postsynaptic recombination intermediates. *FEBS Lett.* **584**, 3709–3716 (2010).
 55. Sommers, J. A. *et al.* FANCI uses its motor ATPase to destabilize protein-DNA complexes, unwind triplexes, and inhibit RAD51 strand exchange. *J. Biol. Chem.* **284**, 7505–7517 (2009).
 56. Simandlova, J. *et al.* FBH1 helicase disrupts RAD51 filaments in vitro and modulates homologous recombination in mammalian cells. *J. Biol. Chem.* **288**, 34168–34180 (2013).
 57. Bugreev, D. V, Brosh Jr, R. M. & Mazin, A. V. RECQ1 possesses DNA branch migration activity. *J. Biol. Chem.* **283**, 20231–20242 (2008).
 58. Bzymek, M., Thayer, N. H., Oh, S. D., Kleckner, N. & Hunter, N. Double Holliday junctions are intermediates of DNA break repair. *Nature* **464**, 937–941 (2010).
 59. Wu, L. & Hickson, I. D. The Bloom’s syndrome helicase suppresses crossing over during homologous recombination. *Nature* **426**, 870–874 (2003).
 60. Yang, J., Bachrati, C. Z., Ou, J., Hickson, I. D. & Brown, G. W. Human topoisomerase III α is a single-stranded DNA decatenase that is stimulated by BLM and RMI1. *J. Biol. Chem.* **285**, 21426–21436 (2010).
 61. Manthei, K. A. & Keck, J. L. The BLM dissolvasome in DNA replication and repair. *Cell. Mol. Life Sci.* **70**, 4067–4084 (2013).
 62. Chaganti, R. S., Schonberg, S. & German, J. A manyfold increase in sister chromatid exchanges in Bloom’s syndrome lymphocytes. *Proc. Natl. Acad. Sci. U. S. A.* **71**, 4508–4512 (1974).
 63. Sarbajna, S. & West, S. C. Holliday junction processing enzymes as guardians of genome stability. *Trends Biochem. Sci.* **39**, 409–419 (2014).
 64. Wyatt, H. D. M., Sarbajna, S., Matos, J. & West, S. C. Coordinated Actions of SLX1-SLX4 and MUS81-EME1 for Holliday Junction Resolution in Human Cells. *Mol. Cell* **52**, 234–247 (2013).
 65. Ciccia, A., Constantinou, A. & West, S. C. Identification and Characterization of the Human Mus81-Eme1 Endonuclease. *J. Biol. Chem.* **278**, 25172–25178 (2003).
 66. Fekairi, S. *et al.* Human SLX4 Is a Holliday Junction Resolvase Subunit that Binds Multiple DNA Repair/Recombination Endonucleases. *Cell* **138**, 78–89 (2009).
 67. Garner, E., Kim, Y., Lach, F. P., Kottmann, M. C. & Smogorzewska, A. Human GEN1 and the SLX4-associated nucleases MUS81 and SLX1 are essential for the resolution of replication-induced Holliday junctions. *Cell Rep.* **5**, 207–215 (2013).
 68. Ip, S. *et al.* Identification of Holliday junction resolvases from humans and yeast. *Nature* **456**, 357–361 (2008).
 69. Wild, P. & Matos, J. Cell cycle control of DNA joint molecule resolution. *Curr. Opin. Cell Biol.* **40**, 74–80 (2016).
 70. Pfander, B. & Matos, J. Control of Mus81 nuclease during the cell cycle. *FEBS Lett.* **591**, 2048–2056 (2017).
 71. Punatar, R. S., Martin, M. J., Wyatt, H. D. M., Chan, Y. W. & West, S. C. Resolution of single and double Holliday junction recombination intermediates by GEN 1. *Proc. Natl. Acad. Sci. U. S. A.* **114**, 443–450 (2017).

72. Sarbajna, S., Davies, D. & West, S. C. Roles of SLX1-SLX4, MUS81-EME1, and GEN1 in avoiding genome instability and mitotic catastrophe. *Genes Dev.* **28**, 1124–1136 (2014).
73. Kramara, J., Osia, B. & Malkova, A. Break-Induced Replication: The Where, The Why, and The How. *Trends Genet.* **34**, 518–531 (2018).
74. Malkova, A., Naylor, M. L., Yamaguchi, M., Ira, G. & Haber, J. E. RAD51-Dependent Break-Induced Replication Differs in Kinetics and Checkpoint Responses from RAD51-Mediated Gene Conversion. *Mol. Cell. Biol.* **25**, 933 LP – 944 (2005).
75. Davis, A. P. & Symington, L. S. RAD51-Dependent Break-Induced Replication in Yeast. *Mol. Cell. Biol.* **24**, 2344 LP – 2351 (2004).
76. Donnianni, R. A. & Symington, L. S. Break-induced replication occurs by conservative DNA synthesis. *Proc. Natl. Acad. Sci.* **110**, 13475–13480 (2013).
77. Lydeard, J. R., Jain, S., Yamaguchi, M. & Haber, J. E. Break-induced replication and telomerase-independent telomere maintenance require Pol32. *Nature* **448**, 820–823 (2007).
78. Mayle, R. *et al.* Mus81 and converging forks limit the mutagenicity of replication fork breakage. *Science (80-.)*. **349**, 742 LP – 747 (2015).
79. Saini, N. *et al.* Migrating bubble during break-induced replication drives conservative DNA synthesis. *Nature* **502**, 389–392 (2013).
80. Štafa, A., Donnianni, R. A., Timashev, L. A., Lam, A. F. & Symington, L. S. Template switching during break-induced replication is promoted by the mph1 helicase in *Saccharomyces cerevisiae*. *Genetics* **196**, 1017–1028 (2014).
81. Costantino, L. *et al.* Break-Induced Replication Repair of Damaged Forks Induces Genomic Duplications in Human Cells. *Science (80-.)*. **343**, 88 LP – 91 (2014).
82. Bhowmick, R., Minocherhomji, S. & Hickson, I. D. RAD52 Facilitates Mitotic DNA Synthesis Following Replication Stress. *Mol. Cell* **64**, 1117–1126 (2016).
83. Dilley, R. L. *et al.* Break-induced telomere synthesis underlies alternative telomere maintenance. *Nature* **539**, 54–58 (2016).
84. Branzei, D. & Foiani, M. Maintaining genome stability at the replication fork. *Nat. Rev. Mol. Cell Biol.* **11**, 208–219 (2010).
85. Prado, F. Homologous Recombination: To Fork and Beyond. *Genes (Basel)*. **9**, 603 (2018).
86. Schlacher, K. *et al.* Double-Strand Break Repair-Independent Role for BRCA2 in Blocking Stalled Replication Fork Degradation by MRE11. *Cell* **145**, 529–542 (2011).
87. Lemaçon, D. *et al.* MRE11 and EXO1 nucleases degrade reversed forks and elicit MUS81-dependent fork rescue in BRCA2-deficient cells. *Nat. Commun.* **8**, 860 (2017).
88. Schlacher, K., Wu, H. & Jasin, M. A distinct replication fork protection pathway connects Fanconi anemia tumor suppressors to RAD51-BRCA1/2. *Cancer Cell* **22**, 106–116 (2012).
89. Hashimoto, Y., Ray Chaudhuri, A., Lopes, M. & Costanzo, V. Rad51 protects nascent DNA from Mre11-dependent degradation and promotes continuous DNA synthesis. *Nat. Struct. Mol. Biol.* **17**, 1305–1311 (2010).
90. Zellweger, R. *et al.* Rad51-mediated replication fork reversal is a global response to

- genotoxic treatments in human cells. *J. Cell Biol.* **208**, 563–579 (2015).
91. Ray Chaudhuri, A. *et al.* Topoisomerase I poisoning results in PARP-mediated replication fork reversal. *Nat. Struct. Mol. Biol.* **19**, 417–423 (2012).
 92. Liberi, G. *et al.* Rad51-dependent DNA structures accumulate at damaged replication forks in *sgs1* mutants defective in the yeast ortholog of BLM RecQ helicase. *Genes Dev.* **19**, 339–350 (2005).
 93. Malik, H. S. & Henikoff, S. Phylogenomics of the nucleosome. *Nat. Struct. Mol. Biol.* **10**, 882–891 (2003).
 94. Talbert, P. B. *et al.* A unified phylogeny-based nomenclature for histone variants. *Epigenetics Chromatin* **5**, 7 (2012).
 95. Zentner, G. E. & Henikoff, S. Regulation of nucleosome dynamics by histone modifications. *Nat. Struct. Mol. Biol.* **20**, 259–266 (2013).
 96. Narlikar, G. J., Sundaramoorthy, R. & Owen-Hughes, T. Mechanisms and functions of ATP-dependent chromatin-remodeling enzymes. *Cell* **154**, 490–503 (2013).
 97. Draizen, E. J. *et al.* HistoneDB 2.0: a histone database with variants—an integrated resource to explore histones and their variants. *Database* **2016**, (2016).
 98. Mattioli, F., D’Arcy, S. & Luger, K. The right place at the right time: chaperoning core histone variants. *EMBO Rep.* **16**, 1454–1466 (2015).
 99. Talbert, P. B. & Henikoff, S. Histone variants on the move: Substrates for chromatin dynamics. *Nat. Rev. Mol. Cell Biol.* **18**, 115–126 (2017).
 100. Foltz, D. R. *et al.* Centromere-specific assembly of CENP-a nucleosomes is mediated by HJURP. *Cell* **137**, 472–484 (2009).
 101. Goshima, G., Kiyomitsu, T., Yoda, K. & Yanagida, M. Human centromere chromatin protein hMis12, essential for equal segregation, is independent of CENP-A loading pathway. *J. Cell Biol.* **160**, 25–39 (2003).
 102. Adam, S., Dabin, J. & Polo, S. E. Chromatin plasticity in response to DNA damage: The shape of things to come. *DNA Repair (Amst)*. **32**, 120–126 (2015).
 103. Clouaire, T. *et al.* Comprehensive Mapping of Histone Modifications at DNA Double-Strand Breaks Deciphers Repair Pathway Chromatin Signatures. *Mol. Cell* **72**, 250–262.e6 (2018).
 104. Gursoy-Yuzugullu, O., House, N. & Price, B. D. Patching Broken DNA: Nucleosome Dynamics and the Repair of DNA Breaks. *J. Mol. Biol.* **428**, 1846–1860 (2016).
 105. Hinde, E., Kong, X., Yokomori, K. & Gratton, E. Chromatin dynamics during DNA repair revealed by pair correlation analysis of molecular flow in the nucleus. *Biophys. J.* **107**, 55–65 (2014).
 106. Marnef, A. & Legube, G. Organizing DNA repair in the nucleus: DSBs hit the road. *Curr. Opin. Cell Biol.* **46**, 1–8 (2017).
 107. Stucki, M. *et al.* MDC1 Directly Binds Phosphorylated Histone H2AX to Regulate Cellular Responses to DNA Double-Strand Breaks. *Cell* **123**, 1213–1226 (2005).
 108. Lou, Z. *et al.* MDC1 Maintains Genomic Stability by Participating in the Amplification of ATM-Dependent DNA Damage Signals. *Mol. Cell* **21**, 187–200 (2006).
 109. Rogakou, E. P., Boon, C., Redon, C. & Bonner, W. M. Megabase Chromatin Domains Involved in DNA Double-Strand Breaks in Vivo. *J. Cell Biol.* **146**, 905–916 (1999).

110. Doil, C. *et al.* RNF168 Binds and Amplifies Ubiquitin Conjugates on Damaged Chromosomes to Allow Accumulation of Repair Proteins. *Cell* **136**, 435–446 (2009).
111. Kolas, N. K. *et al.* Orchestration of the DNA-Damage Response by the RNF8 Ubiquitin Ligase. *Science* (80-.). **318**, 1637 LP – 1640 (2007).
112. Seo, J. *et al.* Genome-wide profiles of H2AX and γ -H2AX differentiate endogenous and exogenous DNA damage hotspots in human cells. *Nucleic Acids Res.* **40**, 5965–5974 (2012).
113. Seo, J. *et al.* Genome-wide reorganization of histone H2AX toward particular fragile sites on cell activation. *Nucleic Acids Res.* **42**, 1016–1025 (2014).
114. Piquet, S. *et al.* The Histone Chaperone FACT Coordinates H2A.X-Dependent Signaling and Repair of DNA Damage. *Mol. Cell* **72**, 888-901.e7 (2018).
115. Pessina, F. & Lowndes, N. F. The RSF1 Histone-Remodelling Factor Facilitates DNA Double-Strand Break Repair by Recruiting Centromeric and Fanconi Anaemia Proteins. *PLoS Biol.* **12**, (2014).
116. Helfricht, A. *et al.* Remodeling and spacing factor 1 (RSF1) deposits centromere proteins at DNA double-strand breaks to promote non-homologous end-joining. *Cell Cycle* **12**, 3070–3082 (2013).
117. Luijsterburg, M. S. *et al.* PARP1 Links CHD2-Mediated Chromatin Expansion and H3.3 Deposition to DNA Repair by Non-homologous End-Joining. *Mol. Cell* **61**, 547–562 (2016).
118. Li, X. & Tyler, J. K. Nucleosome disassembly during human non-homologous end joining followed by concerted HIRA- and CAF-1-dependent reassembly. *Elife* **5**, 1–18 (2016).
119. Yang, X. *et al.* Histone acetyltransferase 1 promotes homologous recombination in DNA repair by facilitating histone turnover. *J. Biol. Chem.* **288**, 18271–18282 (2013).
120. Xu, Y. *et al.* Histone H2A.Z controls a critical chromatin remodeling step required for DNA double-strand break repair. *Mol. Cell* **48**, 723–733 (2012).
121. Gursoy-Yuzugullu, O., Ayrapetov, M. K. & Price, B. D. Histone chaperone Anp32e removes H2A.Z from DNA double-strand breaks and promotes nucleosome reorganization and DNA repair. *Proc. Natl. Acad. Sci.* **112**, 7507–7512 (2015).
122. Alatwi, H. E. & Downs, J. A. Removal of H2A.Z by INO80 promotes homologous recombination. *EMBO Rep.* **16**, 986–994 (2015).
123. Lademann, C. A., Renkawitz, J., Pfander, B. & Jentsch, S. The INO80 Complex Removes H2A.Z to Promote Presynaptic Filament Formation during Homologous Recombination. *Cell Rep.* **19**, 1294–1303 (2017).
124. Bantele, S. C. S. & Pfander, B. Nucleosome Remodeling by Fun30SMARCAD1 in the DNA Damage Response . *Frontiers in Molecular Biosciences* vol. 6 78 (2019).
125. Costelloe, T. *et al.* The yeast Fun30 and human SMARCAD1 chromatin remodellers promote DNA end resection. *Nature* **489**, 581–584 (2012).
126. Xu, C., Xu, Y., Gursoy-Yuzugullu, O. & Price, B. D. The histone variant macroH2A1.1 is recruited to DSBs through a mechanism involving PARP1. *FEBS Lett.* **586**, 3920–3925 (2012).
127. Khurana, S. *et al.* A macrohistone variant links dynamic chromatin compaction to BRCA1-dependent genome maintenance. *Cell Rep.* **8**, 1049–1062 (2014).

128. Kim, J. *et al.* The macroH2A1.2 histone variant links ATRX loss to alternative telomere lengthening. *Nat. Struct. Mol. Biol.* **26**, 213–219 (2019).
129. Wolner, B. & Peterson, C. L. ATP-dependent and ATP-independent Roles for the Rad54 Chromatin Remodeling Enzyme during Recombinational Repair of a DNA Double Strand Break. *J. Biol. Chem.* **280**, 10855–10860 (2005).
130. Sinha, M. & Peterson, C. L. A Rad51 presynaptic filament is sufficient to capture nucleosomal homology during recombinational repair of a DNA double-strand break. *Mol. Cell* **30**, 803–810 (2008).
131. Seeber, A., Hauer, M. H. & Gasser, S. M. Chromosome Dynamics in Response to DNA Damage. *Annu. Rev. Genet.* **52**, 295–319 (2018).
132. Clouaire, T. & Legube, G. A Snapshot on the *Cis* Chromatin Response to DNA Double-Strand Breaks. *Trends Genet.* **35**, 330–345 (2019).
133. Goldberg, A. D. *et al.* Distinct Factors Control Histone Variant H3.3 Localization at Specific Genomic Regions. *Cell* **140**, 678–691 (2010).
134. Tyler, J. K. *et al.* The RCAF complex mediates chromatin assembly during DNA replication and repair. *Nature* **402**, 555–560 (1999).
135. Tagami, H., Ray-Gallet, D., Almouzni, G. & Nakatani, Y. Histone H3.1 and H3.3 Complexes Mediate Nucleosome Assembly Pathways Dependent or Independent of DNA Synthesis. *Cell* **116**, 51–61 (2004).
136. Ahmad, K. & Henikoff, S. The Histone Variant H3.3 Marks Active Chromatin by Replication-Independent Nucleosome Assembly. *Mol. Cell* **9**, 1191–1200 (2002).
137. Ray-Gallet, D. *et al.* HIRA Is Critical for a Nucleosome Assembly Pathway Independent of DNA Synthesis. *Mol. Cell* **9**, 1091–1100 (2002).
138. Delbarre, E. *et al.* Chromatin Environment of Histone Variant H3.3 Revealed by Quantitative Imaging and Genome-scale Chromatin and DNA Immunoprecipitation. *Mol. Biol. Cell* **21**, 1872–1884 (2010).
139. Drané, P., Ouararhni, K., Depaux, A., Shuaib, M. & Hamiche, A. The death-associated protein DAXX is a novel histone chaperone involved in the replication-independent deposition of H3.3. *Genes Dev.* **24**, 1253–1265 (2010).
140. Voon, H. P. J. & Wong, L. H. New players in heterochromatin silencing: Histone variant H3.3 and the ATRX/DAXX chaperone. *Nucleic Acids Res.* **44**, 1496–1501 (2015).
141. Adam, S., Polo, S. E. & Almouzni, G. Transcription recovery after DNA damage requires chromatin priming by the H3.3 histone chaperone HIRA. *Cell* **155**, 963 (2013).
142. Frey, A., Listovsky, T., Guilbaud, G., Sarkies, P. & Sale, J. E. Histone H3.3 Is Required to Maintain Replication Fork Progression after UV Damage. *Curr. Biol.* **24**, 2195–2201 (2014).
143. Luijsterburg, M. S. *et al.* PARP1 Links CHD2-Mediated Chromatin Expansion and H3.3 Deposition to DNA Repair by Non-homologous End-Joining. *Mol. Cell* **61**, 547–562 (2016).
144. Kallappagoudar, S., Yadav, R. K., Lowe, B. R. & Partridge, J. F. Histone H3 mutations—a special role for H3.3 in tumorigenesis? *Chromosoma* **124**, 177–189 (2015).
145. Schwartzenruber, J. *et al.* Driver mutations in histone H3.3 and chromatin remodelling genes in paediatric glioblastoma. *Nature* **482**, 226–231 (2012).

146. Dilley, R. L. & Greenberg, R. A. ALternative Telomere Maintenance and Cancer. *Trends in Cancer* **1**, 145–156 (2015).
147. Lovejoy, C. A. *et al.* Loss of ATRX, genome instability, and an altered DNA damage response are hallmarks of the alternative lengthening of Telomeres pathway. *PLoS Genet.* **8**, 12–15 (2012).
148. Maciejowski, J. & De Lange, T. Telomeres in cancer: Tumour suppression and genome instability. *Nat. Rev. Mol. Cell Biol.* **18**, 175–186 (2017).
149. Huh, M. S. *et al.* Stalled replication forks within heterochromatin require ATRX for protection. *Cell Death Dis.* **7**, e2220 (2016).
150. Juhász, S., Elbakry, A., Mathes, A. & Löbrich, M. ATRX Promotes DNA Repair Synthesis and Sister Chromatid Exchange during Homologous Recombination. *Mol. Cell* **71**, 11-24.e7 (2018).
151. Mansour, W. Y. *et al.* Hierarchy of nonhomologous end-joining, single-strand annealing and gene conversion at site-directed DNA double-strand breaks. *Nucleic Acids Res.* **36**, 4088–4098 (2008).
152. Ray-Gallet, D. *et al.* Dynamics of Histone H3 Deposition In Vivo Reveal a Nucleosome Gap-Filling Mechanism for H3.3 to Maintain Chromatin Integrity. *Mol. Cell* **44**, 928–941 (2011).
153. Kegel, P., Riballo, E., Kühne, M., Jeggo, P. A. & Löbrich, M. X-irradiation of cells on glass slides has a dose doubling impact. *DNA Repair (Amst).* **6**, 1692–1697 (2007).
154. Lukas, C., Falck, J., Bartkova, J., Bartek, J. & Lukas, J. Distinct spatiotemporal dynamics of mammalian checkpoint regulators induced by DNA damage. *Nat. Cell Biol.* **5**, 255–260 (2003).
155. Vítor, A. C., Huertas, P., Legube, G. & de Almeida, S. F. Studying DNA Double-Strand Break Repair: An Ever-Growing Toolbox . *Frontiers in Molecular Biosciences* vol. 7 24 (2020).
156. Beucher, A. *et al.* ATM and Artemis promote homologous recombination of radiation-induced DNA double-strand breaks in G2. *EMBO J.* **28**, 3413–3427 (2009).
157. Löbrich, M. *et al.* γ H2AX foci analysis for monitoring DNA double-strand break repair: Strengths, limitations and optimization. *Cell Cycle* **9**, 662–669 (2010).
158. Biehs, R. *et al.* DNA Double-Strand Break Resection Occurs during Non-homologous End Joining in G1 but Is Distinct from Resection during Homologous Recombination. *Mol. Cell* **65**, 671-684.e5 (2017).
159. Rothkamm, K., Krüger, I., Thompson, L. H. & Löbrich, M. Pathways of DNA Double-Strand Break Repair during the Mammalian Cell Cycle. *Mol. Cell. Biol.* **23**, 5706 LP – 5715 (2003).
160. Moynahan, M. E. & Jasin, M. Mitotic homologous recombination maintains genomic stability and suppresses tumorigenesis. *Nat. Rev. Mol. Cell Biol.* **11**, 196–207 (2010).
161. Koster, D. A., Palle, K., Bot, E. S. M., Bjornsti, M. A. & Dekker, N. H. Antitumour drugs impede DNA uncoiling by topoisomerase I. *Nature* **448**, 213–217 (2007).
162. Xu, Y. & Her, C. Inhibition of topoisomerase (DNA) I (TOP1): DNA damage repair and anticancer therapy. *Biomolecules* **5**, 1652–1670 (2015).
163. Ensminger, M. *et al.* DNA breaks and chromosomal aberrations arise when replication meets base excision repair. *J. Cell Biol.* **206**, 29–43 (2014).

164. Conrad, S., Künzel, J. & Löbrich, M. Sister chromatid exchanges occur in G2-irradiated cells. *Cell Cycle* **10**, 222–228 (2011).
165. Sun, X. *et al.* Development of SNAP-tag fluorogenic probes for wash-free fluorescence imaging. *ChemBioChem* **12**, 2217–2226 (2011).
166. Li, X., Stith, C. M., Burgers, P. M. & Heyer, W. D. PCNA Is Required for Initiation of Recombination-Associated DNA Synthesis by DNA Polymerase δ . *Mol. Cell* **36**, 704–713 (2009).
167. Sebesta, M. *et al.* Role of PCNA and TLS polymerases in D-loop extension during homologous recombination in humans. *DNA Repair (Amst)*. **12**, 691–698 (2013).
168. Green, C. M. & Almouzni, G. Local action of the chromatin assembly factor CAF-1 at sites of nucleotide excision repair in vivo. *EMBO J.* **22**, 5163–5174 (2003).
169. Polo, S. E., Roche, D. & Almouzni, G. New Histone Incorporation Marks Sites of UV Repair in Human Cells. *Cell* **127**, 481–493 (2006).
170. Tagami, H., Ray-Gallet, D., Almouzni, G. & Nakatani, Y. Histone H3.1 and H3.3 Complexes Mediate Nucleosome Assembly Pathways Dependent or Independent of DNA Synthesis. *Cell* **116**, 51–61 (2004).
171. Mejlvang, J. *et al.* New histone supply regulates replication fork speed and PCNA unloading. *J. Cell Biol.* **204**, 29–43 (2014).
172. Sarai, N. *et al.* WHSC1 links transcription elongation to HIRA-mediated histone H3.3 deposition. *EMBO J.* **32**, 2392–2406 (2013).
173. Hardy, J. *et al.* Histone deposition promotes recombination-dependent replication at arrested forks. *PLoS Genet.* **15**, e1008441–e1008441 (2019).
174. Pietrobon, V. *et al.* The Chromatin Assembly Factor 1 Promotes Rad51-Dependent Template Switches at Replication Forks by Counteracting D-Loop Disassembly by the RecQ-Type Helicase Rqh1. *PLOS Biol.* **12**, e1001968 (2014).
175. Teves, S. S. & Henikoff, S. DNA torsion as a feedback mediator of transcription and chromatin dynamics. *Nucleus* **5**, 211–218 (2014).
176. Teves, S. S., Weber, C. M. & Henikoff, S. Transcribing through the nucleosome. *Trends Biochem. Sci.* **39**, 577–586 (2014).
177. Bancaud, A. *et al.* Structural plasticity of single chromatin fibers revealed by torsional manipulation. *Nat. Struct. Mol. Biol.* **13**, 444–450 (2006).
178. Kaczmarczyk, A., Meng, H., Ordu, O., Noort, J. van & Dekker, N. H. Chromatin fibers stabilize nucleosomes under torsional stress. *Nat. Commun.* **11**, 126 (2020).
179. Huang, T.-H. *et al.* The Histone Chaperones ASF1 and CAF-1 Promote MMS22L-TONSL-Mediated Rad51 Loading onto ssDNA during Homologous Recombination in Human Cells. *Mol. Cell* 1–14 (2018) doi:10.1016/j.molcel.2018.01.031.
180. Loyola, A. & Almouzni, G. Marking histone H3 variants: How, when and why? *Trends Biochem. Sci.* **32**, 425–433 (2007).
181. Udugama, M. *et al.* Histone variant H3.3 provides the heterochromatic H3 lysine 9 trimethylation mark at telomeres. *Nucleic Acids Res.* **43**, 10227–10237 (2015).
182. Ayrapetov, M. K., Gursoy-Yuzugullu, O., Xu, C., Xu, Y. & Price, B. D. DNA double-strand breaks promote methylation of histone H3 on lysine 9 and transient formation of repressive chromatin. *Proc. Natl. Acad. Sci.* **111**, 9169–9174 (2014).

183. Chang, F. T. M. *et al.* CHK1-driven histone H3.3 serine 31 phosphorylation is important for chromatin maintenance and cell survival in human ALT cancer cells. *Nucleic Acids Res.* **43**, 2603–2614 (2015).
184. Zapotoczny, G. & Sekelsky, J. Human Cell Assays for Synthesis-Dependent Strand Annealing and Crossing over During Double-Strand Break Repair. *G3 Genes/Genomes/Genetics* **7**, 1191 LP – 1199 (2017).
185. Jasin, M. & Rothstein, R. Repair of Strand Breaks by Homologous Recombination TL - 5. *Cold Spring Harb. Perspect. Biol.* **5 VN-re**, 1–19 (2013).
186. Perry, P. & Evans, H. J. Cytological detection of mutagen–carcinogen exposure by sister chromatid exchange. *Nature* **258**, 121–125 (1975).
187. Solomon, E. & Bobrow, M. Sister chromatid exchanges—A sensitive assay of agents damaging human chromosomes. *Mutat. Res. Mol. Mech. Mutagen.* **30**, 273–277 (1975).
188. Jeggo, P. A., Geuting, V. & Löbrich, M. The role of homologous recombination in radiation-induced double-strand break repair. *Radiother. Oncol.* **101**, 7–12 (2011).
189. Elbakry, A., Juhász, S., Mathes, A. & Löbrich, M. DNA repair synthesis and histone deposition partner during homologous recombination. *Mol. Cell. Oncol.* **5**, (2018).
190. Cole, F. *et al.* Mouse tetrad analysis provides insights into recombination mechanisms and hotspot evolutionary dynamics. *Nat. Genet.* **46**, 1072–1080 (2014).
191. Elliott, B., Richardson, C., Winderbaum, J., Nickoloff, J. A. & Jasin, M. Gene conversion tracts from double-strand break repair in mammalian cells. *Mol. Cell. Biol.* **18**, 93–101 (1998).
192. Bizard, A. H. & Hickson, I. D. The dissolution of double Holliday junctions. *Cold Spring Harb. Perspect. Biol.* **6**, 1–14 (2014).
193. Hickson, I. D. The dissolution of double Holliday junctions. *Cold Spring Harb. Perspect. Biol.* **6**, a016477 (2014).
194. Hu, Y. *et al.* Recq15 and Blm RecQ DNA Helicases Have Nonredundant Roles in Suppressing Crossovers. *Mol. Cell. Biol.* **25**, 3431 LP – 3442 (2005).
195. Ira, G., Malkova, A., Liberi, G., Foiani, M. & Haber, J. E. Srs2 and Sgs1-Top3 suppress crossovers during double-strand break repair in yeast. *Cell* **115**, 401–411 (2003).
196. Di Marco, S. *et al.* RECQ5 Helicase Cooperates with MUS81 Endonuclease in Processing Stalled Replication Forks at Common Fragile Sites during Mitosis. *Mol. Cell* **66**, 658-671.e8 (2017).
197. Zheng, L. *et al.* MRE11 complex links RECQ5 helicase to sites of DNA damage. *Nucleic Acids Res.* **37**, 2645–2657 (2009).
198. Urban, V. *et al.* RECQ5 helicase promotes resolution of conflicts between replication and transcription in human cells. *J. Cell Biol.* **214**, 401–415 (2016).
199. Hu, Y. *et al.* RECQL5/Recq15 helicase regulates homologous recombination and suppresses tumor formation via disruption of Rad51 presynaptic filaments. *Genes Dev.* **21**, 3073–3084 (2007).
200. Schwendener, S. *et al.* Physical interaction of RECQ5 helicase with RAD51 facilitates its anti-recombinase activity. *J. Biol. Chem.* **285**, 15739–15745 (2010).
201. Clynes, D. *et al.* Suppression of the alternative lengthening of telomere pathway by the chromatin remodelling factor ATRX. *Nat. Commun.* **6**, 1–11 (2015).

202. Riballo, E. *et al.* A Pathway of Double-Strand Break Rejoining Dependent upon ATM, Artemis, and Proteins Locating to γ -H2AX Foci. *Mol. Cell* **16**, 715–724 (2004).
203. Heaphy, C. M. *et al.* Altered telomeres in tumors with ATRX and DAXX mutations. *Science* (80-.). **333**, 425 (2011).
204. Chan, Y. W. & West, S. C. A new class of ultrafine anaphase bridges generated by homologous recombination. *Cell Cycle* **17**, 2101–2109 (2018).
205. Chan, Y. W., Fugger, K. & West, S. C. Unresolved recombination intermediates lead to ultra-fine anaphase bridges, chromosome breaks and aberrations. *Nat. Cell Biol.* **20**, 92–103 (2018).
206. Piazza, A., Shah, S., Wright, W. D., Gore, S. K. & Koszul, R. Dynamic Processing of Displacement Loops During Recombinational DNA Repair. **1**, 1–31 (2019).
207. Ralf, C., Hickson, I. D. & Wu, L. The Bloom's Syndrome Helicase Can Promote the Regression of a Model Replication Fork. *J. Biol. Chem.* **281**, 22839–22846 (2006).
208. Szostak, J. W., Orr-Weaver, T. L., Rothstein, R. J. & Stahl, F. W. The double-strand-break repair model for recombination. *Cell* **33**, 25–35 (1983).
209. González-Barrera, S., Cortés-Ledesma, F., Wellinger, R. E. & Aguilera, A. Equal Sister Chromatid Exchange Is a Major Mechanism of Double-Strand Break Repair in Yeast. *Mol. Cell* **11**, 1661–1671 (2003).
210. PERRY, P. & WOLFF, S. New Giemsa method for the differential staining of sister chromatids. *Nature* **251**, 156–158 (1974).
211. Claussin, C. *et al.* Genome-wide mapping of sister chromatid exchange events in single yeast cells using Strand-seq. *Elife* **6**, e30560 (2017).
212. Fabre, F., Chan, A., Heyer, W.-D. & Gangloff, S. Alternate pathways involving Sgs1/Top3, Mus81/ Mms4, and Srs2 prevent formation of toxic recombination intermediates from single-stranded gaps created by DNA replication. *Proc. Natl. Acad. Sci.* **99**, 16887 LP – 16892 (2002).
213. González-Prieto, R., Muñoz-Cabello, A. M., Cabello-Lobato, M. J. & Prado, F. Rad51 replication fork recruitment is required for DNA damage tolerance. *EMBO J.* **32**, 1307–1321 (2013).
214. Davis, L. & Maizels, N. Homology-directed repair of DNA nicks via pathways distinct from canonical double-strand break repair. *Proc. Natl. Acad. Sci.* **111**, E924 LP-E932 (2014).
215. Shor, E. *et al.* Mutations in homologous recombination genes rescue top3 slow growth in *Saccharomyces cerevisiae*. *Genetics* **162**, 647–662 (2002).
216. Wesoly, J. *et al.* Differential contributions of mammalian Rad54 paralogs to recombination, DNA damage repair, and meiosis. *Mol. Cell. Biol.* **26**, 976–989 (2006).
217. Urban, V. *et al.* RECQ5 helicase promotes resolution of conflicts between replication and transcription in human cells. *J. Cell Biol.* **214**, 401–415 (2016).
218. Makrantonis, V. & Marston, A. L. Cohesin and chromosome segregation. *Curr. Biol.* **28**, R688–R693 (2018).
219. Ström, L., Lindroos, H. B., Shirahige, K. & Sjögren, C. Postreplicative Recruitment of Cohesin to Double-Strand Breaks Is Required for DNA Repair. *Mol. Cell* **16**, 1003–1015 (2004).
220. Ström, L. *et al.* Postreplicative Formation of Cohesion Is Required for Repair and

- Induced by a Single DNA Break. *Science* (80-.). **317**, 242 LP – 245 (2007).
221. Ritchie, K. *et al.* Loss of ATRX leads to chromosome cohesion and congression defects . *J. Cell Biol.* **180**, 315–324 (2008).
 222. Lovejoy, C. A., Takai, K., Huh, M. S., Picketts, D. J. & de Lange, T. ATRX affects the repair of telomeric DSBs by promoting cohesion and a DAXX-dependent activity. *PLOS Biol.* **18**, e3000594 (2020).
 223. Ensminger, M. & Löbrich, M. One end to rule them all: Non-homologous end-joining and homologous recombination at DNA double-strand breaks. *Br. J. Radiol.* 20191054 (2020) doi:10.1259/bjr.20191054.
 224. Elango, R. *et al.* Break-induced replication promotes formation of lethal joint molecules dissolved by Srs2. *Nat. Commun.* **8**, 1790 (2017).
 225. Piazza, A., Wright, W. D. & Heyer, W. D. Multi-invasions Are Recombination Byproducts that Induce Chromosomal Rearrangements. *Cell* **170**, 760-773.e15 (2017).
 226. Piazza, A. & Heyer, W.-D. Multi-Invasion-Induced Rearrangements as a Pathway for Physiological and Pathological Recombination. *Bioessays* **40**, e1700249–e1700249 (2018).
 227. Kingston, R. E. *et al.* Histone H3 Mutations in Pediatric Brain Tumors. 6–11 (2014) doi:10.1101/cshperspect.a018689.
 228. Sobinoff, A. P. & Pickett, H. A. Alternative Lengthening of Telomeres: DNA Repair Pathways Converge. *Trends Genet.* **33**, 921–932 (2017).
 229. Cho, N. W., Dilley, R. L., Lampson, M. A. & Greenberg, R. A. Interchromosomal homology searches drive directional ALT telomere movement and synapsis. *Cell* **159**, 108–121 (2014).

8. APPENDIX

8.1 ABBREVIATIONS

53BP1	Tumor suppressor p53-binding protein 1
ALT	Alternative lengthening of telomeres
alt-NHEJ	Alternative non-homologous end-joining
ATM	Ataxia telangiectasia mutated
ATR-X	Alpha-thalassemia mental retardation X-linked protein
BARD1	BRCA1-associated RING domain protein 1
BIR	Break induced replication
BLM	Bloom syndrome protein
bp	Base pair
BRCA1	Breast cancer susceptibility protein 1
BrdU	5-bromo-2'-deoxyuridine
BS	Bloom syndrome
BTR	BLM-TOPOIII α -RMI1/2
CAF-1	Chromatin assembly factor 1
CDK	Cyclin-dependent kinase
CFS	common fragile site
CHD2	Chromodomain-helicase-DNA-binding protein 2
ChIP	Chromatin immunoprecipitation
c-NHEJ	Canonical non-homologous end-joining
CNV	Copy number variation
CO	Crossover
CPT	Camptothecin
CT	Cycle threshold
CtIP	CtBP-interacting protein
DAPI	4',6-diamidino-2-phenylindole
DAXX	Death domain associated protein
DDR	DNA damage response
dHJ	double Holliday junction
D-loop	Displacement loop
DMSO	Dimethyl sulfoxide
DNA	Deoxyribonucleic acid
DNA2	DNA replication ATP-dependent helicase/nuclease DNA2
DSB	Double-strand break
dsDNA	Double-stranded DNA
<i>E. coli</i>	Escherichia coli
EdU	5-ethynyl-2'-deoxyuridine
EXD2	Exonuclease 3'-5' domain-containing protein 2
EXO1	Exonuclease 1

FA	Formaldehyde
G1	Gap phase 1
G2	Gap phase 2
GAPDH	Glyceraldehyde-3-phosphate-dehydrogenase
GC	Gene conversion
GFP	Green fluorescent protein
Gy	Gray
h	Hour
HAT-1	Histone acetyltransferase 1
hDNA	Heteroduplex DNA
HIRA	Histone regulator A
HJURP	Holliday junction recognition protein
HR	Homologous recombination
hTERT	Human telomerase reverse transcriptase
ICL	Interstrand crosslink
IgG	Immunoglobulin G
IR	Ionizing Radiation
JM	Joint molecule
kDa	Kilo Dalton
KU70/80	XRCC6/5, X-ray repair cross-complementing protein 6/5
LIG	DNA ligase
LOH	Loss of heterozygosity
MDC1	Mediator of DNA damage checkpoint protein 1
me	Methylated
MiDAS	Mitotic DNA synthesis
MIR	Multi-invasion-induced rearrangements
MMC	Mitomycin C
MMS	Methyl methanesulfonate
MRE11	Meiotic recombination 11
MRN	MRE11, RAD50, NBS1 complex
NBS1	Nijmegen breakage syndrome 1
PALB2	partner and localizer of BRCA2
PARP1	Poly(ADP-ribose) polymerase 1
PCNA	Proliferating cell nuclear antigen
Pol δ	Polymerase delta
PTM	Post-translational modification
qPCR	Quantitative polymerase chain reaction
RAD51	DNA repair protein RAD51 homolog 1
RFC	Replication factor C
RFP	Red fluorescent protein
RNA	Ribonucleic acid
RNF	E3 ubiquitin protein ligase RING finger protein

RNF168	Ring finger protein 168
RNF8	Ring finger protein 8
RPA	Replication protein A
RSF	Remodeling and spacing factor
RT	Room temperature
<i>S. cerevisiae</i>	<i>Saccharomyces cerevisiae</i>
SCE	Sister chromatid exchange
SD	Standard deviation
SDSA	Synthesis dependent strand annealing
SEM	standard error mean
siRNA	Small interfering RNA
SMARCAD1	SWI/SNF-related matrix-associated actin-dependent regulator of chromatin subfamily A containing DEAD/H box 1
SSB	Single-strand break
ssDNA	Single-stranded DNA
TLS	Translesion synthesis
Top1	Topoisomerase 1
TOPO3 α	Topoisomerase 3 alpha
Ub	Ubiquitinated
UFB	Ultra-fine bridge
UV	ultraviolet
WT	Wild-type
X-IR	X-ray irradiation
XRCC4	X-ray repair cross-complementing protein 4
γ H2AX	gamma H2AX; phosphorylated histone variant H2AX



8.2 EHRENWÖRTLICHE ERKLÄRUNG

Ich erkläre hiermit ehrenwörtlich, dass ich die vorliegende Arbeit entsprechend den Regeln guter wissenschaftlicher Praxis selbstständig und ohne unzulässige Hilfe Dritter angefertigt habe.

Sämtliche aus fremden Quellen direkt oder indirekt übernommenen Gedanken sowie sämtliche von Anderen direkt oder indirekt übernommenen Daten, Techniken und Materialien sind als solche kenntlich gemacht. Die Arbeit wurde bisher bei keiner anderen Hochschule zu Prüfungszwecken eingereicht.

Darmstadt, den 04.05.2020

Amira Elbakry

8.3 CURRICULUM VITAE

Personal information

Name: Amira Elbakry

Place of birth: Giza, Egypt

Education

01.2016-06.2020 Doctor of Philosophy, Radiation Biology and DNA Repair, Technical University of Darmstadt

Thesis title: Factors regulation late stages of homologous recombination and sub-pathway choice in G2.

Supervisor: Prof. Dr. Markus Löbrich

09.2008- 08.2009 Master of Science in Molecular Medicine, University College London

Thesis title: Formation and Repair of Psoralen+UVA-induced DNA Interstrand Crosslinks in Human Cancer Cell Lines. Supervisor Prof. Dr. John Hartley

09.2003-06.2007 Bachelor of Science in Biology (magna cum laude), The American University in Cairo

09.1999-05.2003 American High School Diploma, International School of Choueifat, Cairo

Affiliation

06.2017-03.2020 Fellow, DFG-funded Graduate School (GrK) 1657: Molecular and cellular responses to ionizing radiation at the Technical University of Darmstadt

Publications

Elbakry, A., Juhász, S., Chan, K.C., & Löbrich, M. ATRX and RECQ5 define distinct homologous recombination sub-pathways. *Proc. Nat. Acad. Sci.* 118, e2010370118 (2021).

Elbakry, A., Juhász, S., Mathes, A. & Löbrich, M. DNA repair synthesis and histone deposition partner during homologous recombination. *Mol. Cell. Oncol.* 5, (2018).

Juhász, S., Elbakry, A., Mathes, A. & Löbrich, M. ATRX Promotes DNA Repair Synthesis and Sister Chromatid Exchange during Homologous Recombination. Mol. Cell 71, 11-24.e7 (2018).

Conference Proceedings

Elbakry, A., Juhász, S. & Löbrich, M. **ATR_X and RECQ5 define distinct subpathways of homologous recombination.** Poster presentation at EMBO conference: The DNA damage response in cell physiology and disease, October 2019- Cape Sounio, Greece.

Elbakry, A., Juhász, S., Mathes, A. & Löbrich, M. **ATR_X Promotes DNA Repair Synthesis and Sister Chromatid Exchange during Homologous Recombination.** Poster presentation at Abcam Conference: Mechanisms of Recombination, May 2018- London, United Kingdom.

Elbakry, A., Juhász, S. & Löbrich, M. **The histone variant H3.3 is required for DNA repair synthesis during homologous recombination.** Poster presentation at the 4th German-French DNA Repair Meeting, September 2017- Cologne, Germany. (Travel award).

8.4 ACKNOWLEDGMENTS

The road to finishing this PhD has been long, challenging, with lots of twists and turns but in difficulty lies value, it has been an incredible learning experience. My gratitude goes first to my supervisor, Prof. Dr. Markus Löbrich, who gave me this opportunity, guided and supported me through the years, with many (many) discussions that substantially helped shape my science. Many thanks to my second supervisor, Prof. Dr. Alexander Löwer for his continuous support and advice and to Prof. Dr. Cristina Cardoso and Prof. Dr. Torsten Waldminghaus for being part of my examination committee. Many thanks to members of our graduate college GrK 1657 for the insightful discussions and general good times we had in retreats and meetings. I am also thankful for everyone who contributed to this work and to my educational experience.

My gratitude extends to all members of the Löbrich group, past and present, who have been the best company inside and outside the lab; every single one has made a difference in my life and helped me grow so much professionally and personally. I would like to thank Szilvia Juhász, who taught me a lot in my early time, and all of our incredibly dedicated and supportive technical staff for helping out in all ways possible. Special thanks go out to Monika Gawai, Emilie Renaud and Amir Mofidi, who have left the group but are friends for life who helped me on so many levels with science, and much more; Marta Llorens Agost and Andrés Cruz Garcia for always being there, and also for taking the time to review and comment (extensively) on my thesis, their help was incredibly valuable; Daniel, Holly, Michi, Ann Charlotte and everyone else who was there for me in anyway- I am eternally grateful.

A special mention to the TUD family office, whom have been endlessly helpful throughout the years and provided excellent care for my son to allow me to do my job.

My deepest thanks, appreciation, love and gratitude goes to my family: My parents Salah and Nahed, my sister Eman and my brother Ahmed: you have been my rock all my life and during every challenge; I owe you the world. To my other sisters: Heba, Sarah and Lobna thank you for always being on my side unconditionally. For all my friends, it really does take a village, I could not have made it without your immense support and encouragement. Finally, my son and partner in crime, Youssef, the personification of everything I could ever ask for and my biggest motivation, this is all for you and because of you.

This thesis has been written under exceptionally difficult circumstances, including, but not limited to, a global pandemic (shoutout to COVID-19). I am happy with and proud of this work, and even more proud and extremely lucky to have the amount of love and support I received.

